Studies on the Adjuvant Potential of Synthetic Ligands for Targeting MRSA in Combination Therapy

A Thesis

Submitted in Partial Fulfillment of the Requirements for the Degree of

DOCTOR OF PHILOSOPHY

by

BASU BHATTACHARJEE

Department of Biosciences and Bioengineering
Indian Institute of Technology Guwahati
Guwahati-781039, Assam, India

August 2022

Studies on the Adjuvant Potential of Synthetic Ligands for Targeting MRSA in Combination Therapy

A Thesis

Submitted in Partial Fulfillment of the Requirements for the Degree of

DOCTOR OF PHILOSOPHY

by

BASU BHATTACHARJEE

Department of Biosciences and Bioengineering
Indian Institute of Technology Guwahati
Guwahati-781039, Assam, India

August 2022

In the fond memory of Baba

And

As Heartfelt gratitude to Maa

INDIAN INSTITUTE OF TECHNOLOGY GUWAHATI

DEPARTMENT OF BIOSCIENCES AND BIOENGINEERING

STATEMENT

I do hereby declare that the research findings of this thesis is the result of research work carried out by me in the Department of Biosciences and Bioengineering, Indian Institute of Technology Guwahati, Guwahati, India, under the supervision of Professor Aiyagari Ramesh.

As per the general norms of reporting research findings, due acknowledgements have been made, wherever the research findings of other researchers have been cited in this thesis.

Date: 5 August 2022

Basu Bhattacharjee

INDIAN INSTITUTE OF TECHNOLOGY GUWAHATI

DEPARTMENT OF BIOSCIENCES AND BIOENGINEERING

CERTIFICATE

It is certified that the work described in this thesis entitled " ***Studies on the Adjuvant Potential of Synthetic Ligands for Targeting MRSA in Combination Therapy***" by Mr. Basu Bhattacharjee for the award of degree of Doctor of Philosophy is an authentic record of the results obtained from the research work carried out under my supervision in the Department of Biosciences and Bioengineering, Indian Institute of Technology Guwahati, India, and this work has not been submitted elsewhere for the award of any other degree.

Basu Bhattacharjee
(Candidate)
Roll No. 166106018

CERTIFIED

Aiyagari Ramesh
05/08/2022

Aiyagari Ramesh
(Thesis Supervisor)
Date: 5 August 2022

ACKNOWLEDGEMENT

I would like to take this opportunity to offer my heartfelt gratitude to my family and a number of people who made this journey worthwhile. First and foremost, I would like to express my gratitude to Professor Aiyagari Ramesh, for providing me the platform to learn and accomplish this valuable experience. I wish to further thank him for inculcating in me unique perspective and intellectual thought process towards science which inspired me to retain my trust in science throughout this journey and keep myself highly motivated. His constant zeal towards research and teaching has been my constant source of inspiration. His invaluable guidance, and life lessons throughout my Ph.D. tenure has helped me to grow as an independent researcher, decision maker and as a contented individual. I am thankful to my doctoral committee members, Professor Gurvinder K. Saini, Professor Ranjan Tamuli, and Professor Lal Mohan Kundu for their constructive suggestions, support and motivation, which has helped me to improve the quality of my research experience. I am extremely grateful to Professor Gopal Das, Department of Chemistry for providing me the opportunity to collaborate and learn the interdisciplinary science. I am thankful to sir for the valuable suggestions that often gave new perspectives to my research work.

I sincerely express my gratitude and thanks to Professor Benu Dhawan, All India Institute of Medical Sciences (AIIMS), New Delhi and Professor Kasturi Mukhopadhyay, Jawaharlal Nehru University (JNU), New Delhi for kindly providing the MRSA strain for my work. I am also thankful to Professor Siddhartha Sankar Ghosh, Professor Pranab Goswami, Dr. Biplab Bose and Professor Lingaraj Sahoo for providing an amicable and non-hostile environment to execute my Ph.D. work successfully. I would like to extend my sincere gratitude towards Professor Rakhi Chaturvedi, Head of the Department of Biosciences and Bioengineering, IIT Guwahati, and Professor Latha Rangan; Professor Kannan Pakshirajan, Former Heads of the Department Biosciences and Bioengineering, IIT Guwahati for

providing me the necessary facilities that helped me to pursue my research at IIT Guwahati. I am also grateful to all faculty members and staff of the Department of Biosciences and Bioengineering for supporting me throughout the Ph.D. tenure. I would especially like to thank Nurul Sir, Niranjan Sir and Prarthana Ma'am for helping me whenever I needed. I would like to thank Department of Biosciences and Bioengineering for providing infrastructural facility for my research work. I would also like to thank Central Instruments Facility (CIF) of IIT Guwahati for providing ambient atmosphere of research and high-end equipments to execute my experiments. I would especially like to thank Dr. K.K. Senapati Sir and Dr. Dolly Gogoi Ma'am for letting me use FESEM whenever I needed it, it really saved a lot of my crucial time.

I acknowledge the state-of-art facility at the Center for Excellence under the aegis of Program Support Grant provided by Department of Biotechnology (DBT), Government of India. I am grateful to Department of Biotechnology (DBT) and Science and Engineering Board (SERB), Department of Science & Technology (DST) for supporting my research through grants. I am also grateful to Ministry of Human Resource Department (MHRD) and IIT Guwahati for providing research fellowship. I am grateful to our collaborators Dr. Utsab Manna, Dr. Senjuti Halder, Dr. Ashes Das, Megha Basak and Sagnik Dey, from the Department of Chemistry, IIT Guwahati for the scientific collaboration and helping me out whenever I needed them. I sincerely acknowledge my M. Tech thesis supervisor Dr. Munia Ganguli, Principal Scientist, CSIR-IGIB and Prof. Amit Asthana, Associate Dean (R&D), NIPER Hyderabad for providing me the opportunities to explore the field of nanobiotechnology which was the stepping stone for me to venture into translational research.

I would also like to thank my seniors Dr. Thiyagarajan, Dr. Sandipan Mukherjee, Dr. Poulomi Dey and Dr. Priya Mullick for their helpful guidance at the initial stages of my

research work. They painstakingly made efforts to teach me the knitty-gritties of lab related work and work culture in general. It is my pleasure to thank my current lab members Barlina, Shubhangi and former lab members Tabassum, Narahari, Dipanjali, Gopika, Bhagyashree, Sanket, and Muskan for their support and unconditional gesture of assistance in the time of need especially during the pandemic. I wish to thank my friends Dr. Anitha, Dr. Deepa, Saddam, Manish, Abhishek, Juhi, Jaishree, Shweta, Ankita, Pankaj, Bhaskar and Kishore for their constant support and motivation throughout the course of my Ph.D. because of whom my stay at IIT Guwahati has become more memorable and wonderful. I also wish to thank all my furry friends all around the campus for greeting me with compassion every time I have met them even if I didn't have anything to offer them then. They taught me to be forgiving, playful and most importantly being compassionately humane. I would also like to thank Dr. Rajib Shome, Dr. Smita Das, Plaboni Sen, Puja Rani Kuri, Barlina Konwar, Muktashree Saha, Riddhi Bannerjee and Gaurav Bhatt for their valuable suggestions in my personal and professional life.

Lastly, I would like to thank Mrs. Purnima Bhattacharjee (my mother), Mrs. Madhu Chatterjee (my sister) and Mrs. Debashree Debasmita (my wife) for always backing me up in every aspect of life. I would also like to thank my father and especially his lessons about how to tackle obstacles and conduct life in-general.

Basu Bhattacharjee

CONTENTS

CHAPTER 2: Potential of Urea-based Ligands as an Efflux Pump Inhibitor to Counter Ciprofloxacin Resistance in MRSA

CHAPTER 3: Development of C8-loaded Nanocarrier as an Adjuvant for Mitigation of MRSA in Combination Therapy

CHAPTER 5: Potential of Quinoxaline-based Antimicrobial (C2) in Combination Therapy for Mitigation of MRSA in an *In-Vitro* Bone Cell Infection Model

ABBREVIATIONS

µg	Microgram
µL	Microliter
µM	Micromolar
A_{600}	Absorbance at 600 nm
AFM	Atomic Force Microscope
agrC	Accessory gene regulator gene
ANOVA	Analysis of variance
ATR-FTIR	Attenuated total reflectance Fourier-transform infrared spectroscopy
bp	Base pairs
cFDA-SE	5(and 6)-carboxyfluorescein diacetate succinimidyl ester
CFU	Colony forming unit
cps	Counts per second
cnbA	Collagen binding protein gene
C_T	Cycle threshold
CV	Crystal violet
DAPI	4′,6-diamidino-2-phenylindole
DLS	Dynamic light scattering
DMEM	Dulbecco's modified eagles medium
DMSO	Dimethyl sulfoxide
DNA	Deoxyribonucleic acid
EDTA	Ethylenediamine tetraacetic acid
EDX	Energy Dispersive X-Ray Analysis
FBS	Fetal bovine serum
FESEM	Field emission scanning electron microscope
FETEM	Field emission transmission electron microscope
FTIR	Fourier-transform infrared spectroscopy
fnbA	Fibronectin binding protein gene
HEK	Human embryonic Kidney
HEPES	N-2-Hydroxyethyl Piperazine N-2 Ethane Sulphonic acid
IC_{50}	half maximal inhibitory concentration
MBC	Minimum bactericidal concentration
MBEC	Minimum Biofilm Eradication Concentration
MBIC	Minimum Biofilm Inhibitory Concentration

Abbreviations

mg	Milli grams
MG-63	Human osteosarcoma cells
MIC	Minimum inhibitory concentration
MKC	Minimum killing concentration
mL	Milliliter
mM	Millimolar
MTT	3-(4,5-Dimethylthylthiazol-2-yl)-2,5-diphenyltetrazolium bromide
nm	Nanometer
NPs	Nanoparticles
norA	Nor A Efflux pump gene specific to fluoroquinolones
OD_{600}	Optical density at 600 nm
PBS	Phosphate buffered saline
qRT-PCR	Real-Time Quantitative Polymerase Chain Reaction
RNA	Ribonucleic acid
rpm	Revolutions per minute
RT	Room temperature
SBF	Simulated body fluid
SD	Standard deviation
TW	Titanium wire
w/v	Weight/volume
λ_{Em}	Emission wavelength
λ_{Ex}	Excitation wavelength

भारतीय प्रौद्योगिकी संस्थान गुवाहाटी
Indian Institute of Technology Guwahati

LIST OF TABLES

CHAPTER 4

CHAPTER 5

CHAPTER 6

LIST OF SCHEMES AND FIGURES

Chapter 1

Introduction and Literature Review

भारतीय प्रौद्योगिकी संस्थान गुवाहाटी
Indian Institute of Technology Guwahati

Introduction

The prevalence of antibiotic-resistant pathogenic bacteria is a contemporary and global healthcare problem. The consequences of infections caused by antibiotic-resistant bacteria are adverse as the ramifications may be profound in the realm of clinics and public healthcare. Antibiotic-resistant pathogenic bacteria possess a plethora of attributes, that empower the bacteria to counter therapeutic antibiotics, such as (i) presence of a membrane permeability barrier that impedes drug diffusion and uptake, (ii) presence of an efflux pump that expels drugs from the cell and reduces their availability at target sites, (iii) alterations in molecular targets of antibiotics, (iv) presence of a metabolic bypass that renders the cell insensitive to the antibiotic and (v) presence of antibiotic-altering and antibiotic-degrading enzymes. Further, rampant use of antibiotics in the clinics may escalate resistance development in cells and transmission of the resistance trait can also be facilitated through horizontal gene transfer, leading to dissemination of the resistance trait on an enormous scale. The problem of antibiotic-resistance is further compounded by the innovation gap and the arduous track in drug discovery research. In order to cope up with this serious healthcare crisis, there is a compelling need for a prudent drug discovery program that is committed to tackle the global problem and mitigate infections caused by antibiotic-resistant bacteria.

Considering the limitations of antibiotic monotherapy and the scarcity of new and effective antibiotics, it is conceived that the combination of two or more antibacterial agents during a treatment regimen can be a viable approach to alleviate severe bacterial infections. Combinations of antibiotics are likely to render therapeutic dividends such as (i) providing a broad empiric coverage, (ii) facilitating multimodal spectra of activity, (iii) hindering emergence of resistance and (iv) generating a synergistic effect. However, combinations of antibiotics can also be counterproductive as antagonism can emerge owing to drug interactions. In addition, antibiotic-mediated drug toxicity and cost-intensive therapy can be significant impediments in harnessing the therapeutic potential of antibiotic combinations. On the other hand, combination of non-antibiotic molecules with antibiotics offers an exciting prospect in the realm of medicinal chemistry and drug discovery as it opens up the untapped library of bioactive synthetic molecules. In particular, there is an enormous scope to rationally design synthetic small molecules that can directly counter the core resistance mechanism in pathogenic bacteria. Conceivably, such molecules can emerge as therapeutic adjuvants and minimize resistance

development, reduce host-directed toxicity and restore activity of therapeutic antibiotics for clinical use.

Based on the aforementioned tenet, the present investigation is an endeavor towards the generation of rationally designed synthetic small molecules and exploring their prospect as adjuvants in combinatorial antibacterial chemotherapy. The present investigation holds significance as the fundamental understanding emerging from the study is likely to yield a guideline to develop effective adjuvants for combinatorial antibacterial therapy and thereby address a very serious global healthcare problem.

Literature Review

1.1. An Overview of Antibiotic-Resistant Pathogenic Bacteria

Antibiotic-resistant pathogenic bacteria display inherent resistance mechanisms against commonly used therapeutic agents. In addition, indiscriminate use of antibiotics has escalated the evolution of drug-resistant strains. Considering the grave concerns associated with antibiotic-resistance, a large number of seminal review articles have critically articulated the implications of antibiotic-resistant pathogenic bacteria (Peterson and Kaur 2018; Petchiappan and Chatterjee, 2017; de Kraker *et al*., 2016; Fair and Tor 2014, Wright, 2011; Davies and Davies, 2010; Fischbach and Walsh 2009, Nikaido, 2009). Literature reports categorize the clinically-prevalent drug-resistant bacterial pathogens as: (i) β-lactam resistant Pneumococci, (ii) penicillin and chloramphenicol-resistant *Neisseria meningitides*, (iii) vancomycin-resistant enterococci (VRE), (iv) vancomycin- resistant *Staphylococcus aureus* (VRSA), (v) methicillin-resistant *Staphylococcus aureus* (MRSA), (vi) penicillin-resistant *Streptococcus pneumoniae*, (vii) multidrug-resistant *Salmonella typhimurium* (MRST), (viii) multidrug-resistant *Acinetobacter*, carbapenem-resistant Enterobacteriaceae (CRE) and others (Kaye and Kaye, 2000; Lee *et al*., 2018; Tong *et al*., 2015; Lowy, 2003; Mather *et al*., 2013; Fair and Tor, 2014). Amongst the drug-resistant pathogens, the emergence of *Klebsiella pneumonia* NDM-1 has caused lot of concern, as the pathogen is life-threatening and displays high resistance towards critical antibiotics such as penicillin, cephalosporins and other lactams, and this trait is attributed to the presence of a metallo-β-lactamase-resistance gene (blaNDM.1) (Yong *et al*., 2009; Nordmann *et al*., 2011; Brink *et al*., 2012; Jin *et al*., 2015; Arpin *et al*., 2012).

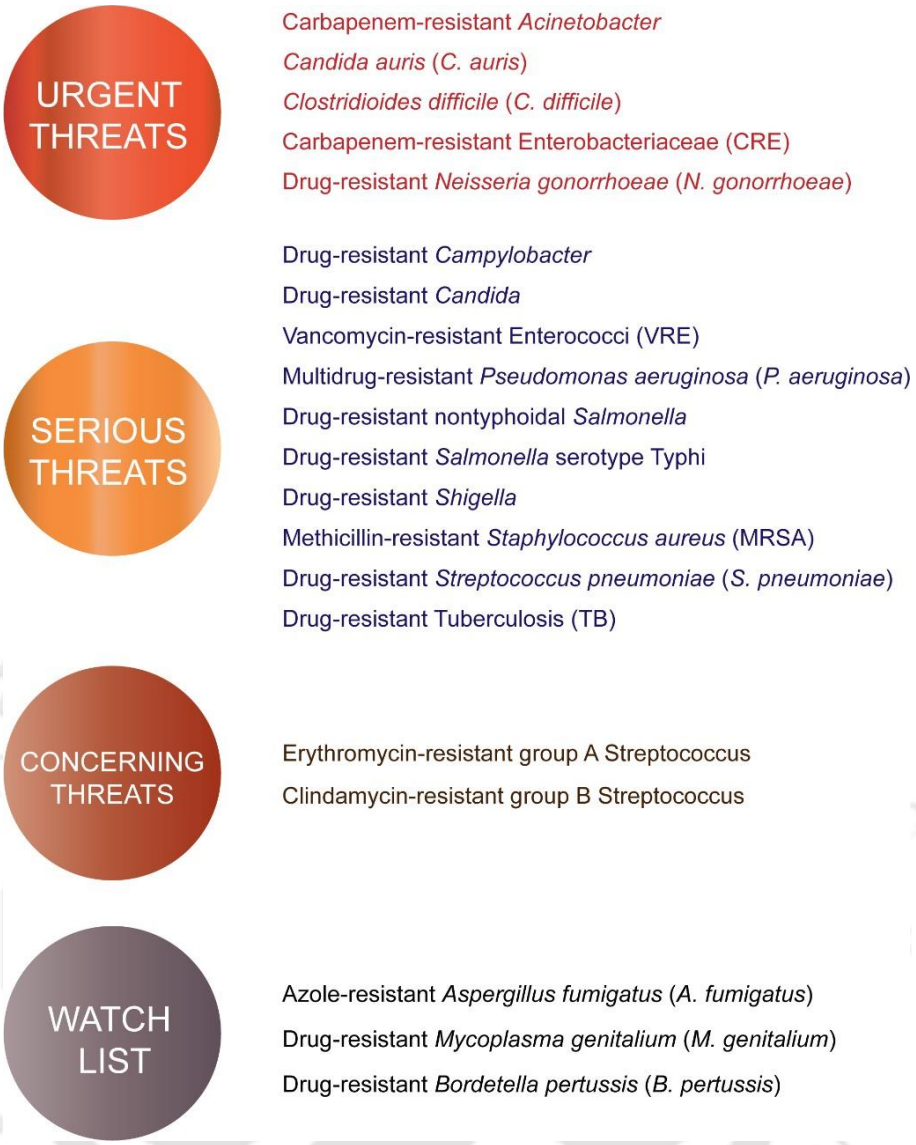

Figure 1.1. Antibiotic-resistant pathogenic microbes classified on the basis of the threat levels. The threat levels are based on CDC report 2019.

The Centers for Disease Control and Prevention (CDC) in the USA and the World Health Organization (WHO) have also published reports that emphasize the implications with regard to antibiotic-resistant pathogens. On the basis of the threat level, CDC has proposed a classification of antibiotic-resistant microbes consisting of four categories (CDC Report, 2019). A schematic representation of the various categories and the pathogens belonging to each category is illustrated in Figure 1.1. The World Health Organization (WHO) has proposed a priority list consisting of three categories namely, critical, high, and medium priority and have catalogued various antibiotic-resistant pathogenic bacteria under the three lists (Tacconelli *et al.*, 2017; WHO report 2014). A schematic representation of the various pathogens belonging to

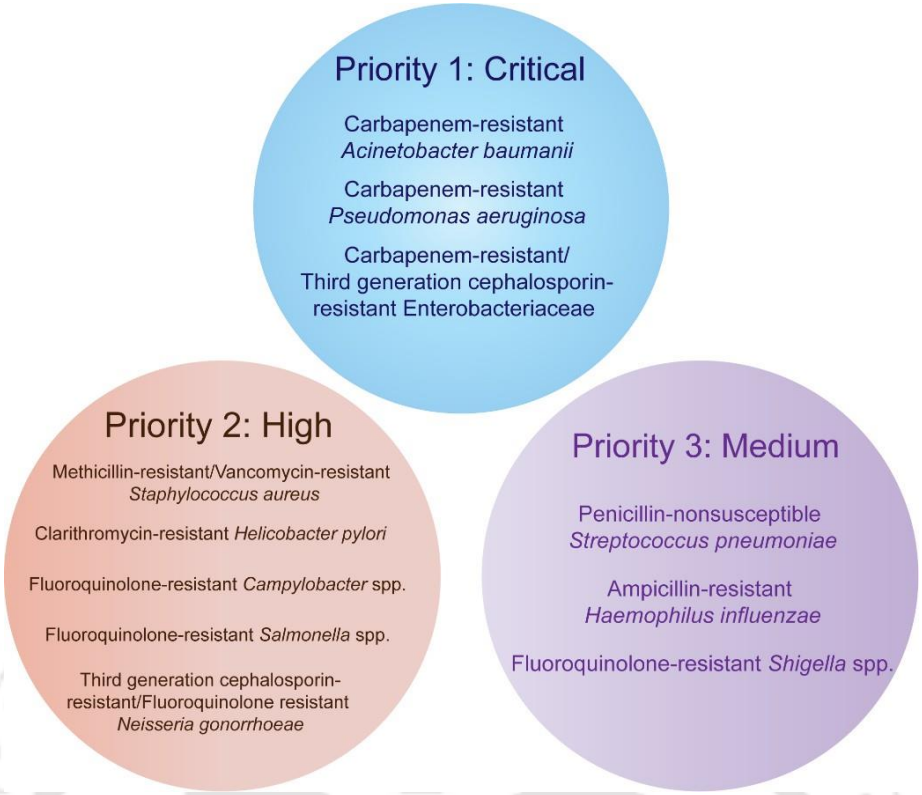

Figure 1.2. Representative antibiotic-resistant pathogenic bacteria belonging to various priority list as proposed by WHO. The priority list is based on WHO report 2014.

each category is illustrated in Figure 1.2. The implications of antibiotic-resistant microbe with regard to the healthcare burden is quite serious. This tenet is indeed reflected in the CDC report of 2019, wherein it was reported that in excess of 2.8 million antibiotic-resistant infections are recorded in the United States each year, and more than 35,000 people die as a result of these infections. A nuanced analysis on the timeline of the discovery of various classes of antibiotics indicate that a large number of antibiotics were discovered between 1930s-1960s. Since the 1960s, the number of approved new drug scaffolds were only six spanning over a nearly thirty-year innovation gap (Fair and Tor 2014; Silver 2011; Fischbach and Walsh 2009). An alternate paradigm of the timeline of antibiotic discovery from 1925-2025 suggests four major periods namely: (a) the golden era, (b) medicinal chemistry era, (c) resistance era and (d) narrow-spectrum era (Brown and Wright, 2016).

1.2. Key Mechanisms of Antibiotic-Resistance in Pathogenic Bacteria

Conventional antibiotics are known to target fundamental physiological and metabolic processes in cells. Hence, these antibiotics can interfere with DNA synthesis (Collin *et*

al., 2011; Kohanski *et al*., 2010) or prevent cell wall synthesis (Hurdle *et al*., 2011) or perturb protein synthesis and folate synthesis (McCoy *et al*., 2011; Wilson, 2014; Lange *et al*., 2007; Palmer and Kishony, 2014). Pathogenic bacteria are however known to possess various attributes to circumvent the action of these antibiotics. Extensive literature reports are available that describe the mechanisms of antibiotic-resistance prevalent in pathogenic bacteria. Based on these studies, the well-established modes of resistance include (a) presence of a permeability barrier that hampers antibiotic diffusion and cellular uptake, (b) presence of an active efflux pump that can expel some antibiotics and thus decrease its availability at target sites, (c) modifications of molecular targets, (d) presence of a metabolic bypass mechanism, which lowers the sensitivity of the target cell to the drug, (e) presence of enzymes that are known to either alter or destroy antibiotics (Nikaido, 2010; Wright, 2011; Weidenmaier and Peschel, 2008; Chambers and DeLeo, 2009; Gutsmann and Seydel, 2010; Gootz, 2010). Further, an overuse of antibiotics in the clinics can render a biased selection of resistant cells, which in turn can transmit the resistance trait to other cells by horizontal gene transfer, resulting in large scale manifestation of antibiotic-resistance trait in pathogenic bacteria (Davies and Davies 2010; Fair and Tor 2014, Toprak *et al*., 2012).

1.3. Methicillin-Resistant Staphylococcus aureus (MRSA)

In the present investigation, the potential of the generated synthetic ligands as a bactericidal, antibiofilm and an adjuvant molecule was tested against a clinical strain of MRSA. In the following section, a brief overview on the essential features of the pathogen is presented. MRSA is a serious human pathogen, that is known to be prevalent in both healthcare as well as the community sphere. The pathogen is a major causative agent of a number of ailments such as bacteremia, endocarditis, skin and soft tissue infections, bone and joint infections and other hospital-associated infections (Lee *et al*., 2018; Turner *et al*., 2019; Tong *et al*., 2015; Craft *et al*., 2019). Since its first emergence in the clinics in 1960, an extensive community spread of MRSA has been witnessed. The healthcare burden of MRSA has a global footprint extending from a relatively low occurrence in Scandinavia to high prevalence in certain regions of North America and Asia (Lee *et al*., 2018). In the United States, the number of cases of MRSA infection in hospitalized patients in 2017 was estimated to be around 323,700 of which 10,600 deaths were recorded (CDC Report, 2019). With regard to mitigation of MRSA infection in the clinic, the widespread resistance of the pathogen to a large number of therapeutic β-

lactam antibiotics poses a fundamental problem (Lee *et al*., 2018; Craft *et al*., 2019). Moreover, MRSA expresses a plethora of virulence factors such as adhesins, toxins, immune-evasive factors and tissue-degrading enzymes, which enable initiation, establishment and persistence of invasive infections in the host (Lee *et al*., 2018; Turner *et al*., 2019; Spaan *et al*., 2017; Laabei *et al*; 2014; Thammavongsa *et al*., 2015).

1.4. MRSA Biofilm and Implant Infection

MRSA cells are physiologically adaptive and can readily form biofilms in tissues and medical implants. The biofilm matrix can protect the underlying cells from the host immune system and can also present a permeability barrier for chemotherapeutic agents and antibiotics (Craft *et al*., 2019; Arciola *et al*., 2018; Stoodley, *et al*., 2011; Oliveira *et al*., 2018; Hall and Mah, 2017). A major proportion of hospital-acquired infections are caused by biofilm formation on medical implants, resulting in tissue destruction, systemic spread of the pathogen and deterioration in the efficacy of the implant, which can ultimately have fatal consequences (Hall-Stoodley *et al*., 2004; Bryers, 2008; Darouiche, 2001). During implant colonization by MRSA biofilm, matrix proteins such as collagen, can accumulate on the implant's surface and facilitate initial adhesion of MRSA cells, which can subsequently bolster biofilm formation on the implant (Lee *et al*., 2018; Foster *et al*., 2014).

1.5. Prevailing Mechanisms of Antibiotic Resistance in MRSA

1.5.1. Mobile Genetic Elements Encoding Antibiotic Resistance

The acquisition of mobile genetic elements (MGEs) carrying antibiotic-resistance genes by MRSA is a well-established phenomenon. MRSA is known to possess a 20-65 kb *SCCmec* element that contains the *mecA* gene complex accounting for the methicillin-resistance trait in the pathogen (Turner *et al*., 2019). In MRSA, the MGEs acquired by a process of horizontal transfer are essentially responsible for manifestation of resistance against a large number of antibiotics such as aminoglycoside, penicillin, chloramphenicol, trimethoprim, macrolide, mupirocin, methicillin, tetracycline and others (Turner *et al*., 2019).

1.5.2. Expanded β-lactam Resistance

Manifestation of methicillin resistance in MRSA is essentially due to a drug target modification strategy adopted by the pathogen. MRSA is known to express an accessory

penicillin-binding protein (PBP), termed as PBP2a, having low affinity for all β-lactams. Owing to the presence of this protein, a large number of β-lactams such as penicillin, cephalosporin and carbapenem are ineffective against MRSA (Craft *et al*., 2019).

1.5.3. Vancomycin-Resistance

Vancomycin is a key therapeutic antibiotic for mitigation of MRSA infections. The clinical use of this antibiotic assumes greater significance as β-lactams have become increasing ineffective against MRSA. However, the presence of vancomycin-resistant staphylococci has also been reported in a previous study (Weigel *et al*., 2003; Rossi *et al*., 2014).

1.5.4. Efflux Pump-Mediated Resistance

Efflux pumps are significantly implicated in development of resistance against therapeutic agents in staphylococci (Li and Nikaido, 2009; Costa *et al*., 2015; Jang, 2016). Efflux pumps are essentially membrane proteins involved in the export of antibiotics, biocides, and toxic metals. Multidrug efflux pumps prevalent in *S. aureus* largely belong to five categories of membrane protein families: (a) the major facilitator superfamily (MFS), (b) the small multidrug resistance (SMR) family, (b) the multidrug and toxin extrusion (MATE) family, (d) the ATP-binding cassette (ABC) superfamily, and (e) the resistance-nodulation-division (RND) superfamily (Jang, 2016). Amongst all the efflux pumps present in staphylococci, the MFS type pumps have been studied in great detail. A brief overview on various types of staphylococcal MFS efflux pumps and the notable antibiotics affected by the efflux activity is illustrated in Table 1.1.

In *S. aureus*, the NorA efflux pump is the most extensively characterized efflux system. Studies have revealed that NorA protein consists of 388 amino acids and encompasses 12 transmembrane segments (Yoshida *et al*., 1990). A large number of studies have demonstrated that NorA can expel chemically and structurally divergent compounds, such as the fluoroquinolones norfloxacin and ciprofloxacin, dyes and quaternary ammonium compounds (Neyfakh *et al*., 1993; Kaatz *et al*., 1993). In MRSA, the *norA* gene codes for an efflux pump protein involved in the export of

Table 1.1. Overview of representative Major Facilitator Superfamily (MFS) efflux pumps present in *Staphylococcus aureus*.

Sl. No.	Efflux Pump	Affected Antibiotic	Coding Element	Reference
1.	NorA	Norfloxacin, Enoxacin, Ofloxacin, Ciprofloxacin, Ethidium bromide, Acriflavine	Chromosome	Truong-Bolduc *et al*., 2003; Kaatz *et al*., 2005; Truong-Bolduc and Hooper 2007
2.	NorB	Ciprofloxacin, Norfloxacin Sparfloxacin, Gemifloxacin Premafloxacin	Chromosome	Truong-Bolduc and Hooper 2010
3.	SdrM	Norfloxacin	Chromosome	Yamada *et al*., 2006
4.	LmrS	Linezolid, Chloramphenicol, Trimethoprim Erythromycin, Lincomycin	Chromosome	Floyd *et al*., 2010
5.	QacA	Cetrimide, Chlorhexidine	Plasmid	Rouch *et al*., 1990; Brown and Skurray 2001

ciprofloxacin ciprofloxacin (Jang, 2016). A recent study has also demonstrated that NorA is implicated in resistance development against ciprofloxacin in *S. aureus* (Papkou *et al*., 2020). Mechanistic studies have revealed that NorA-mediated efflux of norfloxacin is affected by protonophores and hence coupled to membrane proton gradient (Ng *et al*., 1994).

1.6. Overview of Antibiotic-Mediated Anti-MRSA Therapy

The current therapeutic antibiotics, which have been routinely used in the clinic for countering MRSA infections include vancomycin, daptomycin, linezolid, sulfamethoxazole and trimethoprim (Lee *et al*., 2018; Turner *et al*., 2019). Besides, other antibiotics which have emerged for therapeutic intervention against MRSA include ceftaroline, telavancin, delafloxacin, tedizolid and others (Lee *et al*., 2018). The glycopeptide vancomycin has prevailed in the clinics as a critical arsenal for treatment of MRSA systemic infections (Liu *et al*., 2011; Gould *et al*., 2012). Studies have revealed

the antagonistic potential of the lipopeptide daptomycin against MRSA (Smith *et al*., 2009; Arbeit *et al*., 2004). Additional studies have documented the utility of linezolid and telavancin for anti-MRSA therapy (Wunderink *et al*., 2012; Stryjewski *et al*., 2008). However, with increasing emergence of resistance development in MRSA against a critical antibiotic like vancomycin (Weigel *et al*., 2003; Rossi *et al*., 2014), there is a compelling need for an alternative intervention against MRSA.

1.7. Antibiotic-based Combination Therapy Against MRSA

The use of multiple antibiotics in combination therapy has been used as an effort towards achieving a better clinical outcome against MRSA infections. This approach essentially consists of using a cocktail of antibiotics, which differ in their (a) mode of action in different pathways or (b) site of action within the same pathway (Worthington and Melander 2013). The various attributes. which makes combinatorial therapy more favorable than monotherapy encompass (i) increased antibacterial spectrum, (ii) prevention of poly-microbial infections, (iii) minimization of emergence of resistant trait and (iv) rendering synergistic effect, (v) lowering doses and decreasing drug toxicity of antibiotic combinations. The benefit of combination therapy was captured in a study which revealed that vancomycin in combination with oxacillin or rifampicin was synergistically effective against MRSA (Yu *et al*., 2020). In another study, it was illustrated that rifampin potentiates the efficacy and synergizes with fusidic acid, tigecycline, against MRSA biofilm (Tang *et al*., 2013). A combination of tedizolid and rifampicin could suppress MRSA biofilm formation and deter emergence of rifampicin-resistance in MRSA (Gidari *et al*., 2020). A meta-analysis study indicated that the combination of daptomycin and cephalosporin could yield a beneficial outcome against MRSA (Wang *et al*., 2020). In another study, it was demonstrated that a combination of oritavancin and rifampin was effective against MRSA and this combination may be considered as a potential therapeutic option for mitigation of prosthetic joint infections (Yan *et al*., 2018).

1.8. Small Synthetic Molecules as Adjuvants in Combination Therapy Against MRSA

Despite the potential benefits, combination therapy with antibiotics have limitations as antagonism can result owing to drug interactions. Further, if a broad-spectrum

Table 1.2. Small synthetic molecules used in combination with antibiotics for mitigation of MRSA.

Sl. No.	Small Synthetic Molecule	Antibiotic in Combination	Reduction in MIC of Antibiotic	Reference
1.	D-Norvaline	Oxacillin	~ 82-fold	Lee *et al*., 2022
2.	Auranofin	Linezolid	4-8-fold	She *et al*., 2019
3.	Palmitic Acid and Span85	Oxacillin	~ 82-fold	Song *et al*., 2020
4.	Sanguisorbigenin	Linezolid Gentamicin Vancomycin Amikacin Amoxicillin Ceftazidime	4-16-fold	Wang *et al*., 2022
5.	Lipopeptide Surfactin	Platensimycin	4-fold	Xiong *et al*., 2022
6.	Enterocin	Kanamycin Erythroycin	8-fold 16-fold	Atya *et al*., 2016

antibiotic is used in combination; it is likely to favor growth of opportunistic pathogens such as *Clostridium difficile*. In addition, toxicity and cost-prohibitive therapy are significant roadblocks in leveraging the therapeutic potential of antibiotic combinations. In this context, combination of low molecular weight synthetic molecules with antibiotics offers an exciting prospect in the realm of medicinal chemistry and drug discovery as it opens up the untapped sphere of a plethora of rationally designed bioactive synthetic molecules. A good number of review articles provide a comprehensive analysis on the potential of small molecules as adjuvants in combination therapy directed against antibiotic-resistant pathogenic bacteria including MRSA (Namivandi-Zangeneh *et al*., 2021; Vermote and Van Calenbergh, 2017; Melander and Melander, 2017; Hawas *et al*., 2022; Cascioferro *et al*., 2021). Synthetic molecules can be rationally designed to breach the resistance in target cells and restore susceptibility of the pathogen to therapeutic antibiotics. To this end, some recent studies have indeed validated this premise and have demonstrated the use of various rationally designed small molecules as adjuvants for rendering an efficient combination therapy directed against MRSA (Namivandi-Zangeneh *et al*., 2021; Wang *et al*., 2022; Berndsen *et al*., 2022). Additional illustrative examples on the use of small molecules to potentiate therapeutic antibiotics against MRSA are depicted in Table 1.2.

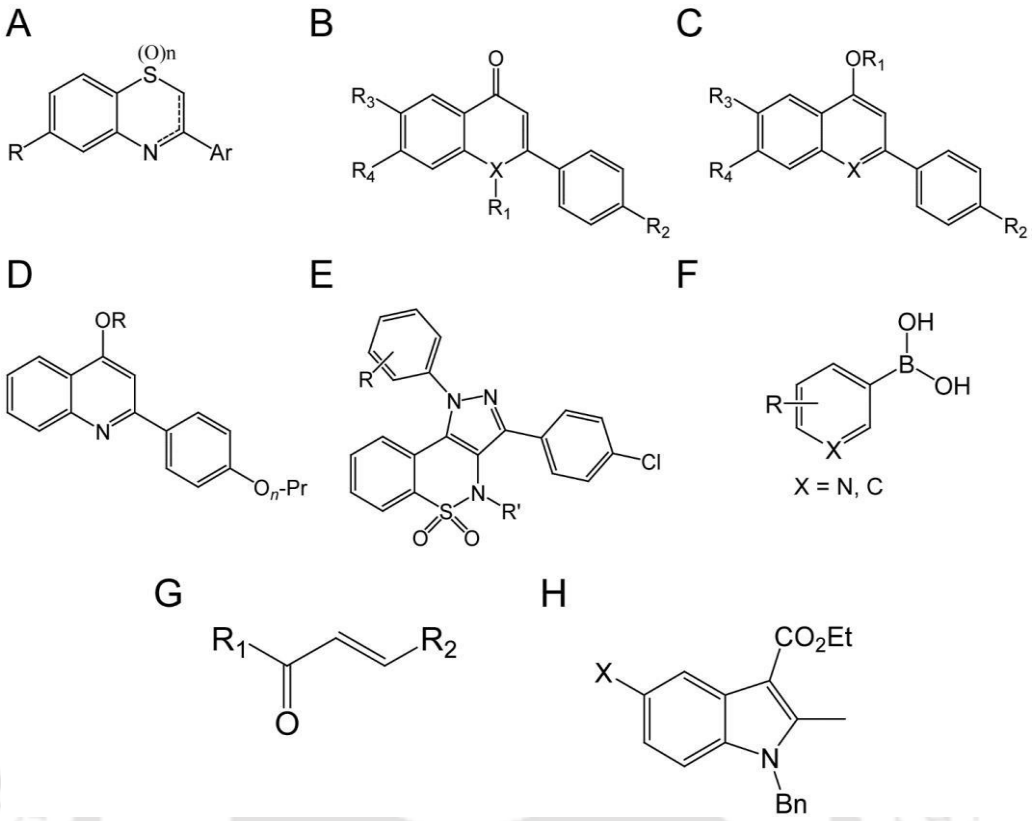

Figure 1.3. Molecular structure of representative efflux pump inhibitors. (A) Benzothiazine derivatives (Sabatini et al., *J. Med. Chem.*, **2008**, *51*, 4321-4330), (B-C) Quinolone and hydroxyquinoline derivatives (Sabatini et al., *J. Med. Chem.*, **2011**, *54*, 5722-5736), (D) Phenylquinoline derivatives (Sabatini et al., *J. Med. Chem.*, **2013**, *56*, 4975-4989), (E) Benzothiazine derivatives (Sabatini et al., *J. Med. Chem.*, **2012**, *55*, 3568-3572), (F) Pyridine and benzene boronic derivatives (Fontaine et al., *J. Med. Chem.*, **2014**, *57*, 2536-2548), (G) Substitute chalcone derivatives (Gaur et al., *RSC Adv.*, **2015**, *5*, 5830-5845), (H) Indole derivatives (Lepri et al., *J. Med. Chem.*, **2016**, *59*, 867-891).

1.9. Efflux Pump Inhibitors (EPIs) for Anti-MRSA Therapy

Efflux pump activity has been shown to be associated with resistance against biocides and therapeutic antibiotics in staphylococci (Li and Nikaido 2009; Jang 2016; Floyd *et al.*, 2010; Kaatz *et al.*, 2005). Hence, it is conceived that the efflux pump in *S. aureus* can be a rational drug target for effective anti-MRSA intervention. Previous studies have reported the potential of small synthetic molecules as EPI against *S. aureus* (Pieroni *et al.*, 2010; Sabatini *et al.*, 2011; Ganesan *et al.*, 2016).

Table 1.3. Representative EPIs used in combination with antibiotic to targetMRSA.

Inhibitor	Mode of Action	Antibiotic Substrate	Fold reduction in MIC of Antibiotic	Reference
Nerol derivatives	NorA Inhibition	Norfloxacin	3-fold	Coelho *et. al*., 2016
Benzochromene derivatives	NorA Inhibition	Ciprofloxacin	32-fold	Ganesan *et. al*., 2016
Benzothiazone derivatives	NorA Inhibition	Ciprofloxacin	16 – fold	Sabatini *et. al*., *J. Med. Chem*. 2008
Pyridine-3- Boronic compounds	NorA Inhibition	Ciprofloxacin	4-fold	Fontaine *et. al*., *J. Med. Chem*. 2014
Benzothiazine derivatives	NorA Inhibition	Ciprofloxacin	16-fold	Sabatini *et. al*., 2012
Pinostrobin	NorA Inhibition	Ciprofloxacin	128-fold	Lowrence *et.al*., 2015
Quinoline derivative	NorA inhibition	Ciprofloxacin	16-fold	Sabatini *et. al*., 2011
Dihydro-naphthalene derivatives	NorA inhibition	Ciprofloxacin	16-fold	Handzlik *et. al*., 2013
Indole derivatives	NorA inhibition	Ciprofloxacin	8-fold	Tambat *et. al*., 2019
Benzocyclohexane oxide derivatives	NorA inhibition	Norfloxacin	4-fold	Zhong *et. al*., 2016

Based on an extensive literature report, it is evident that EPIs are structurally diverse ranging from benzothiazine, quinoline, boronic, chalcone, indole and other derivatives (Sabatini *et al*., 2008; Sabatini *et al*., 2011; Sabatini *et al*., 2013; Sabatini, *et al*., 2012; Fontaine, *et al*., 2014; Gaur *et al*., 2015; Lepri *et al*., 2016). The general structure of these EPIs is depicted in Figure 1.3. The structural descriptors that account for the activity of EPIs is also known from previous studies. For instance, a medium molecular size, a noteworthy polar surface area, hydrophobicity and the presence of H-bond donor/acceptor groups are key attributes that define the activity of synthetic EPIs (Sabatini *et al*., 2011; Lepri *et al*., 2016; Brincat *et al*., 2012). A large number of reports highlight the structure-activity correlation of synthetic EPIs. For instance, the efflux pump inhibition activity and antibiotic-potentiating activity of celecoxib derivatives was

influenced by charge, electronegative functional group(s) and relative positioning of the functional groups on the aromatic core (Sabatini *et. al.*, 2012). In another study, it was shown that the EPI could be modulated by the nature of the chain (aromatic or aliphatic or inorganic or just H-atom) (Fontaine *et. al.*, 2014). EPIs can increase the sensitivity of the pathogen towards antibiotic(s) by facilitating cellular accumulation of drugs and thus provides a complimentary mechanism to suppress drug- resistance. A few illustrative examples of the antibiotic-potentiating activity of EPIs for anti-MRSA therapy is represented in Table 1.3.

1.10. Membrane-Targeting Compounds for Combating MRSA

Synthetic molecules that can target the membrane can be effective as antibacterials against antibiotic-resistant pathogens. Antibiotics perturb specific biochemical, physiological and synthesis processes in the target cells and are thus more likely to trigger resistance development. However, the likelihood of resistance development against membrane-targeting agents is comparatively less as it involves large-scale renovation of membrane, which is extremely challenging for the target bacteria (van Bambeke *et al*., 2008; Hurdle *et al*., 2011). As a prototype membrane-targeting agent, antimicrobial peptides (AMPs) are promising candidates (Wright, 2011; Wimley and Hristova, 2011). However, there are several bottlenecks in exploring their therapeutic potential owing to their high cost of manufacturing, poor pharmacokinetics, proteolytic inactivation and low *in vivo* efficacy (Chen *et al*., 2012; Marr *et al*., 2006). On the other hand, AMP-mimicking synthetic amphiphiles hold interesting prospect and numerous studies have indeed illustrated the membrane-targeting as well as potent antibacterial activity of these molecules (Kuroda and DeGrado 2005, Findlay *et al*., 2010; Hoque *et al*., 2012; Gokel and Negin 2012; Bera *et al*., 2010; Goswami *et al*., 2013; Thiyagarajan *et al*., 2014; Dey *et al*., 2018). It is also conceived that membrane-targeting molecules can be promising adjuvants in combination therapy against MRSA as they are likely to breach the permeability barrier associated with membranes and enhance antibiotic uptake. Several studies have validated this premise and have demonstrated that membrane-acting molecules indeed enhance the therapeutic efficacy of antibiotics in combination therapy (Thiyagarajan et al., 2017; Dey *et al*., 2018; Kim *et al*., 2018; Kang *et al*., 2021; Thappeta *et al.*, 2020; Xiong *et al*., 2022).

MOTIVATION AND OBJECTIVES OF THE PRESENT INVESTIGATION

भारतीय प्रौद्योगिकी संस्थान गुवाहाटी
Indian Institute of Technology Guwahati

MOTIVATION AND OBJECTIVES OF THE PRESENT INVESTIGATION

The origin of the present research investigation and the principal motivating factors stem from the following considerations:

1. The high prevalence of serious MRSA infections in the clinics and the restricted number of antibiotics that are active against MRSA underscores a pressing need for an effective therapeutic strategy against the pathogen. In this regard, combination therapy can be considered as a viable option as it is conceived that the synergy between drugs may enhance the overall bactericidal effect, reinstate susceptibility of the target cells and prevent the emergence of resistance during therapy.

2. Combinations of antibiotics may be a viable therapeutic option against MRSA. However, such a combination can be counterproductive as the interaction between antibiotics could lead to manifestation of antagonism and also trigger toxic side-effects. On the other hand, deployment of small synthetic molecules is an exciting prospect in the sphere of drug discovery. In particular, molecules that can breach the fundamental resistance mechanism and potentiate the bactericidal efficacy of a frontline antibiotic will provide significant therapeutic dividend.

3. In MRSA, efflux pumps are significantly implicated in conferring resistance against therapeutic antibiotics. Thus, development of small molecules as efflux pump inhibitor (EPI) and their use in combination with antibiotics can be a viable therapeutic approach.

4. The bacterial membrane is acknowledged as an Achilles heel and thus membrane-targeting synthetic antibacterials are likely to contravene the membrane-mediated resistance mechanism in MRSA and boost the uptake and bactericidal efficacy of a therapeutic antibiotic.

5. There is a considerable scope to adopt a rational design principle and generate small molecule adjuvants that display high solubility in biological fluids and efficient transit across membrane barriers. A fundamental understanding of the structure-activity relationship is likely to yield a broad structural guideline that can pave the way for developing effective adjuvants for combinatorial antibacterial therapy.

6. It is pertinent that the potential of synthetic EPIs and membrane-targeting antibacterial in combination therapy is validated through models, which can mimic clinical problems such as extracellular matrix, bone cell and orthopaedic implant-associated MRSA infection and also ascertain the toxic potential of the candidate molecules.

Objectives:

Based on the prospect of efflux pump inhibitors and membrane-acting antibacterials as adjuvants in combination therapy for mitigation of MRSA, the essential objectives of the Ph.D. thesis were as follows:

1. Evaluation of urea-based ligands as efflux pump inhibitor for countering ciprofloxacin resistance in MRSA.
2. Development of a urea-based ligand-loaded therapeutic nanocomposite for adjuvant-mediated anti-MRSA therapy.
3. Evaluation of bactericidal activity, membrane-directed activity and antibiofilm activity of quinoxaline-based ligands for targeting MRSA.
4. Assessment of the potential of quinoxaline-based ligand in combination therapy for mitigation of MRSA in an *in vitro* bone cell infection model.
5. Development of a quinoxaline-based ligand-loaded therapeutic nanocomposite for anti-MRSA therapy and alleviation of MRSA invasion in an orthopaedic implant.

भारतीय प्रौद्योगिकी संस्थान गुवाहाटी
Indian Institute of Technology Guwahati

Chapter 2

Potential of Urea-based Ligands as an Efflux Pump Inhibitor to Counter Ciprofloxacin Resistance in MRSA

This chapter describes the potential of a set of rationally designed urea-based synthetic ligands as an efflux pump inhibitor (EPI) against MRSA. The potential of C8, the most potent EPI, in rendering effective killing of MRSA in combination with ciprofloxacin is also presented in this chapter.

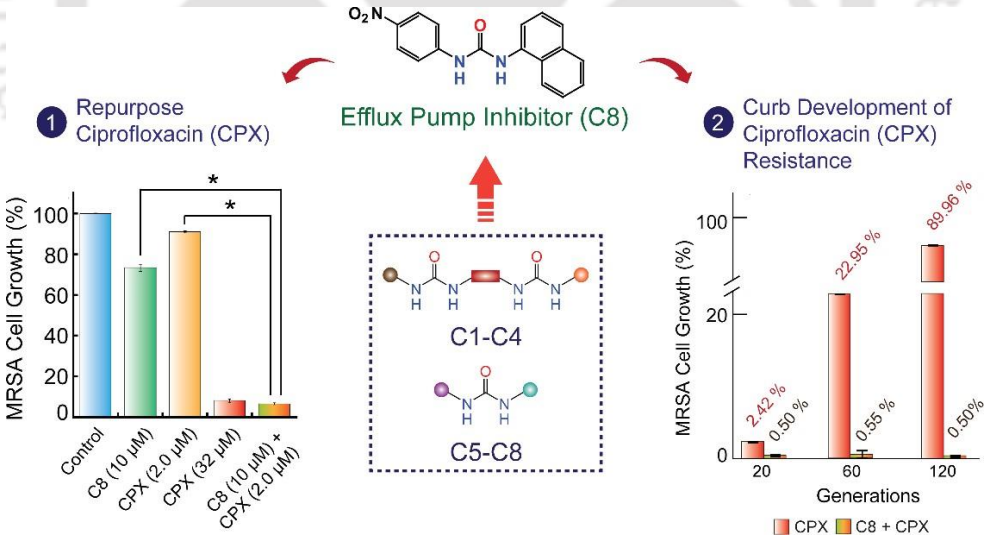

भारतीय प्रौद्योगिकी संस्थान गुवाहाटी
Indian Institute of Technology Guwahati

ABSTRACT

In this chapter, the potential of synthetic ligands (C1-C8) based on urea scaffold to inhibit the efflux pump in a clinical MRSA strain is presented. Initial screening experiments with varying concentrations of the ligand (5.0 µM - 80 µM) revealed that the ligands did not display any significant antibacterial activity against the MRSA strain *S. aureus* 4s. The efflux pump in MRSA was inhibited by ligands C1, C5, C6 and C8 as ascertained by an EtBr efflux assay. On a comparative basis, C8 displayed was most potent in terms of efflux inhibition in the MRSA strain (~95 %) and was even superior than reserpine, a known efflux pump inhibitor (EPI). Ligands C1 and C8 also supported considerable cellular accrual of EtBr. The potent EPI activity of C8 was garnered to augment ciprofloxacin (CPX) accrual in MRSA, wherein the CPX level was significantly higher (~232 nM/mg cell) as compared to MRSA subjected to treatment with CPX (~148 nM/mg cell). In MRSA cells treated with C8, there was a remarkable downregulation of *norA* gene encoding a major efflux pump protein implicated in efflux of CPX in MRSA. Interestingly, there was a 16 × reduction in the MIC of CPX when MRSA cells were treated with 10 µM C8 and 2.0 µM CPX. Further, the combinatorial treatment regimen could significantly hinder MRSA cell growth (~6.0 % growth) as compared to the growth evidenced in cells treated with either C8 or CPX. Significant annihilation of MRSA in the combination treatment was also corroborated by FESEM. An *in vitro* resistance study over multiple generations indicated that MRSA cell growth was arrested only till 40 generations, when grown in presence of 32 µM CPX. However, in presence of 10 µM C8 and 2.0 µM CPX, MRSA cell growth was remarkably subdued upto 120 generations.

2.1. Introduction

Methicillin-resistant *Staphylococcus aureus* (MRSA) is a human pathogen, which is often associated with nosocomial and community-associated infections (Lee *et al*., 2018; Turner *et al*., 2019; Chambers and Deleo, 2010). The current therapeutic antibiotics deployed for treatment of severe MRSA infections include vancomycin, daptomycin or linezolid (Lee *et al*., 2018; Liu *et al*., 2011). Besides, other antibiotics which are in the horizon for therapeutic intervention against MRSA are ceftaroline, telavancin, delafloxacin and others (Lee *et al*., 2018). However, with the increasing prevalence of resistance development against a key antibiotic like vancomycin in MRSA (Weigel *et al*., 2003; Rossi *et al*., 2014), there is a critical need for an alternative and effective therapeutic intervention against MRSA. To address this concern, the concept of combination therapy against MRSA has emerged as a viable option as it is conceived that they can foster synergy to enhance the bactericidal efficacy, restore susceptibility of the pathogen and also hinder resistance development during the therapeutic window (Fischbach, 2011; Worthington and Melander, 2013; Thangamani *et al*., 2016; Davis, *et al*., 2015). To this end, mitigation of *S. aureus*-mediated infection has been documented in case of treatment with gentamicin in combination with antibiotics like daptomycin and vancomycin (Tsuji *et al*., 2005; Houlihan, *et al*., 1997). The therapeutic prospect of treatment with cefoxitin and β-lactams has also been highlighted (Banerjee *et al*., 2013). It can be conjectured that the use of different antibiotics in combination against MRSA would not only enhance the bactericidal efficacy, but would also reduce the concentration of the antibiotic required for killing the pathogen. This outcome is particularly beneficial for treatment using certain class of antibiotics such as aminoglycoside, fluoroquinolone and glycopeptides, as these antibiotics bear toxic implications on the host (Cosgrove *et al*., 2009; Owens *et al*., 2005; Finch and Eliopoulos, 2005). In a combination therapy regimen, a biocompatible synthetic warhead capable of countering the innate antibiotic resistance in MRSA and reestablish vulnerability of the pathogen against the antibiotic can hold interesting prospect. Efflux pumps contribute significantly towards development of resistance against therapeutic agents in staphylococci (Li and Nikaido, 2009; Costa, *et al*., 2015; Jang, 2016). Hence, efflux pumps are potential targets and deployment of an efflux pump inhibitor (EPI) can be considered as a promising therapeutic approach to curb MRSA infections.

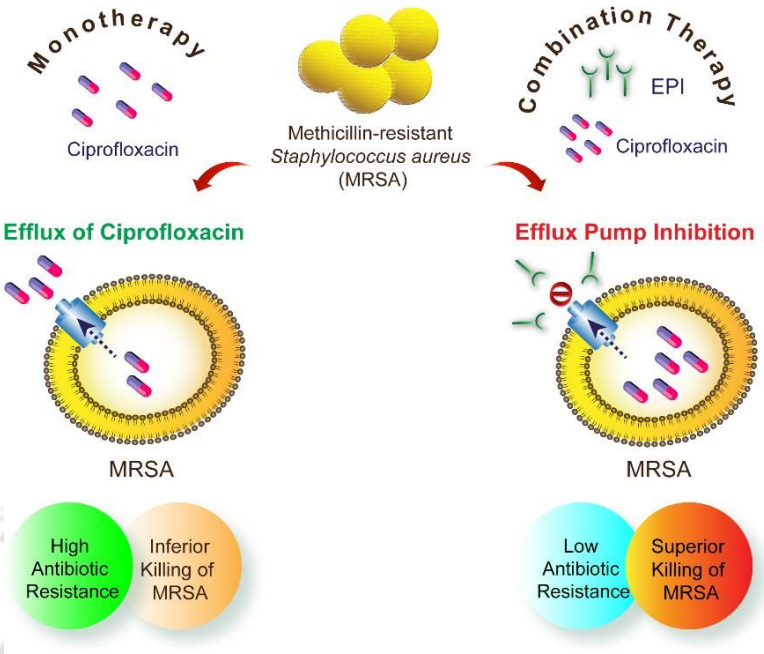

Scheme 2.1. A schematic illustration of the potential outcome of using synthetic efflux pump inhibitor (EPI) to hinder ciprofloxacin resistance and mediate effective annihilation of MRSA.

In MRSA, an efflux pump associated with the export of ciprofloxacin (CPX) is the NorA protein (Jang, 2016). Studies have demonstrated that NorA is indeed involved in the emergence of resistance development against CPX in *S. aureus* (Papkou *et al*., 2020). Hence, it is anticipated that targeting MRSA with CPX alone is likely to trigger resistance development, which can lead to ineffective elimination of MRSA (Scheme 2.1). Conversely, deployment of a synthetic EPI and CPX in tandem is likely to counter the resistance through efflux pump inhibition, which would subsequently lead to higher killing of MRSA by CPX (Scheme 2.1). This principle has indeed been documented in previous studies (Sabatini *et al*., 2008; Sabatini *et al*., 2011; Sabatini *et al*., 2013; Radix *et al*., 2018; Sundaramoorthy *et al*., 2018).

Previous studies have highlighted the structure features of synthetic EPIs (Sabatini *et al*., 2008; Sabatini *et al*., 2011; Sabatini *et al*., 2013; Sabatini *et al*., 2012; Fontaine *et al*., 2014; Gaur *et al*., 2015; Lepri *et al*., 2016). Based on structure-activity relationship emerging from these studies, it is apparent that a medium molecular size, a prominent polar surface area, hydrophobicity and the presence of H-bond donor/acceptor groups are critical EPI activity (Sabatini *et al*., 201; Lepri *et al*., 2016; Brincat *et al*., 2012). For potential therapeutic applications against MRSA, non-bactericidal EPIs will be desirable as resistance against such molecules is likely to be lower. On the basis of this premise, the current investigation explores the efficacy of urea-based ligands

(C1-C8) as an EPI. The investigation demonstrates that the ligand C8 displayed the highest efficacy as an EPI and could downregulate expression of *norA*gene transcript in MRSA. The study also reveals that C8 heightened the potency of CPX and curbed emergence of CPX-resistance in MRSA across several generations.

2.2. Materials and Methods

2.2.1. Compounds and Reagents

Ethidium bromide (EtBr), ciprofloxacin and reserpine, were procured from Sigma-Aldrich (USA). Brain-Heart Infusion (BHI) broth was procured from HiMedia, Mumbai, India. Dimethyl sulfoxide (DMSO) was obtained from Merck, India.

2.2.2. MRSA Strain and Culture Condition

Staphylococcus aureus 4s, a clinical MRSA strain was used in the present investigation. The strain was kindly provided by Prof. Benu Dhawan, All India Institute of Medical Sciences (AIIMS), New Delhi and Prof. Kasturi Mukhopadhyay, Jawaharlal Nehru University (JNU), New Delhi. *S. aureus* 4s was grown in BHI broth at 37 °C and 180 rpm for 12 h. The MRSA strain was revived from frozen stock culture and subcultured prior to the experiments.

2.2.3. Synthetic Ligands

Synthesis of the ligands (C1-C8) was accomplished by standard procedures reported previously (Manna *et al*., 2016a; Manna *et al*., 2016b; Jose *et al*., 2007; Casula *et al*., 2017). Stock solution for each ligand (10 mg/mL) was prepared in DMSO.

2.2.4. Anti-MRSA Activity of Urea-based Ligands and Ciprofloxacin (CPX)

S. aureus 4s was inoculated (1% inoculum) in 96 well microtiter plates having BHI medium and grown overnight at 37 °C and 180 rpm in separate sets in presence of varying concentrations of the ligands C1-C8 (5.0 µM - 80 µM each) or CPX (1.0 µM - 512 µM). In a separate control experiment, the target cells were grown in the absence of the ligands or CPX. Growth of the MRSA strain was monitored by measuring absorbance at 600 nm in a microtiter plate reader (Infinite M200, TECAN, Switzerland). The minimum inhibitory concentration (MIC) of CPX was determined as the lowest antibiotic concentration, which resulted in A_{600} reading of <0.1. The antibacterial activity of the

ligands and CPX against the MRSA strain was calculated from three independent experiments, each having three replicas. Data analysis and calculation of standard deviation was performed with Microsoft Excel 2010 (Microsoft Corporation, USA).

2.2.5. Efflux Pump Inhibition Assay

In order to ascertain the EPI activity of the ligands, a solution-based assay was performed using a previously reported method (Thiyagarajan *et al*., 2017). The assay was performed with *S. aureus* 4s cells incubated with EtBr (5.0 µg/mL) for 1 h at 37 ˚C in separate sets with C1-C8 (5.0, 10 and 40 µM each) or the standard EPI reserpine (40 µM). Following incubation, excess EtBr was removed by centrifugation at 10000 rpm for 3.0 min and the cells were washed twice with sterile PBS. Subsequently, the cells were resuspended in sterile PBS containing 0.4 % glucose and the relative decrease in fluorescent intensity of EtBr was ascertained periodically over a period of 10 min by measuring the fluorescence emission between 530-720 nm at an excitation wavelength of 515 nm (using FluoroMax-4, HORIBA). Fluorescence emission intensity for control cells (without treatment with glucose) was also recorded. All the experiments were performed in triplicates. Data analysis and calculation of standard deviation was performed with Microsoft Excel 2010 (Microsoft Corporation, USA). The relative end-point fluorescence values were used for one-way analysis of variance (ANOVA). Quantitative estimation of efflux activity (expressed as %) was ascertained as described in a previous method (Lepri *et al*., 2016). Experiments were also performed to estimate the accumulation of EtBr in MRSA in presence of ligands or the standard EPI reserpine as described previously (Thiyagarajan *et al*., 2017).

2.2.6. CPX Accumulation Assay

Accumulation of CPX in *S. aureus* 4s cells incubated with C8 (10 µM) was measured by following a previously described method (Thiyagarajan *et al*., 2017). Overnight grown cells of *S. aureus* 4s were harvested by centrifugation at 8000 rpm for 3.0 min. The cell pellet was washed twice with sterile 50 mM sodium phosphate buffer (pH 7.0) and resuspended in the same buffer (A_{600} = 1.0) for 10 min at 37 ˚C. In separate sets, the cell suspension was incubated with 8.0 µM CPX (final concentration) and 0.5 mL sample was removed from each tube intermittently over a period of 9.0 min. The cells were then incubated in separate sets with either C8 (10 µM) or reserpine (40 µM) and samples were

collected every 3.0 min from the tubes over a period of 12 min. To each sample, 1.0 mL of ice-cold 50 mM sodium phosphate buffer (pH 7.0) was added and the tubes were incubated in ice (4 $^{\circ}$C) to stop the reaction. The samples were then centrifuged at 7000 rpm for 5.0 min and washed once with 1.0 mL ice cold 50 mM sodium phosphate buffer (pH 7.0). The cell pellet was resuspended in 0.1 M Glycine-HCl buffer (pH 3.0) and incubated for 15 h in 4 $^{\circ}$C. Subsequently, the samples were centrifuged at 8000 rpm for 5.0 min and the fluorescence emission of the supernatant was measured at 447 nm by exciting the sample at 279 nm (using FluoroMax-4, HORIBA). The concentration of CPX present in the supernatant was determined from a previously generated calibration plot of CPX (10 nM to 2000 nM) and expressed as nanomolar of ciprofloxacin per milligram (dry weight) of bacterial cells. All the experiments were performed in triplicates. Data analysis and calculation of standard deviation was performed with Microsoft Excel 2010 (Microsoft Corporation, USA). A schematic representation of the CPX accumulation assay in shown in Figure 2.1.

2.2.7. Effect of C8 on norA Gene Expression in MRSA

S. aureus 4s cells (~ 10^6 CFU/mL) were grown in separate sets at 37 ºC and 180 rpm for 24 h in BHI media in presence of C8 (10 µM, 25 µM and 50 µM). Total RNA was isolated from the grown cells using TRIzol Max Bacterial RNA Isolation Kit (Invitrogen, USA). The RNA yield was estimated by measuring the absorbance (IMPLEN NanoPhotometer NP80) and 200 ng of RNA from each sample was used in quantitative real-time PCR (qRT-PCR). Gene-specific primers were designed for *16S rRNA* and *norA* genes using Primer3 (v. 0.4.0). The sequence of the primers is represented in Table 2.1. qRT-PCR was performed for each sample by using a SYBR 1-STEP qRT-PCR kit (Thermo, USA) on a 36-well rotor QIAGEN RotorGene Q qRT-PCR machine. Reverse transcription was performed at 50 $^{\circ}$C for 3 min. Subsequently, PCR was performed under the following conditions: (1) initial hold at 94 $^{\circ}$C for 2 min, (2) cycling step encompassing denaturation 94 $^{\circ}$C for 30 sec, annealing at 55 $^{\circ}$C for 1.0 min, extension at 72 $^{\circ}$C for 1.0 min for a total of 45 cycles. qRT-PCR data was analyzed by LinRegPCR (2014.x) software and the cycle threshold (C_T) values were calculated following baseline correction. The fold change in *norA* gene expression was

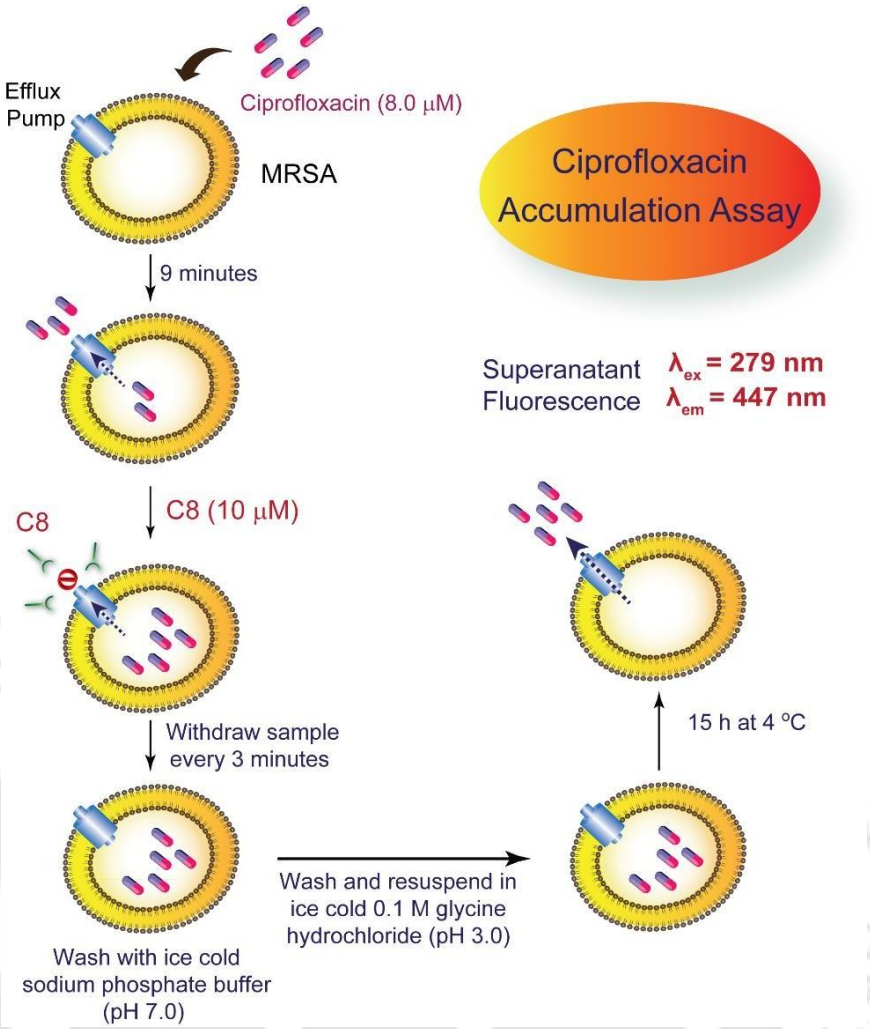

Figure 2.1. Cartoon illustrating the protocol for ciprofloxacin accumulation assay conducted with cells of the MRSA strain *S. aureus* 4s in presence of the urea-based ligand C8.

Table 2.1. Sequence of primers used in quantitative real-time PCR-based gene expression studies.

Sl. No.	Target Gene	Oligo Sequence (5' to 3')	Amplicon size
1.	*16S rRNA*	Forward: GAAAGCCACGGCTAACTACG Reverse: CATTTCACCGCTACACATGG	202 bp
2.	*norA*	Forward: ATCGGTTTAGTAATACCAGTCTTGC Reverse: GCGATATAATCATTTGAGATAACGC	100 bp

determined by the $\Delta\Delta C_T$ method (Livak *et al*., 2001). ANOVA was conducted for fold change in *norA* gene expression (Sigma Plot version 11.0).

2.2.8. Effect of Combination Treatment of C8 and CPX on MRSA

S. aureus 4s cells (~10^6 CFU suspended in BHI) were grown in BHI medium in a sterile 96-well microtiter plate and subjected to a checkerboard assay having varying concentrations of C8 (5.0 µM, 10 µM, 20 µM and 40 µM) and CPX (2.0 µM - 32 µM). During the assay, MRSA cells were incubated at 37 °C and 180 rpm for 12 h. Growth of cells following treatment was estimated by measuring absorbance at 600 nm (Infinite M200, TECAN, Switzerland). In a separate set of experiment, the growth of MRSA cells was determined in presence of varying levels of CPX or C8. For the combination treatment sets, the reduction in the MIC of CPX was ascertained.

The combined effect of C8 and CPX on MRSA cells was also ascertained by FESEM analysis. Herein, untreated as well as treated MRSA cells were collected by centrifugation, washed with sterile PBS and sterile MilliQ water and finally resuspended in sterile MilliQ water. A 10 µL aliquot of each sample was spotted on separate aluminium foil (1.0 cm x 1.0 cm square) and air dried overnight in a laminar hood. The samples were then mounted on a carbon tape covered metal stub and gold (Au) coating was accomplished twice for 180 seconds each. Finally, the samples were analyzed in a field emission scanning electron microscope (Zeiss Sigma, USA) at 3.0-5.0 kV and their images were recorded.

2.2.9. Estimation of Doubling Time of MRSA

S. aureus 4s cells (~10^6 CFU/mL) were inoculated in BHI medium and incubated at 37 °C and 180 rpm. At intermittent time intervals (0 h, 0.25 h, 0.5 h, 1 h, 1.5 h, 2 h, 2.5 h, 3 h, 3.5 h, 4 h and 4.5 h) the absorbance of the cultures was measured at 600 nm in a spectrophotometer (Lambda 25, Perkin-Elmer). The absorbance values for the samples were used to construct a growth curve (A_{600} versus time). The specific growth rate (μ) of the cells was determined from the slope of the curve (Zwietering *et al*., 1990) and used to estimate the doubling time (t_d) for MRSA cells (Doran, 2013). The number of generations for *S. aureus* 4s cells grown in BHI medium was calculated from the doubling time and total time of cell growth for each treatment cycle.

2.2.10. In Vitro Resistance Development in MRSA against CPX

S. aureus 4s cells were grown in 3.0 mL BHI media (1% inoculum) in separate test tubes containing (a) 10 µM C8, (b) 32 µM CPX and (c) 10 µM C8 and 2.0 µM CPX

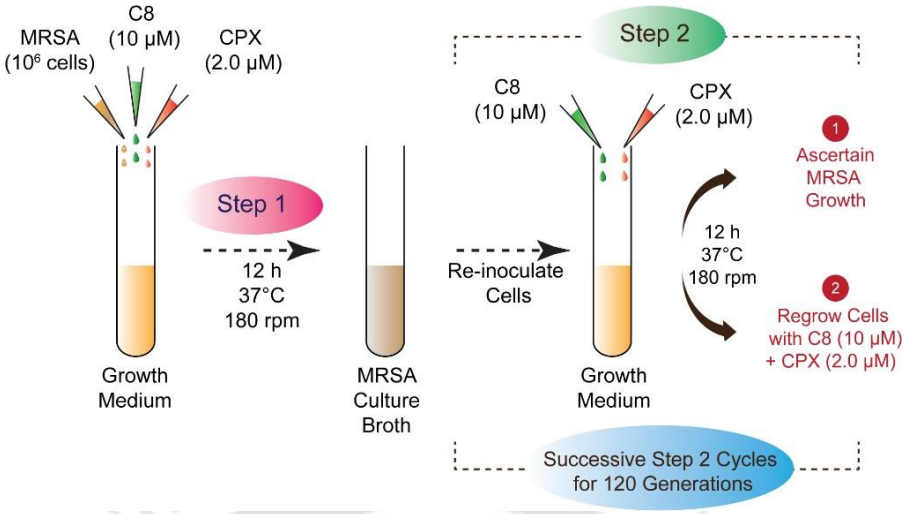

Figure 2.2. Protocol to ascertain *in vitro* development of ciprofloxacin resistance in *S. aureus* 4s in presence of the urea-based ligand C8.

Subsequently, the growth of MRSA cells was monitored by recording the absorbance at 600 nm (Lambda 25, Perkin-Elmer). From the treatment set, a 30 μL aliquot of MRSA cell suspension was again grown in separate test tubes and subjected to a similar treatment cycle, which was repeated independently to achieve 120 generations of growth. A schematic of the protocol to ascertain CPX resistance in MRSA against C8 is indicated in Figure 2.2.

2.3. Results and Discussion

2.3.1. Design Rational of Ligands

Based on earlier studies, that articulated the structural determinants of effective EPIs (Sabatini *et al*., 2011; Lepri *et al*., 2016; Brincat *et al*., 2012), in the present study ligands bearing urea as the main scaffold were synthesized (Figure 2.3) by standard methods (Manna *et al*., 2016a; Manna *et al*., 2016b; Jose *et al*., 2007; Casula *et al*., 2017). Notably, the central urea moiety can form H-bond mediated assemblies. Ligands C1-C4 bear two urea units as against one in C5-C8 and hence are more likely to self-assemble. Further, ligands C1-C4 are more hydrophilic. Further, the polarity of C8 is higher with the nitro group present in the para position and the hydrophobicity of C8 is also higher than C6. Thus, it would be interesting to compare how these subtle differences in structure, hydrophobicity and polarity amongst the ligands impart an effect on efflux pump inhibition.

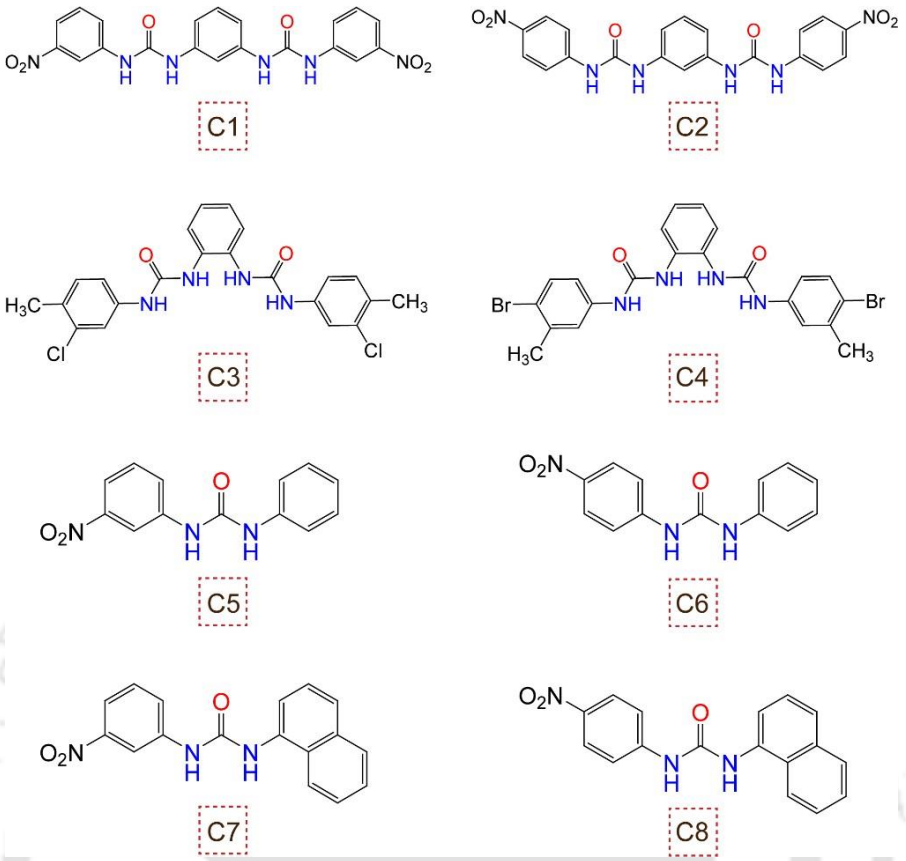

Figure 2.3. Molecular structure of urea-based synthetic ligands (C1-C8).

The characterization spectra for ligands C1-C8 conformed with the data reported in previous publications (Manna *et al*., 2016a; Manna *et al*., 2016b; Jose *et al*., 2007; Casula *et al*., 2017). Hence, the identity, structure and purity of the compounds was assured prior to initiating the biological studies.

2.3.2. Bactericidal Activity of Ligands Against MRSA

The antagonistic activity of ligands C1-C8 against *S. aureus* 4s was determined prior to ascertaining their potential to inhibit efflux pump. It was conjectured that non-bactericidal EPIs would bear significant therapeutic implications as the possibility of developing resistance against such ligands is likely to be reduced. The essential observation from the antibacterial assay was that none of the ligands exhibited any significant antibacterial activity against the MRSA strain (Figure 2.4). Further, it was observed that ligands C1, C2, C3 and C4 could inhibit growth of MRSA cell more effectively at lower concentrations (Figure 2.4). Self-assembly of ligands C1-C4 in solution is more likely due to the presence of two urea units as against a single urea group

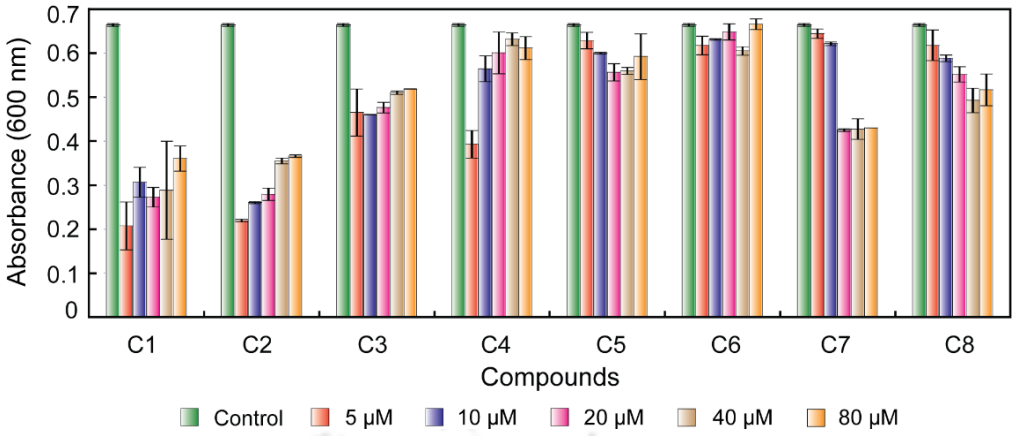

Figure 2.4. Bactericidal activity of urea-based ligands (C1-C8) against the MRSA strain *S. aureus* 4s.

in C5-C8 (Figure 2.3). Besides, this phenomenon of self-assembly is likely to manifest even more at higher concentrations of the ligands C1-C4. Perhaps, the facile self-assembly of ligands C1-C4 particularly at higher concentrations likely hinders their bactericidal activity.

2.3.3. Effect of Urea-based Ligands on Efflux Pump in MRSA

The potential of the ligands C1-C8 to inhibit efflux pump in *S. aureus* 4s was determined by a standard efflux assay (Viveiros *et al*., 2008). According to the assay principle, it was anticipated that in presence of glucose, efflux of EtBr would ensue and efflux pump inhibition by the ligands can be verified by recording high EtBr-associated fluorescence in MRSA (Figure 2.5A). In the EtBr efflux assay, MRSA cells displayed copious efflux of EtBr in presence of glucose as captured in the rapid decline in the emission of the dye over a period of 10 mins (Figure 2.5B). However, for the control sample (without glucose) as well for cells treated with reserpine, a standard EPI, no significant EtBr efflux activity was manifested. This indicated that the tested MRSA strain *S. aureus* 4s did display efflux pump activity (Figure 2.5B). At equimolar concentration (10 µM), ligands C1, C5, C6 and C8 rendered efflux pump inhibition, (Figure 2.5B), with ligand C8 being most potent and superior to reserpine (Figure A2.1 in Appendix, Table 2.2). Further, quantitative analysis revealed that the magnitude of efflux pump inhibition rendered by C1, C5, C6 and C8 in the tested MRSA strain was ~ 66 %, ~ 34 %, ~ 46 % and ~95 %, respectively. The comparatively higher efflux pump inhibition observed with C8 was also evident when the ligands were used at a

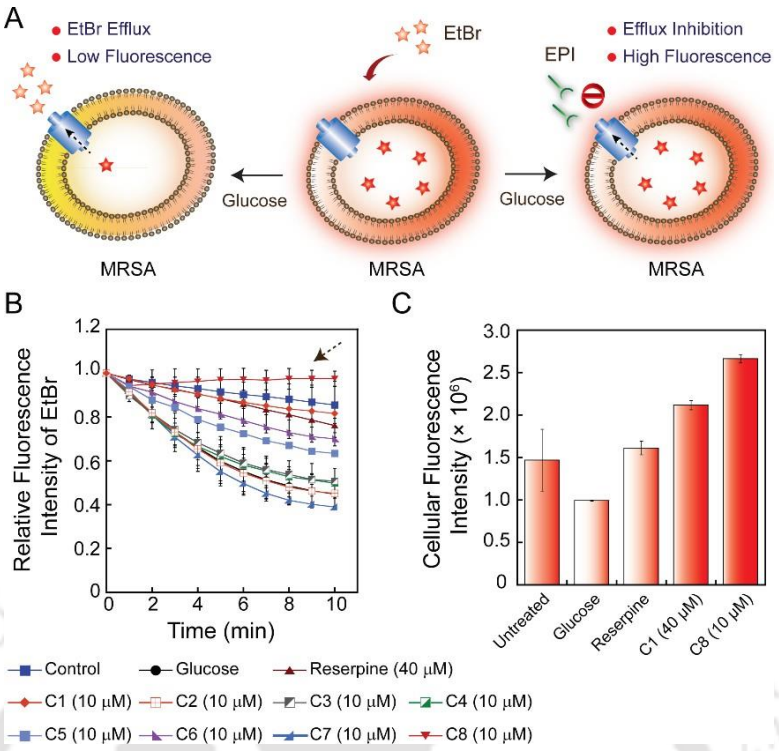

Figure 2.5. (A) Schematic representation of the principle of EtBr-based efflux pump assay. (B) Effect of urea-based ligands on EtBr efflux in *S. aureus* 4s cells. The trace obtained with C8 is indicated by an arrow. (C) EtBr fluorescence associated with *S. aureus* 4s cells treated with C1 and C8. For both the assays in (B) and (C), reserpine (40 μM) was used as positive control.

Table 2.2. Analysis of relative end-point fluorescence and inhibition of EtBr efflux activity in *S. aureus* 4s cells treated with equimolar concentration of urea-based ligands.

Sl. No.	Statistical Analysis for Relative End-Point Fluorescence		Concentration of Ligands in EtBr Efflux Assay
	Comparison Group	Significant Difference*	
1.	C8 versus Control (+ glucose)	Yes	10 μM
2.	C8 versus C2	Yes	
3.	C8 versus C3	Yes	
4.	C8 versus C4	Yes	
5.	C8 versus C5	Yes	
6.	C8 versus C6	Yes	
7.	C8 versus C7	Yes	

* Significant difference implies p value < 0.001 in analysis of variance (ANOVA) followed by all pair wise multiple comparisons (Holm-Sidak method) of relative end-point fluorescence measured in EtBr efflux assay.

concentration of 5.0 μM and 40 μM each (Figure A2.2 in Appendix). Notably, the relative fluorescence intensity of EtBr was nominally less in presence of 40 μM C8 as

compared to the intensity obtained with 5.0 µM of C8 (Figure A2.2 in Appendix). Possibly, at higher ligand concentration, self-assembly of the ligand in aqueous medium is likely, which may in turn reduce the local concentration of C8. This may account for the lesser EtBr-associated fluorescence intensity at 40 µM C8 in the efflux assay (Figure A2.2 in Appendix).

Further, *S. aureus* 4s cells displayed significant accumulation of EtBr when subjected to treatment with the ligands (Figure 2.5C). Herein, although the concentration of C1 (40 µM) was higher than C8 (10 µM), EtBr fluorescence was higher in case of C8 (Figure 2.5C). This observation again suggested that C8 was most effective as an EPI. It was also noted that EtBr accumulation was significantly higher in MRSA cells treated with C8 as against cells treated with reserpine (Table A2.1 in Appendix). Based on the results emerging from the EtBr-efflux and accumulation assays, C8 was most effective as an EPI. When compared with C5-C8, the ligands C1-C4 possess two urea units each and thus can readily self-assemble in solution. Consequently, interaction of the ligands with the target efflux pump may be hindered resulting in a decrease in their efficacy as an EPI. It may be noted that C8 bears an electron-withdrawing nitro group, is more hydrophobic than C5 and C6 and is more polar than C7. Collectively these traits may account for its higher potency as an EPI, as substantiated by analogous features described in other EPIs (Sabatini *et al*., 2011; Sabatini *et al*., 2012; Lepri *et al*., 2016; Brincat *et al*., 2012).

2.3.4. Effect of C8 on CPX Accumulation and norA Gene Expression in MRSA

On the basis of a fluorescence-based assay (Giraud *et al*., 2000) it was observed that in cells treated with CPX (control sample) there was a steady increase in the accumulation of CPX, which attained a saturation value of ~140 nM/mg of cell, after an incubation period of 9.0 min (Figure 2.6A). Notably, upon subsequent addition of 10 µM C8, there was a prominent increase in CPX accumulation in MRSA (~232 nM/mg of cell) after a total incubation period of 21 min. The level of CPX accumulated in C8-treated cells was distinctly higher than in MRSA treated with CPX only (~148 nM/mg of cell) after a total incubation period of 21 min (Figure 2.6A). Collectively, these results clearly suggested that C8 hindered the efflux phenomenon and thereby favored CPX accrual in MRSA cells.

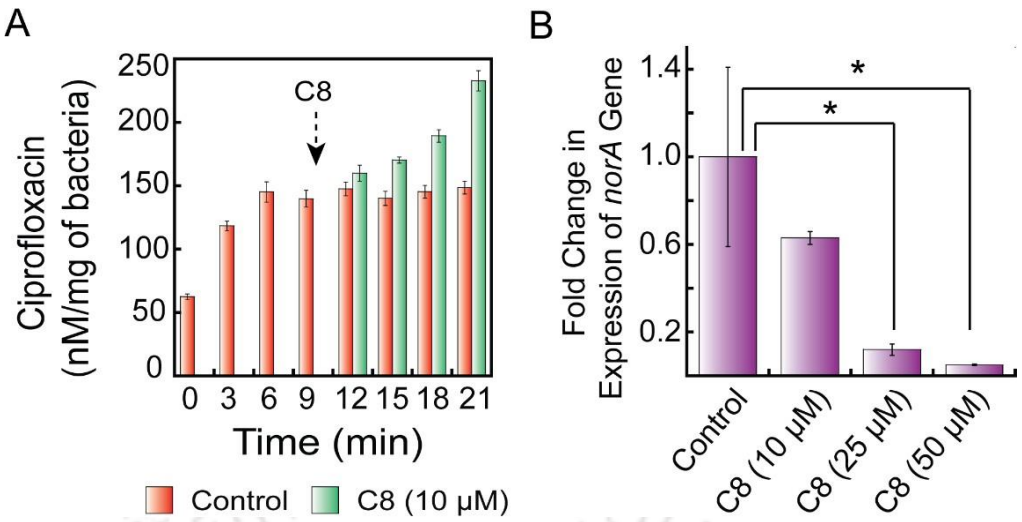

Figure 2.6. (A) Determination of the level of accumulation of ciprofloxacin (CPX) in *S. aureus* 4s cells treated with 10 µM C8. (B) Effect of C8 on *norA* gene expression in *S. aureus* 4s cells. * indicates *p* value < 0.001 in one-way ANOVA.

Manifestation of efflux pump activity in *S. aureus* 4s (Figure 2.5B-2.5C) suggested the presence of NorA protein, given that in clinical MRSA strains NorA is associated with efflux of EtBr and CPX (Li and Nikaido 2009; Jang, 2016). To this end, the presence of *norA* gene in *S. aureus* 4s strain was indeed observed as PCR revealed the presence of a gene specific amplicon having an expected size of ~ 100 bp in the MRSA strain (Figure A2.3 in Appendix). Interestingly, qRT-PCR based experiments indicated a prominent reduction in *norA* gene expression level (~0.63-fold) in *S. aureus* 4s cells treated with 10 µM C8 as against untreated cells (Figure 2.6B). In the presence of 25 µM and 50 µM C8, *norA* gene expression levels in MRSA was remarkably suppressed, with the fold-change in gene expression levels amounting to ~0.12 and ~0.03, respectively (Figure 2.6B). The significant suppression of *norA* gene expression in MRSA by C8 may hold potential therapeutic implications.

2.3.5. Effect of Combinatorial Treatment of C8 and CPX on MRSA

The MIC of CPX against *S. aureus* 4s was measured as 32 µM (10.6 µg/mL), akin to the reported MIC in a previous study (Thiyagarajan *et al.*, 2017) A checkerboard assay in the combinatorial treatment experiments indicated that the MIC of CPX was reduced with an increase in the concentration of C8 (Table 2.3). Notably, the MIC of CPX against the MRSA strain was reduced to 4.0 µM in combination with 5.0 µM, 20 µM and 40 µM C8 (Table 2.3). It may be mentioned here that in the presence of 10 µM C8,

Table 2.3. Absorbance values (A_{600} ± standard deviation) obtained in the checkerboard assay to ascertain the combined effect of C8 and ciprofloxacin on *S. aureus* 4s cells.

C8 (µM)	Concentration of Ciprofloxacin (µM)				
	2.0	**4.0**	**8.0**	**16**	**32**
0	0.651 ± 0.085	0.750 ± 0.025	0.696 ± 0.029	0.560 ± 0.033	0.024 ± 0.022*****
5.0	0.165 ± 0.029	0.036 ± 0.023*****	0.024 ± 0.021	0.024 ± 0.020	0.026 ± 0.019
10	0.070 ± 0.041*****	0.052 ± 0.025	0.026 ± 0.023	0.040 ± 0.020	0.045 ± 0.030
20	0.204 ± 0.022	0.043 ± 0.022*****	0.025 ± 0.022	0.044 ± 0.021	0.048 ± 0.033
40	0.230 ± 0.127	0.061 ± 0.011*****	0.044 ± 0.014	0.062 ± 0.018	0.052 ± 0.023

* Indicates minimum inhibitory concentration (MIC) of ciprofloxacin (CPX) obtained in the checkerboard assay. MIC of CPX was assigned as the lowest concentration of the antibiotic, which resulted in A_{600} value of <0.1 in the checkerboard assay.

the MIC of CPX was 2.0 µM and reduced by 16-fold (Table 2.3). With regard to decrease in the MIC of CPX in presence of C8, a dose-response relationship was evident in presence of 5.0 µM and 10 µM C8 (Table 2.3). However, this dose-response relationship could not be observed at 20 µM and 40 µM of C8 (Table 2.3). At higher concentrations, C8 is likely to self-assemble in aqueous medium, leading to a decrease in the effective concentration of the ligand. Consequently, the tandem effect in presence of 20 µM and 40 µM C8 was not as significant as with 10 µM C8 and a dose-response effect was not captured. An analogous phenomenon was also noted in EtBr efflux assay, wherein inhibition of EtBr efflux was less in presence of 40 µM C8 as compared to that observed in presence of 5.0 µM C8 (Figure A2.2 in Appendix). It is also probable that C8 at higher concentrations (20 µM and 40 µM) can undergo self-assembly and CPX may interact with the assembly thereof, leading to a decrease in the effective concentration and potency of CPX against MRSA during combination treatment.

In the combinatorial treatment regimen, C8 (10 µM) was essentially non-bactericidal as considerable growth of MRSA cells could be observed (~73% growth) (Figure 2.7A). Cell growth was robust when MRSA cells were grown in presence of 2.0 µM CPX (~91% growth) (Figure 2.7A). Interestingly, in presence of 10 µM C8 and 2.0 µM CPX, growth of MRSA was remarkably suppressed (~6.0 % growth) (Figure 2.7A). The magnitude of inhibition of MRSA observed in presence of 10 µM C8 and 2.0 µM CPX was on par with 32 µM CPX alone (~8.0 % growth). FESEM analysis

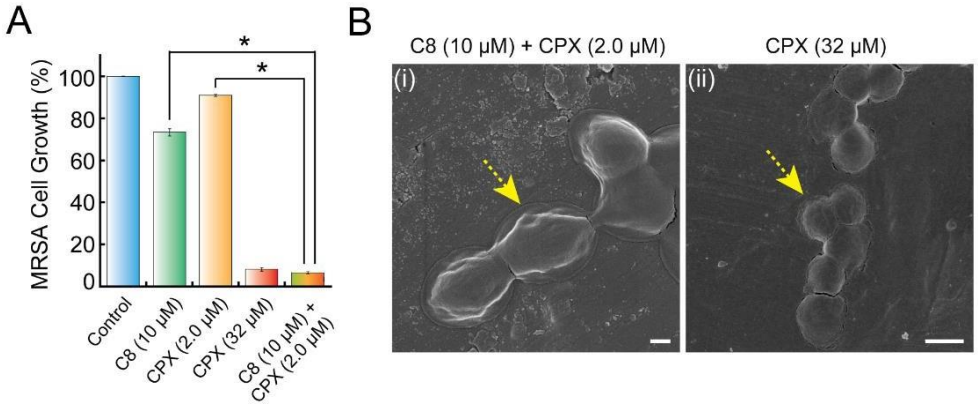

Figure 2.7. (A) Growth of *S. aureus* 4s cells upon treatment with C8 and CPX. * indicates *p* value < 0.001 in one-way ANOVA. (B) FESEM-based images of *S. aureus* 4s cells treated with (i) C8 and CPX and (ii) CPX alone. Arrow in the panels denote perturbation of cell morphology. Scale bar in panel (i) and (ii) is 300 nm and 1.0 µm, respectively.

revealed a significant morphological distortion in *S. aureus* 4s cells treated with 10 µM C8 and 2.0 µM CPX and this effect was similar to that observed upon treatment with 32 µM CPX (Figure 2.7B). The remarkable cell disruption noted in MRSA upon treatment with 10 µM C8 and 2.0 µM CPX was also evident when compared to untreated cells as well as cells treated with C8 or CPX (Figure A2.4 in Appendix). In essence, the combinatorial treatment assay revealed that C8 heightened the antibacterial effect of CPX and rendered annihilation of MRSA in presence of very low levels of CPX.

2.3.6. Potential of C8 in Preventing Development of Ciprofloxacin Resistance in MRSA

In order to establish the potential of C8 as an adjuvant in combination therapy targeting MRSA, it was worthwhile to determine the ability of C8 in preventing development of CPX-resistance in MRSA subjected to an extended combinatorial treatment with C8 and CPX. To this end, in separate sets *S. aureus* 4s cells were treated for 120 generations with either 32 µM CPX or a combination of 10 µM C8 and 2.0 µM CPX. When treated with 32 µM CPX alone (equal to MIC of CPX against *S. aureus* 4s), MRSA cell growth was arrested only till 40 generations (Figure 2.8A). Thereafter, MRSA cells displayed a notable recovery of growth, which reached ~90% after 120 generations (Figure 2.8A-2.8B). These results indicated that when the antibiotic was used alone, development of CPX-resistance in the target MRSA increased as the cells traversed through successive

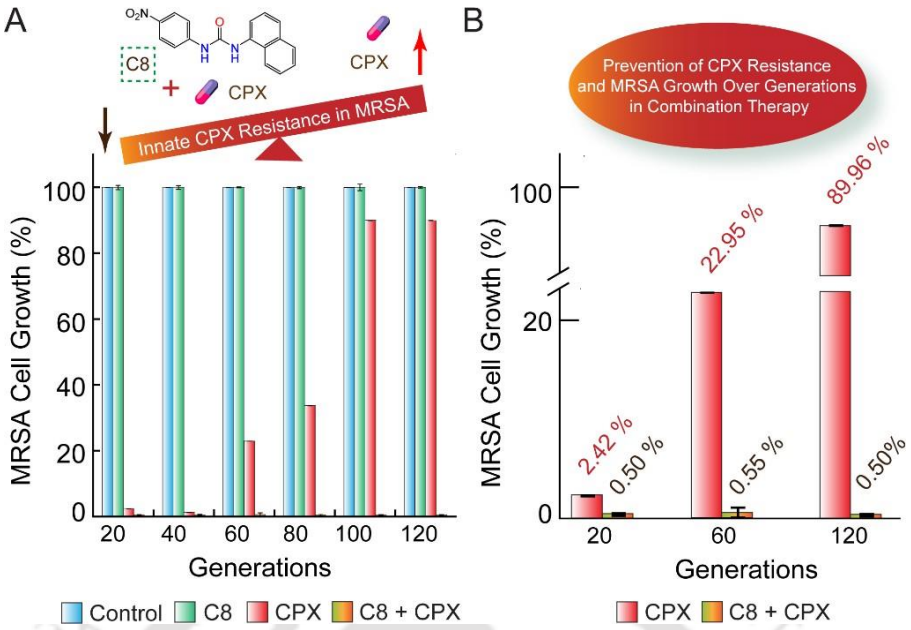

Figure 2.8. (A) Estimation of the growth of *S. aureus* 4s cells propagated for several generations either in presence of CPX or a combination of C8 and CPX. (B) Magnified view of (A) indicating the percentage growth of MRSA cells attained over several generations.

growth cycles and reached large number of generations. This phenomenon can perhaps be accounted by the presence of an efflux phenomenon in MRSA cells as evidenced in earlier studies (Figure 2.5B). However, when MRSA cells were treated with 10 µM C8 and 2.0 µM CPX, cell growth was completely arrested till 120 generations (Figure 2.8A-2.8B). This suggested that as a consequence of inhibition of MRSA efflux pump rendered by C8, the development of ciprofloxacin resistance in the target cells was effectively suppressed. Hence, in the combination treatment format, C8 holds considerable potential to counter a fundamental resistance mechanism and mediate killing of MRSA by CPX during therapy extending over several generations of cell growth.

2.4. Significant Findings

The salient findings of the present study can be enlisted as follows:

1. Amongst a set of urea ligands, C8 was most effective as an EPI (~95 % efflux inhibition) and was even superior than reserpine, a known efflux pump inhibitor.
2. C8 could elevate the magnitude of ciprofloxacin (CPX) accumulation in MRSA cells as well curb expression of *norA* gene implicated in efflux of CPX in MRSA.
3. A combination of 10 µM C8 and 2.0 µM CPX could lead to a 16-fold reduction in the MIC of CPX against MRSA and the growth inhibition rendered on target MRSA cells was remarkable (only ~6.0 % growth) as compared to equivalent levels of C8 (~73 % growth) or CPX alone (only ~91 % growth).
4. Interestingly, upon treatment with 10 µM C8 and 2.0 µM CPX, resistance development against CPX in MRSA cells was prevented and cell growth was completely arrested till 120 generations.

Based on the aforementioned results, it is apparent that C8 holds considerable promise as an adjuvant to flout CPX-resistance and enhance CPX-mediated killing of MRSA. However, to leverage the therapeutic potential of C8, development of a biocompatible cargo, which will favor sustained release of C8 is pertinent. To this end, generation of a C8-loaded nanocarrier for potential therapeutic applications targeting MRSA is described in the next chapter.

भारतीय प्रौद्योगिकी संस्थान गुवाहाटी
Indian Institute of Technology Guwahati

Chapter 3

Development of C8-loaded Nanocarrier as an Adjuvant for Mitigation of MRSA in Combination Therapy

This chapter illustrates the generation of C8-loaded PLGA nanocarrier (C8-PNC) and its application as an adjuvant in combination therapy for effective killing of MRSA and for prevention of MRSA adhesion onto collagen.

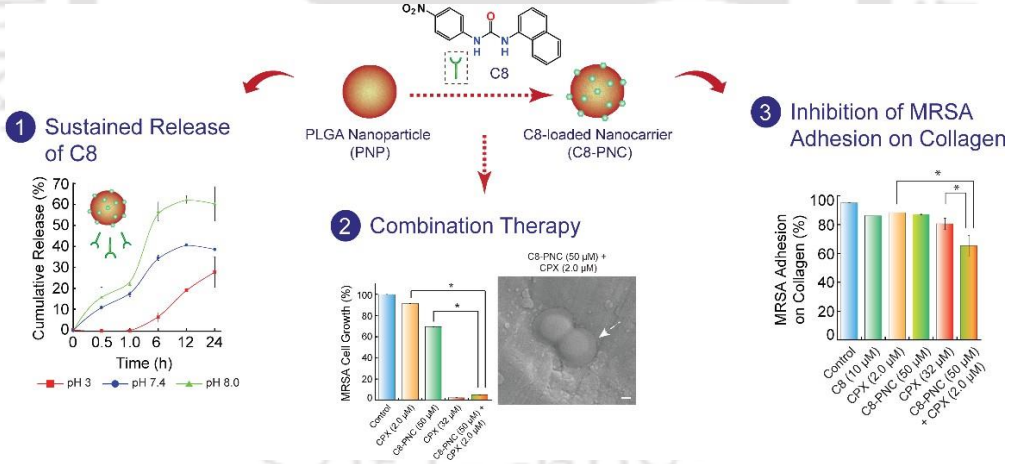

ABSTRACT

This chapter described the development of a payload nanocarrier and ascertains its potential in combination therapy for targeting MRSA. C8-loaded PLGA nanocarrier (C8-PNC) was generated by incubating PLGA nanoparticle (PNP) with varying concentration of C8. C8-PNC was spherical having an average particle size of ~250 nm. The loading efficiency (LE) was observed to saturate at ~60 µM of C8 and at the maximum concentration of 70 µM C8, LE was ~86%. In HEPES buffer and simulated body fluid (SBF), both having a physiologically relevant pH, release of C8 from the loaded nanocarrier was sustained and the magnitude of cumulative release of the ligand following 24 h of incubation was estimated to be ~38% (~30 µM) and ~60% (~48 µM), respectively. An EtBr efflux assay revealed that C8-PNC could render considerable reduction in efflux activity exhibited by the tested MRSA strain *S. aureus* 4s. Interestingly, in presence of C8-PNC (loaded with 50 µM C8) and CPX (2.0 µM) MRSA cell growth was significantly arrested (~7.0 % growth) and the MIC of CPX was reduced 16-fold. A similar combinatorial treatment could also render a substantial reduction of MRSA cell adhesion onto collagen as against MRSA treated with 2.0 µM CPX or 32 µM CPX. Further, qRT-PCR analysis indicated a remarkable suppression of *norA* gene expression in non-adhered MRSA cells when MRSA cells were subjected to adhesion assay in presence of C8-PNC (having a loading concentration of 50 µM C8) and 2.0 µM CPX. An MTT assay indicated that C8-PNC was essentially non-toxic to cultured HEK 293 cells.

3.1. Introduction

The prevalence of drug-resistant MRSA in the clinics is a serious healthcare concern. Given that efflux pumps in MRSA are largely associated with the resistance phenotype observed against therapeutic antibiotics, it is conceived that a viable strategy to counter the menace of MRSA is to deploy synthetic molecules that can effectively target efflux pump present in the pathogen. Earlier studies (Chapter 2) revealed that the rationally designed urea ligand C8 could effectively hinder efflux activity prevalent in MRSA, potentiate cellular uptake of CPX and reinstate susceptibility of the pathogen to low concentrations of CPX. Moreover, in a combinatorial therapy regimen, ligand C8 could thwart development of CPX resistance in MRSA over several generations when the target cells were grown in presence of C8 and CPX.

In order to leverage the leads obtained in the previous study and explore the prospect of C8 in combination therapy against MRSA, development of a robust delivery system that can ensure sustained release and enhance the bioavailability of ligand C8 in a physiological milieu is critical. In this regard, the use of nanoscale materials for encapsulation and delivery of bioactive ligands is an interesting option. Particularly, the high surface area to volume ratio and unique physicochemical traits of nanomaterials are favorable to attain a heightened antibacterial activity. The application of nanoscale materials for facile delivery of antibacterial agents as well as to render enhanced solubility, sustained and stimuli-responsive release of drug is well documented (Huh and Kwon, 2011; Goswami, *et al*., 2014; Duncan *et al*., 2015; Thiyagarajan *et al*., 2017; Yeh *et al*., 2020). Various types of nanoscale materials have been used to develop antibacterial agents ranging from metallic nanoparticles (Bajaj *et al*., 2017; Adhikari *et al*., 2013), polymeric nanoparticles (Silva *et al*., 2015; Radovic-Moreno *et al*., 2012), liposomes (Yamakami *et al*., 2013), lipid-based nanoparticles (Lewies *et al*., 2017) mesoporous silica nanoparticles (Tenland *et al*., 2019) and others.

Amongst various choices for developing nanocarriers as a cargo for delivery of antibacterial agents, poly(lactide-co-glycolide) (PLGA)-based nanoparticle is particularly selected in therapeutic applications as the polymer is generally regarded as safe (GRAS) and approved by FDA, exhibits biocompatibility and biodegradability and can render protection and extended residence time for the entrapped drug (Danhier et al., 2012; Swider et al., 2018). To this end, development of effective bactericidal agents based on PLGA nanoparticles as a delivery system has been demonstrated (Thiyagarajan *et al*., 2017; Wan *et al*., 2020; Zhang *et al*., 2022). Based on the aforementioned rationale,

in the present study a C8-loaded PLGA nanocarrier (C8-PNC) was generated for potential therapeutic applications targeting MRSA. The payload nanocarrier displayed EPI activity, reinstate CPX-mediated elimination of the pathogen and also effectively hinder adhesion of MRSA onto collagen in presence of CPX.

3.2. Materials and Methods

3.2.1. Compounds and Reagents

5 (and 6)-carboxyfluorescein diacetate succinimidyl ester (cFDA-SE), ethidium bromide (EtBr), poly(D,L-lactide-co-glycolide) lactide:glycolide (50:50), molecular weight 30,000-60,000 (PLGA) , poly(vinyl alcohol) average molecular weight 85,000-124,000, 87-89% hydrolyzed (PVA), ciprofloxacin, reserpine, collagen type IV, Dulbecco's Modified Eagle Medium (DMEM), trypsin-EDTA and 3-(4,5-dimethyl-2-thiazolyl)-2,5-diphenyl-2H-tetrazolium bromide (MTT) were procured from Sigma-Aldrich (USA). Brain-Heart Infusion (BHI) broth was procured from HiMedia, Mumbai, India. Dimethyl sulfoxide (DMSO) was obtained from Merck, India. Fetal bovine serum (FBS) was obtained from PAA Laboratories, USA. N-2- hydroxyethyl piperazine N-2 ethane sulphonic acid (HEPES buffer) was procured from Sisco Research Laboratories SRL, Mumbai, India.

3.2.2. Development of C8-loaded Nanocarrier

Initially PLGA nanoparticle (PNP) was prepared as described previously (Carteria *et al*., 2009). Subsequently, PNPs (1.0 mg/mL in sterile MilliQ water) and C8 (1.25 µM - 100 µM) were incubated overnight in separate sets under shaking conditions at room temperature. Following incubation, the samples were subjected to centrifugation at 10000 rpm for 5.0 min to recover C8-loaded PLGA nanocarrier (C8-PNC), which was then stored at -20 ºC prior to subsequent use. Microscopic and spectroscopic techniques were used to characterized PNPs and C8-PNC as described in the following section.

3.2.3. Characterization of PNP and C8-PNC

3.2.3.1. FESEM and FETEM Analysis

To accomplish FESEM analysis, a 10 µL aliquot each of PNP (1.0 mg/mL in sterile MilliQ water) and C8-PNC (1.0 mg/mL PNP having 50 µM C8) was separately drop-casted onto aluminium foil. The sample was then dried overnight in a laminar hood, visualized in a field emission scanning electron microscope (Zeiss Sigma, USA) and the

obtained images were recorded. In case of FETEM analysis, 10 µL aliquot each of PNP (1.0 mg/mL in sterile MilliQ water) and C8-PNC (1.0 mg/mL PNP loaded with 50 µM C8) were separately drop-casted onto a carbon-coated copper grid. The sample was then dried overnight in a laminar hood, analyzed by FETEM (Model 2100F, JEOL) operating at 200 kV and their images were captured.

3.2.3.2. Atomic Force Microscope (AFM) Analysis

A 10 µL aliquot of PNP (1.0 mg/mL in sterile MilliQ water) and C8-PNC (1.0 mg/mL PNP loaded with 50 µM C8) was separately spotted onto a sterile glass cover slip (18 mm × 18 mm). The cover slip was then air dried overnight in a laminar hood. AFM images were acquired in non-contact mode over a 10 µm × 10 µm area at a scan rate of 0.5-1.0 line/s (Oxford Instruments plc, U.K). Cantilevers made up of silicon nitride were used having a resonant frequency of ca. 150 to 200 kHz. Analysis of the amplitude channel and topographic images was accomplished by using the WSxM v5.0 Develop 6.5 image viewer software.

3.2.3.3. Dynamic Light Scattering (DLS) Analysis

In order to estimate the particle size, PNPs were resuspended in sterile MilliQ water (1.0 mg/ml) and 0.2 ml aliquot of the sample was further dispersed in 0.8 ml sterile MilliQ and subjected to DLS analysis (Zetasizer, Malvern, UK). In a separate set, C8-PNC (1.0 mg/mL PNP loaded with 50 µM C8) was dispersed in sterile MilliQ water (final volume of 1.0 mL). A 0.1 mL aliquot of this solution was further diluted in sterile MilliQ water to a final volume of 1.0 mL and subjected to particle size estimation by DLS. The DLS experiments were performed in three independent sets and every set consisted of three replicates.

3.2.3.4. UV-Visible Absorbance Spectroscopy

The absorbance spectra of C8 (50 µM), PNP (1.0 mg/mL) and C8-PNC (1.0 mg/mL PNP loaded with 50 µM C8) was recorded in a spectrophotometer (Lambda 25, Perkin-Elmer) in scanning mode from 200 nm to 800 nm. Absorbance measurements were acquired from three independent experimental samples.

3.2.4. Loading Efficiency (LE) and Adsorption Isotherm

In order to estimate the loading efficiency, PNPs (1.0 mg/mL) were incubated in separate sets with variable concentrations of C8 (1.25 µM - 70 µM) for 12 h on a rocker at room temperature. Following incubation, the solution was subjected to centrifugation at 10000 rpm for 10 min and C8-PNC was recovered as the pellet and was resuspended in sterile MilliQ water. In every set, the concentration of C8 in the supernatant (free or residual C8) was ascertained by using a previously generated calibration plot for C8. The loading efficiency (LE) was calculated as follows:

$$LE = \frac{W_{Total\ C8} - W_{Free\ C8}}{W_{Total\ C8}} \times 100\%$$

where $W_{Total\ C8}$ is the total amount of C8 used during preparation of C8-PNC and $W_{Free\ C8}$ is the amount of free or residual C8 recovered in the supernatant by centrifugation. All the experiments were performed in triplicates. Data analysis and calculation of standard deviation was performed with Microsoft Excel 2010 (Microsoft Corporation, USA).

In order to measure the adsorption isotherm, C8 in varying concentrations (1.25 µM - 80 µM) were added in separate sets to PNPs (1.0 mg/mL) in a total working volume of 1.0 mL and then incubated for 30 min at room temperature under mild shaking. Subsequently, the samples were subjected to centrifugation at 10000 rpm for 10 min. The residual C8 present in the supernatant was aspirated and its absorbance was measured UV-visible spectroscopy. The absorbance value was then used to calculate the concentration of the residual or non-adsorbed C8 using a previously generated calibration plot. The adsorption capacity, q_e (mg/mg) was calculated as described in a previous method (Saha *et al*., 2011). All the experiments were carried out in triplicates and data analysis and calculation of standard deviation was performed with Microsoft Excel 2010 (Microsoft Corporation, USA).

.

3.2.5. Potential of C8-PNC in Efflux Pump Inhibition

To ascertain inhibition of efflux pump activity rendered by C8-PNC or PNP, an EtBr efflux assay was conducted as described earlier in section 2.2.5.

3.2.6. Potential of C8-PNC in Combination Therapy against MRSA

In a 96-well microtitre plate, *S. aureus* 4s (~10^6 CFU in BHI medium) was grown in separate sets in presence of C8-PNC (loaded with 50 µM C8) and CPX (2.0 µM) at 37 ºC and 180 rpm for 6 h. In separate sets, MRSA cells were also grown in presence of either CPX (2.0 µM or 32 µM) or C8-PNC (loaded with 50 µM C8). Following incubation, the growth of cells was ascertained by recording the absorbance of the culture at 600 nm in a microtitre plate reader (Infinite M200, TECAN, Switzerland). FESEM analysis was also performed to determine the effect of the combination treatment of C8-PNC and CPX on MRSA. The protocol followed for FESEM analysis was similar to that described in section 2.2.8.

3.2.7. MRSA Cell Adhesion onto Collagen in Presence of C8 and C8-PNC

A standard collagen adhesion assay was performed as outlined in an earlier study (Mukherjee and Ramesh, 2015). Initially, a tissue culture plate (six well) was coated with collagen solution (final concentration of 500 µg/mL) overnight at 4 ºC, followed by washing and blocking of the wells as described previously (Mukherjee and Ramesh, 2015). For the adhesion assay, *S. aureus* 4s cells were labelled with cFDA-SE (Singh *et al*., 2012) and the solution-based fluorescence of cells recorded at 518 nm (excitation wavelength of 488 nm) was noted as total fluorescence (F_T). cFDA-SE labelled *S. aureus* 4s cells were then added to collagen-coated wells (1.0 mL aliquot each) and incubated in separate sets for 1 h at 4 ºC in presence of (i) C8 (10 µM), (b) CPX (2.0 µM), (c) C8-PNC (loaded with 50 µM C8), (d) CPX (32 µM) and (e) combination of CPX (2.0 µM) and C8-PNC (loaded with 50 µM C8). Subsequently, the non-adhered cells were carefully pipetted and their fluorescence emission intensity at 518 nm was noted as a measure of non-adhered cells (F_{NA}). A quantitative estimation of MRSA cells adhered onto collagen (F_A) was derived by determining the between F_T and F_{NA}. A schematic representation of the collagen adhesion assay in shown in Figure 3.1. In a separate experiment, RNA was extracted from non-adhered *S. aureus* 4s cells harvested from the tissue culture wells following various treatment in adhesion assay and the expression of *norA* gene in non-adhered cells was ascertained by qRT-PCR analysis as mentioned before in section 2.2.7. Detection of collagen-adhered MRSA cells was accomplished by fluorescence microscope analysis (Eclipse Ti-U, Nikon, USA). A schematic representation of the CPX accumulation assay in shown in Figure 3.1.

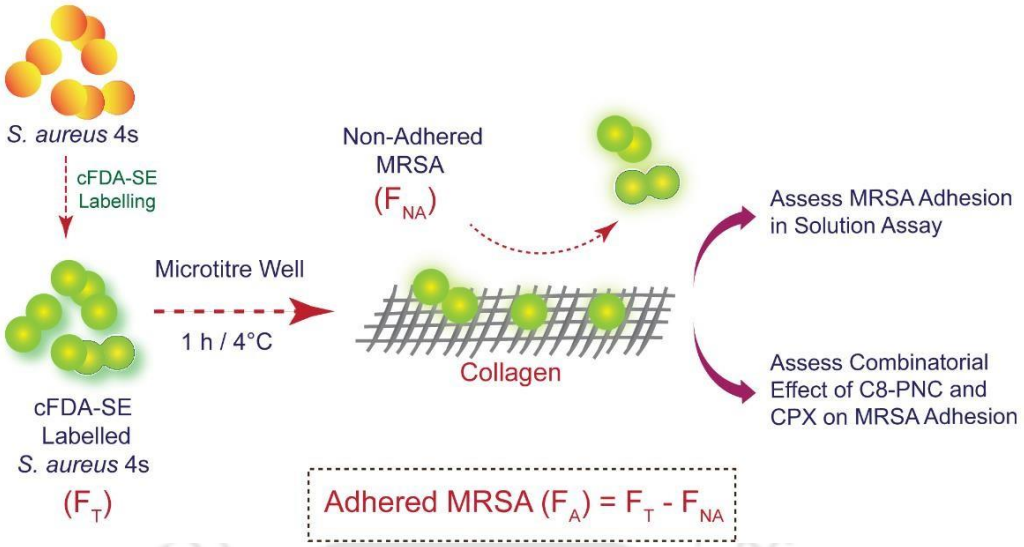

Figure 3.1. Schematic of the protocol followed for estimation of MRSA cell adhesion onto collagen in presence of C8-PNC and CPX.

3.2.8. Cytotoxic Potential of C8 and C8-PNC

An MTT-based assay was conducted to ascertain the cytotoxic potential of C8 (5.0 μM - 40 μM) and C8-PNC (loaded with 1.25 μM - 70 μM of C8) against HEK 293 cells (human embryonic kidney cells). The growth conditions for HEK 293 cells and the protocol for conducting the MTT assay was similar to the method described in an earlier study. (Thiyagarajan *et al*., 2017)

3.3. Results and Discussion

3.3.1. C8-loaded PLGA Nanocarrier (C8-PNC)

The potential of C8 as an adjuvant for combination therapy against MRSA was clearly established from the results obtained in the previous Chapter (Chapter 2). However, to leverage the therapeutic prospect of C8, a biocompatible delivery vehicle, which will favor slow release of the payload will be required. To this end, PLGA nanoparticle (PNP) was synthesized by a single emulsion method (Carteria *et al*., 2009) and chosen as a delivery agent as it was conceived that PNPs will be biocompatible and would support sustained delivery of the payload C8. FESEM analysis of PNPs indicated that the nanoparticles were spherical in shape with an average particle size of ~200 nm (Figure 3.2A). The spherical shape of PNPs was also evidenced in TEM and AFM analysis (Figure 3.2B-3.2C). The average height profile of PNP as ascertained by AFM was ~225 nm (Figure 3.2D-3.2E). The average hydrodynamic radius of PNP

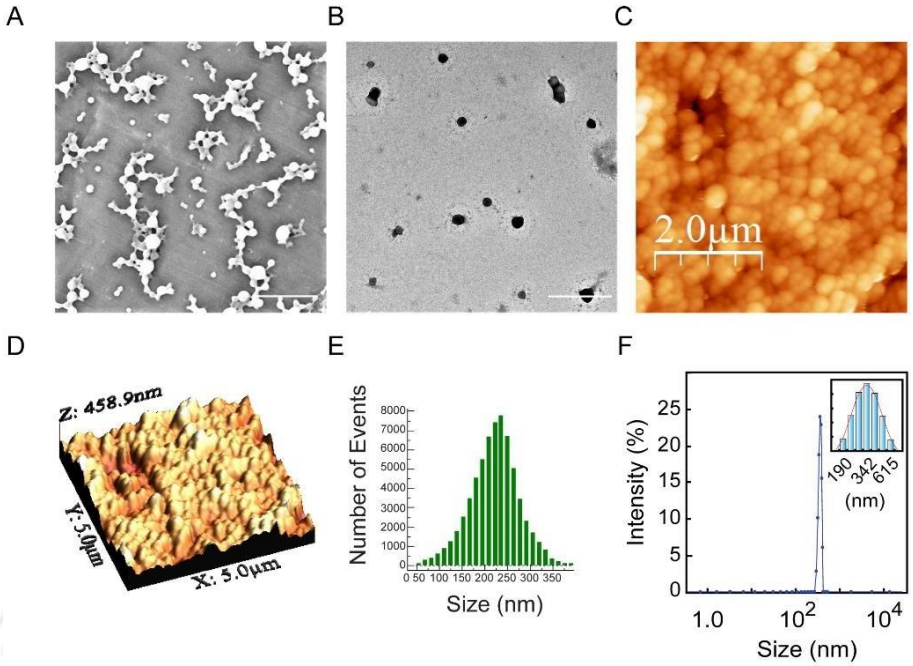

Figure 3.2. Characterization of PLGA nanoparticle (PNP) by (A) FESEM, (B) TEM,(C-E) AFM analysis and (F) dynamic light scattering (DLS) analysis. Scale bar in (A) and (B) is 1.0 µm. (C) and (D) indicate 2D and 3D topography AFM image of PNP, respectively. (E) Height profile of PNPs determined by analysis of the image in (D). (F) Estimation of hydrodynamic radius of PNP by DLS. Inset depicts size distribution histogram.

determined by DLS was ~396 nm (Figure 3.2F). Akin to PNPs, C8-PNC was also spherical (Figure 3.3A-3.3B). However, FESEM analysis indicated that compared to PNPs, C8-PNC was larger in size (average particle size of ~250 nm as against ~200 nm for PNPs). The larger size of C8-PNC as compared to PNPs was further substantiated as the average height profile of C8-PNC was ~421 nm (Figure A3.1A-A3.1B in Appendix) and the average hydrodynamic radius of C8-PNC was ~531 nm (Figure 3.3C). Loading of C8 in C8-PNC was confirmed as UV-visible absorbance spectroscopy could clearly reveal the presence of the characteristic absorbance peak of C1 in the loaded nanocarrier (Figure A3.1C in Appendix). With regard to the loading efficiency (LE) of C8, it was observed that there was a significant increase in the magnitude of LE with an increase in the concentration of C8 and at ~60 µM of C8, a saturation effect was apparent (Figure 3.3D). Further, in presence of 70 µM C8 (maximum loading concentration of C8), LE was ~86% (Figure 3.3D). Determination of the parameters in adsorption studies with C8 revealed that the nature of adsorption of

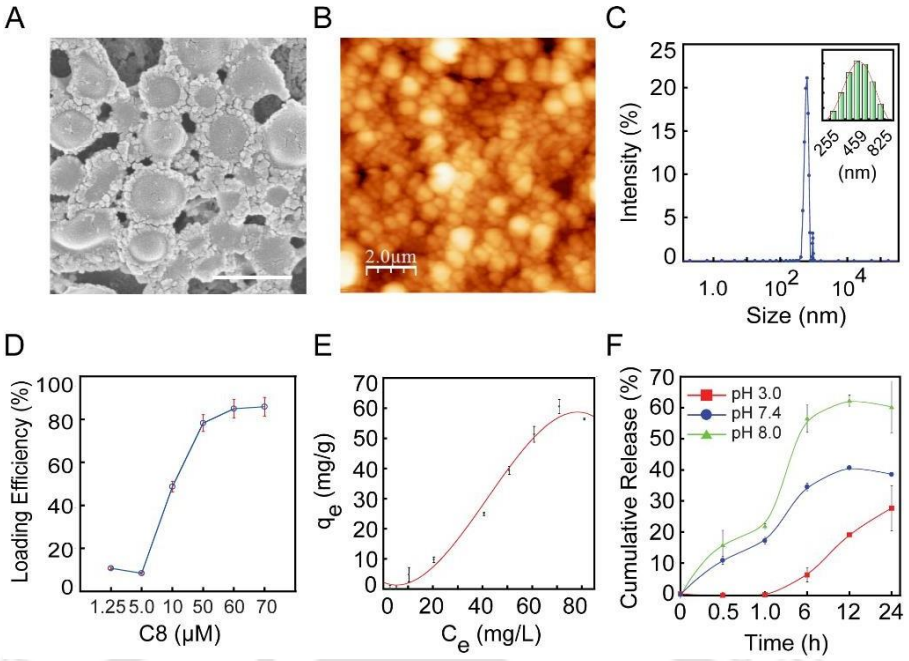

Figure 3.3. (A) FESEM analysis of C8-loaded PLGA nanocarrier (C8-PNC). Scale bar is 1.0 μm. (B) AFM analysis of C8-PNC. (C) DLS analysis of C8-PNC. Inset represents size distribution histogram. (D) Estimation of the loading efficiency of C8 in PLGA nanoparticle. (E) Adsorption isotherm profile of C8. (F) Estimation of the cumulative release of C8 from C8-PNC incubated in various buffer systems.

C8 onto PNPs followed a Langmuir isotherm model (Figure 3.3E), which implied homogeneous and a monolayer type of adsorption (Saha *et al*., 2011). It can be conjectured that the efficacy of a candidate adjuvant in the host associated physiological ambience would depend on its effective concentration, which in turn will be largely governed by its interactions with host plasma proteins, body fluids and tissue. Hence for therapeutic intervention, it is desirable to use high levels of the adjuvant in order to guarantee bioavailability and achieve the desired levels of therapeutic dose. Based on this tenet, in the current investigation, C8-PNC loaded with 80 μM C8 was used in the release kinetics studies. Upon incubation for 24 h in an acidic buffer (pH 3.0), the cumulative release of C8 was quite low, amounting to ~27% (Figure 3.3F). Interestingly, in HEPES buffer (pH of 7.4) and SBF (pH 8.0), a sustained release profile for C8 was evident and the magnitude of cumulative release of C8 was apparently higher than that observed in case of the acidic citrate buffer (Figure 3.3F). A quantitative estimation revealed that the cumulative release of C8 in HEPES buffer and SBF was ~38% and ~60%, respectively, following 24 h (Figure 3.3F). It is significant to mention that the quantum of C8 released in HEPES buffer and SBF was ~30 μM and ~48 μM,

respectively, which is in excess of the effective dose of the ligand required for efflux pump inhibition in *S. aureus* 4s strain. This suggested that the favorable release profile of C8 rendered by C8-PNC is likely to be amicable for therapeutic applications against the MRSA strain.

3.3.2. Potential of C8-PNC as an EPI and in Combination Therapy against MRSA

The favorable release profile of C8 obtained from C8-PNC in buffer solution having physiological relevance was encouraging. The subsequent aim of the investigation was to ascertain whether the efflux pump inhibition rendered by ligand C8 against MRSA was also manifested when MRSA cells were treated with C8-PNC. To this end, a prominent inhibition of EtBr efflux was indeed noted in *S. aureus* 4s cells treated with C8-PNC (Figure 3.4A, Table A3.1 in Appendix), which was similar to the trend observed earlier with MRSA cells treated with C8 (Figure 2.5B). Further, it was also noted that upon treatment of MRSA cells with C8-PNC, a nominal efflux of EtBr was observed till 2.0 min, following which prominent inhibition of EtBr efflux was recorded (Figure 3.4A). This phenomenon suggested that the cumulative release of C8 from C8-PNC during the initial 2.0 min perhaps lead to attainment of an effective concentration of C8 in solution. Consequently, a significant inhibition of efflux pump activity in MRSA cells was observed thereof.

With regard to the effect on cell growth, it was observed that although *S. aureus* 4s displayed appreciable growth upon treatment with C8-PNC (~70% growth) or 2.0 µM CPX (~91% growth) (Figure 3.4B), a significant growth inhibition (only ~7.0 % growth) was observed when the target pathogen was grown in presence of both C8-PNC (having 50 µM C8) and CPX (2.0 µM) (Figure 3.4B). The magnitude of growth inhibition rendered by the combination treatment of C8-PNC and CPX was on par with 32 µM CPX (Figure 3.4B). Further, the MIC of CPX was reduced 16 × in case of the combination treatment. The antagonistic effect of the combination treatment on MRSA cells was also captured in FESEM analysis, which indicated prominent perturbation of MRSA cell morphology in comparison to control cells (Figure 3.4C). Thus, C8-PNC could not only render sustained release of C8 but could also effectively reduce the dose of CPX required to eliminate MRSA.

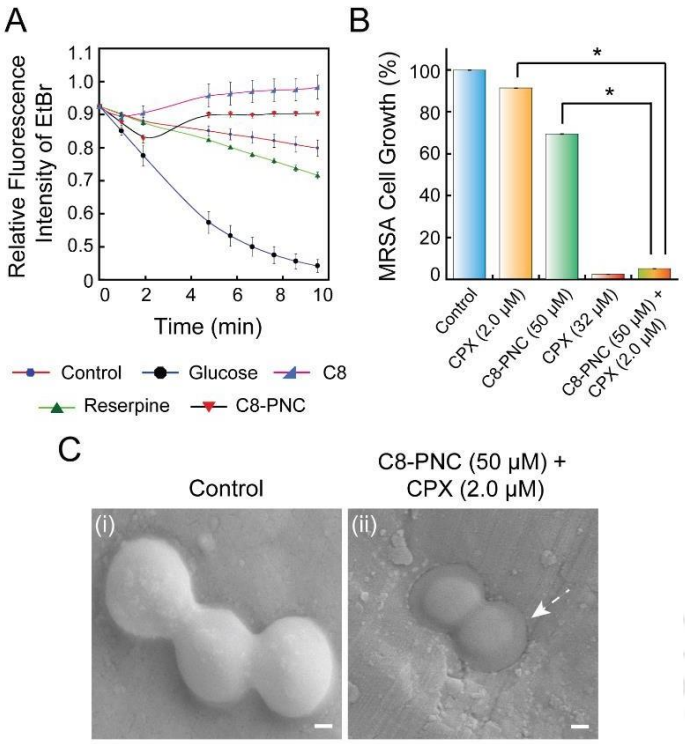

Figure 3.4. (A) Measurement of EtBr efflux in *S. aureus* 4s cells treated with C8-PNC. Positive control encompassed cells treated with 40 µM reserpine. (B) Growth of MRSA cells in presence of C8-PNC (having 50 µM C8) and CPX (2.0 µM). * represents *p* value < 0.001 in one-way ANOVA. (C) FESEM analysis of (i) Untreated MRSA cells and (ii) MRSA cells treated with C8-PNC and CPX. White arrow in panel (ii) specifies perturbation of characteristic cell morphology. Scale bar is 200 nm.

3.3.3. Effect of Combination Treatment with C8-PNC and CPX on Adhesion of MRSA onto Collagen

It is widely acknowledged that adhesion of *S. aureus* cells onto collagen can serve as a trigger to initiate large-scale infection of extracellular matrix by the pathogen (Lee *et al*., 2018; Foster *et al*., 2014). Hence, it is perceived that inhibiting the adhesion of MRSA cells onto collagen can be a rational therapeutic approach to hinder MRSA-mediated infection. In the current study, it was encouraging to observe that C8-PNC in combination with CPX could efficiently eliminate MRSA cells. Hence, it was conjectured that this combination treatment regimen may also serve to inhibit MRSA cell adhesion onto collagen. To ascertain this tenet a collagen adhesion assay was performed, wherein untreated MRSA cells could adhere onto collagen in high numbers (~95% adhesion). Upon treatment with C8-PNC (having 50 µM C8) or CPX (2.0 µM),

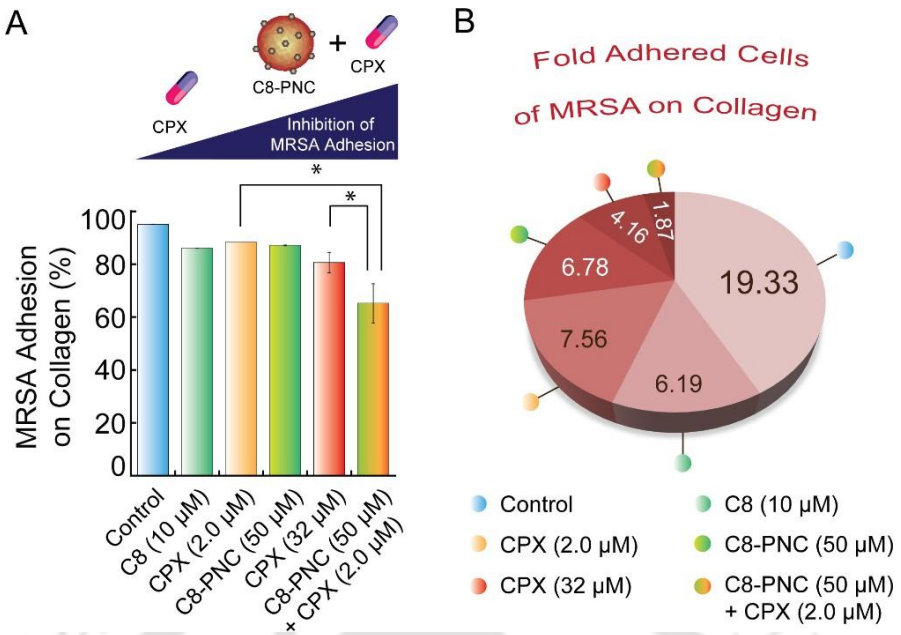

Figure 3.5. (A) Estimation of *S. aureus* 4s cell adhesion onto collagen in different treatment sets. * in (A) represents *p* value of <0.001 in one-way ANOVA. (B) Fold adhered cells of *S. aureus* 4s estimated during collagen adhesion assay performed in various treatment sets.

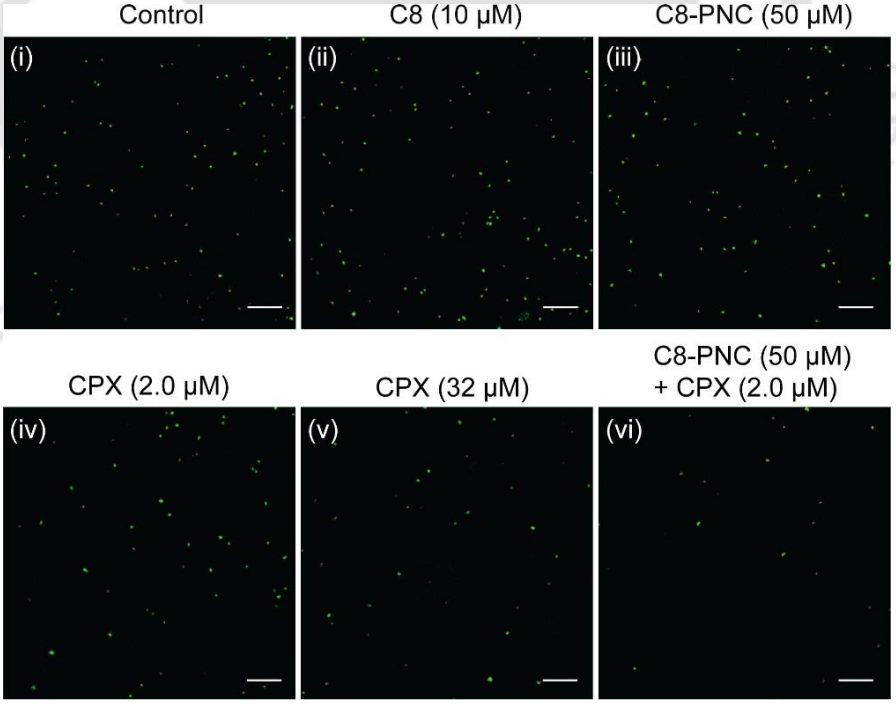

Figure 3.6. Fluorescence microscope analysis of *S. aureus* 4s cells adhered onto collagen in case of different treatment sets. Scale bar is 20 μm.

the extent of adhesion was decreased to a marginal extent and measured to be ~87% and ~88% adhesion, respectively (Figure 3.5A). Interestingly, there was a significant

decrease in MRSA cell adhesion onto collagen (~65% adhesion) when the cells were subjected to the adhesion assay in presence of C8-PNC (having 50 µM C8) in combination with 2.0 µM CPX (Figure 3.5A). Further, MRSA cell adhesion onto collagen in presence of the combinatorial treatment with C8-PNC and CPX was significantly lower in comparison to the adhesion of cells treated with 2.0 µM or 32 µM CPX (Figure 3.5A). A quantitative estimation of the fold adhered cells (adhered: non-adhered MRSA cells) also revealed that proportion of MRSA cells adhered onto collagen was significantly lower in combination treatment regimen (~1.87 fold) in comparison to cellssubjected to treatment with either 2.0 µM CPX (~7.56 fold) or 32 µM CPX (~4.16 fold)(Figure 3.5B).

Fluorescence microscope analysis could also corroborate the results as the numbered of adhered MRSA cells observed upon combinatorial treatment was distinctly less in comparison to untreated (control) as well as other treatment sets (Figure 3.6). Based on the results of the adhesion assay, it was apparent CPX alone may not hinder MRSA cell adhesion onto collagen. However, in the combination treatment regimen, C8-PNC (having 50 µM C8) likely countered efflux pump activity and enhanced the potency of CPX against target MRSA cells leading to in a significant reduction in MRSA cell adhesion onto collagen.

3.3.4. Effect of C8-PNC and CPX on norA Gene Expression in MRSA During Collagen Adhesion

During collagen adhesion assay, treatment of *S. aureus* 4s cells with 2.0 µM CPX could induce a notable increase in *norA* gene expression (~4.0 - fold) in non-adhered cells (Figure 3.7). Literature reports indicate that *norA* is associated with CPX efflux in MRSA (Li and Nikaido, 2009; Jang, 2016) In the light of this premise, *norA* gene transcription level is likely to be high in MRSA cells treated with 2.0 µM CPX. When *S. aureus* 4s cells were treated with 32 µM CPX (equivalent to MIC against the MRSA strain), *norA* gene expression in non-adhered cells was quite high (~3.0-fold upregulation), albeit slightly reduced as compared to cells treated with 2.0 µM CPX (Figure 3.7). When used at MIC level, CPX perhaps can render copious physiological or cellular perturbations in *S. aureus* 4s cells, leading to a reduction in the level of *norA* gene transcription in comparison to MRSA cells treated with 2.0 µM CPX. This tenet can be verified through more rigorous experiments in the future. Interestingly, when *S. aureus* 4s cells were treated with C8-PNC (having 50 µM C8) singularly or in conjunction with

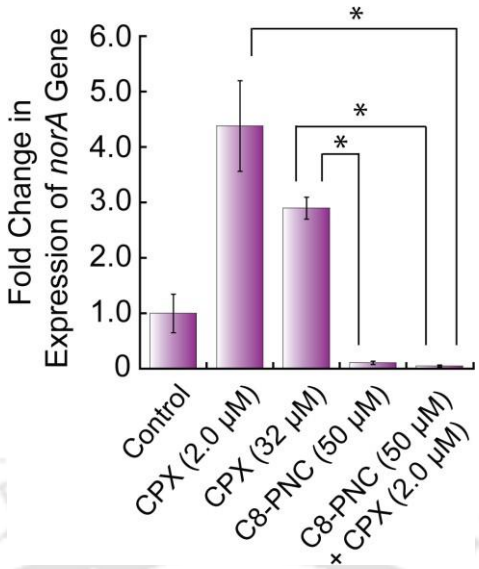

Figure 3.7. Quantitative real-time PCR analysis to estimate the fold change in *norA* gene expression in non-adhered MRSA cells subjected to various treatment sets in collagen adhesion assay. * indicates *p* value < 0.001 in one-way ANOVA.

2.0 μM CPX, a remarkable suppression in the level of *norA* gene expression was observed in non-adhered as against untreated cells (Figure 3.7). Collectively, the aforementioned results suggest that during collagen adhesion, C8-PNC in conjunction with low levels of CPX can downregulate the expression of *norA* gene in MRSA cells and thus bears interesting prospect as an anti-adhesion agent for mitigation of MRSA infection in collagen.

3.3.5. Cytotoxic Potential of C8-PNC

In order to deploy C8-PNC as a potential adjuvant for therapeutic intervention against MRSA, it is vital that the developed payload nanocarrier is biocompatible towards host cells. To this end, an MTT assay revealed that C8-PNC was not detrimental to cultured HEK 293 cells, with the viability of cells being greater than 80% even with a loading concentration of 50 μM C8 (Figure 3.8). It may be mentioned here that C8-PNC loaded with 50 μM C8 exhibited EPI activity and could eliminate MRSA in conjunction with 2.0 μM CPX (Figure 3.4A-3.4B). It was also worth noting that although 10 μM C8 displayed EPI activity (Figure 2.5B), the ligand per se was toxic and could significantly hamper the growth of HEK 293 cells (~42% viability) (Table A3.2 in Appendix). Conceivably, upon treatment with C8, the concentration of the ligand in the vicinity of HEK 293 cells is expected to be high, and consequently a cytotoxic effect is

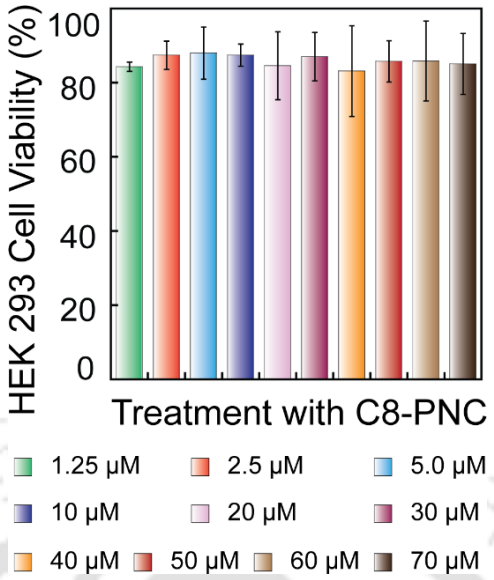

Figure 3.8. MTT assay-based estimation of the cytotoxic effect imparted by C8-PNC on cultured HEK 293 cells. The loading concentration of C8 is depicted in the figure. Data point obtained from six experimental samples were used to ascertain mean ± standard deviation.

manifested. On the contrary, when HEK 293 cells are treated with C8-PNC, sustained release of the payload can decrease the local concentration of C8 and thus reduce the toxic implications.

3.4. Significant Findings

The key findings of the present study can be stated as follows:

1. In order to harness the potential of C8 as an efflux pump inhibitor, C8-loaded PLGA nanocarrier (C8-PNC) was developed having a loading efficiency of ~86% in presence of 70 µM C8.

2. In HEPES buffer and simulated body fluid (SBF), a sustained release profile of C8 from the nanocarrier was observed, with the cumulative release of C8 being ~38% (~30 µM) and ~60% (~48 µM) after 24 h of incubation.

3. C8 could elevate the magnitude of ciprofloxacin (CPX) accumulation in MRSA cells as well curb expression of *norA* gene implicated in efflux of CPX in MRSA.

4. C8-PNC (loaded with 50 µM C8) in conjunction with 2.0 µM CPX could render a remarkable suppression of MRSA cell growth (~7.0 % growth) as well as lower the MIC of CPX by 16-fold.

5. Interestingly, C8-PNC (having 50 µM C8) and CPX (2.0 µM) could also effectively hinder MRSA cell adhesion onto collagen as well as suppress the expression of *norA* gene in non-adhered MRSA cells.

6. C8-PNC (loaded with 50 µM C8) was observed to be non-toxic to cultured HEK 293 cells.

Based on the salient results obtained in this study, it is apparent that the developed nanomaterial holds prospect as a therapeutic in combination therapy to mitigate MRSA cell adhesion onto collagen. In future, these leads can perhaps be substantiated through separate *in vivo* invasive MRSA infection models in soft tissue. In the constant endeavor to overcome the scarcity of therapeutic approaches against MRSA infections, an interesting prospect is in the development of membrane-targeting synthetic adjuvants. Conceivably, resistance development against such antibacterials acting on a vital target such as the membrane is less likely. Further, the potential of combining such membrane-targeting adjuvants with therapeutic antibiotics for eradication of MRSA is also worth exploring. To this end, in the subsequent chapter, quinoxaline ligands are screened for their membrane-targeting bactericidal activity against MRSA planktonic cells and biofilm is ascertained.

भारतीय प्रौद्योगिकी संस्थान गुवाहाटी
Indian Institute of Technology Guwahati

Chapter 4

Bactericidal Potential, Membrane-directed Activity and Antibiofilm Activity of Quinoxaline-based Ligands for Targeting MRSA

This chapter describes the antibacterial potential of quinoxaline-based synthetic ligands C1-C4 against MRSA. The membrane-targeting activity and antibiofilm potential of C2, the most potent molecule is also presented in this chapter.

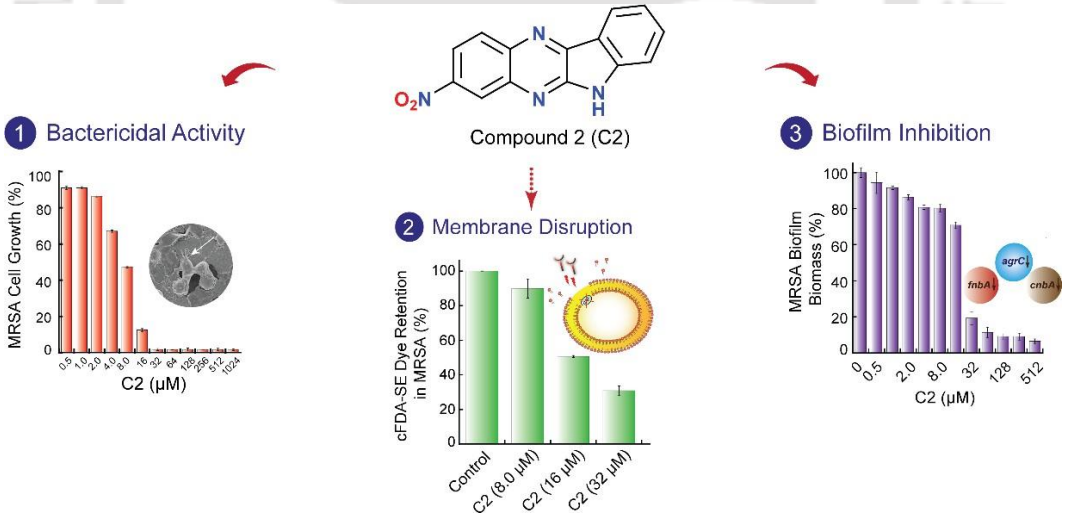

ABSTRACT

In this study, the antibacterial potential of quinoxaline-based synthetic ligands (C1-C4) against MRSA is evaluated. Amongst the tested ligands, only C2 exhibited notable antibacterial activity against the clinical MRSA strain *S. aureus* 4s, with an MIC of 32 µM against the pathogen. FETEM analysis could substantiate the anti-MRSA activity of C2, wherein copious cellular damage and distortion of the salient morphology manifested in cells treated with 32 µM C2. A dose-dependent membrane-directed activity rendered by C2 on MRSA cells was evidenced through a cFDA-SE dye-based assay. Solution-based crystal violet and MTT assay revealed that C2 imparted a dose-dependent effect on the biomass and metabolic activity of MRSA biofilm. The minimum biofilm inhibitory concentration (MBIC) of C2 against the *S. aureus* 4s biofilm was observed to be 32 µM. The antagonistic effect of C2 on MRSA biofilm was also evident in FESEM and AFM analysis, wherein the prominent cell-cell adhesion typically observed in MRSA biofilm was disrupted. A quantitative real-time PCR analysis indicated that the expression of *agrC*, which is implicated in the regulation of adhesins in *S. aureus* decreased in a dose-dependent manner upon treatment with C2. The antibiofilm potential of C2 was also corroborated by downregulation of the adhesin genes *fnbA* and *cnbA* in *S. aureus* 4s cells upon treatment with C2.

4.1. Introduction

The emergence of MRSA in the clinics is a contemporary and global healthcare problem as the pathogen is armed with efficient countermeasures that can evade the action of many therapeutic antibiotics (Lee *et al*., 2018; Turner *et al*., 2019; Chambers and Deleo, 2010; Liu *et al*., 2011). Most of the therapeutic antibiotics are known to perturb essential cellular processes such as DNA synthesis, cell wall synthesis, protein synthesis and folate synthesis (Collin *et al*., 2011; Hurdle *et al*., 2011; McCoy *et al*., 2011; Lange *et al*., 2007). However, the use of therapeutic antibiotics to curb MRSA infection has been undermined since the pathogen has acquired resistance traits, foil the action of antibiotics, evade the host defense mechanism and thereby pose a persistent challenge in the clinics (Lee *et al*., 2018; Turner *et al*., 2019; Mwangi *et al*., 2007; Chen *et al*., 2015; Weigel *et al*., 2003).

The bacterial cell membrane has a characteristic organization, which enables it to render a host of critical physiological functions. Hence, it is conceived that bactericidal agents that can breach the membrane or disrupt its function hold significant prospect as a therapeutic (Chen *et al*., 2010; Van Bambeke *et al*., 2008; Hurdle *et al*., 2011). In contrast to antibiotics, which essentially target basic cellular processes and are thus liable to trigger resistance development, the prospect of developing resistance against membrane-acting agents would necessitate large-scale renewal of damaged membrane components, which can be a physiologically demanding task for the bacteria (Steinbuch and Fridman, 2016). In this context, membrane-acting antimicrobial peptides (AMPs) that exhibit broad-spectrum antibacterial activity are promising candidates (Wright 2011; Wimley and Hristova, 2011). However, there are acute challenges in leveraging their therapeutic potential due to an incumbent high cost of manufacturing, inferior pharmacokinetics, susceptibility to proteolysis and lower *in vivo* efficacy (Chen *et al*., 2012; Marr *et al*., 2006). In order to overcome these limitations, AMP-mimicking synthetic amphiphiles hold considerable therapeutic potential owing to their facile synthesis, a large repertoire of synthetic variants that can be exploited for activity, their resistance to proteolysis and high membrane-directed activity (Findlay *et al*., 2010). Several studies have indeed described the membrane-targeting and bactericidal activity of synthetic amphiphilic molecules (Kuroda and DeGrado 2005, Findlay *et al*., 2010; Hoque *et al*., 2012; Gokel and Negin 2012; Bera *et al*., 2010; Goswami *et al*., 2013; Thiyagarajan *et al*., 2014; Dey *et al*., 2018). Studies have also demonstrated the potential of membrane-targeting synthetic amphiphiles against MRSA (Thiyagarajan *et al*., 2017; Moretti *et al*., 2019; Tyuleva *et al*., 2019; Dey *et al*., 2020).

In the light of the aforementioned tenet, the bactericidal and membrane-directedactivity of rationally designed quinoxaline-based ligands (C1-C4) is evaluated in this chapter. A detailed characterization of the membrane-directed activity and antibiofilm activity of the most potent antimicrobial C2 against the MRSA strain *S. aureus* 4s is also reported in this chapter.

4.2. Materials and Methods

4.2.1. Materials

5 (and 6)-carboxyfluorescein diacetate succinimidyl ester (cFDA-SE), alamar blue, 3-(4,5-dimethyl-2-thiazolyl)-2,5-diphenyl-2H-tetrazolium bromide (MTT) were procured from Sigma-Aldrich (USA). Brain-Heart Infusion (BHI) broth was procured from HiMedia, Mumbai, India. Dimethyl sulfoxide (DMSO) was obtained from Merck,India. TRIzol™ Max™ Bacterial RNA Isolation Kit and superscript III platinum SYBRgreen qRT-PCR 1 step kit was obtained from Invitrogen.

4.2.2. MRSA Growth Conditions

Staphylococcus aureus 4s strain was cultured in BHI broth at 37 ºC and 180 rpm for 12 h as mentioned previously in section 2.2.2.

4.2.3. Quinoxaline-based Ligands

Synthesis and characterization of the quinoxaline-based ligands (C1-C4) is described in the Appendix of Chapter 4. The ligands were kindly provided by Professor Gopal Das, Department of Chemistry, Indian Institute of Technology Guwahati. Stock solution for each ligand (10 mg/mL) was prepared in DMSO and the specific working concentration of each ligand required for a particular experiment was prepared fresh from the stock solution.

4.2.4. Bactericidal Activity of Ligands against MRSA

4.2.4.1. Microtitre Broth Dilution Assay

The bactericidal activity of the ligands C1-C4 (0.5 µM-1024 µM each) against *S. aureus* 4s strain was ascertained in a 96-well microtitre plate using a broth dilution assay as outlined in section 2.2.4. The anti-MRSA activity of the synthetic ligands was calculated from three independent experiments, each having three replicas. Data analysis and calculation of standard deviation was performed with Microsoft Excel 2010 (Microsoft Corporation, USA).

4.2.4.2. Alamar Blue Assay

S. aureus 4s cells were grown in presence of the ligands C1-C4 (0.5 µM-1024 µM each) in BHI medium incorporated with alamar blue dye (30 µg/mL final concentration). Following overnight incubation of MRSA cells with the ligands, the absorbance of a 100 µL aliquot of medium from each sample was measured at 570 nm as well as 600 nm in a multiplate reader (Infinite M200, TECAN, Switzerland). The proliferation of cells was determined based on % resazurin reduction in the alamar blue dye reduction assay (Das *et al*., 2013) The dye reduction assay was ascertained from three independent experiments, each having three replicas. Data analysis and calculation of standard deviation was performed with Microsoft Excel 2010 (Microsoft Corporation, USA).

4.2.4.3. Microscopic Analysis

The antibacterial activity of C2 against MRSA was also ascertained by FESEM, FETEM and AFM analysis. Overnight grown cells of *S. aureus* 4s were recovered by centrifugation, washed twice with sterile PBS and resuspended in the same. The cells were then treated with 32 µM of C2 in separate sets for 6 h and 12 h at 37°C. Following incubation, untreated as well as treated cells were collected by centrifugation, washed with sterile PBS and sterile MilliQ water and finally suspended in sterile MilliQ water. In case of FESEM, the samples were prepared as described earlier in section 2.2.8.

For FETEM analysis, 10 µL aliquots of untreated and C2-treated MRSA cells suspended in sterile MilliQ water were separately drop-casted onto a carbon-coated copper grid and dried overnight in a laminar hood. The samples were then analyzed by FETEM (Model 2100F, JEOL) operating at 200 kV and their images were recorded.

In case of AFM analysis, aliquots of untreated and C2-treated MRSA cells suspended in sterile MilliQ water were separately spotted onto a sterile glass cover slip (18 mm × 18 mm) and air dried overnight in a laminar hood. Atomic force microscopic images were then acquired in non-contact mode for a 10 µm × 10 µm area at a scan rate of 0.5-1.0 line/s (Oxford Instruments plc, U.K). Cantilevers made up of silicon nitride were used having a resonant frequency of ca. 150 to 200 kHz. Analysis of the amplitude channel and topographic images was performed using the WSxM v5.0 Develop 6.5 image viewer software.

4.2.5. Membrane-targeting Activity of C2 against MRSA

The membrane-targeting activity of C2 against *S. aureus* 4s was ascertained by cFDA-SE assay. Initially, *S. aureus* 4s cells were labelled with cFDA-SE as described earlier (Thiyagarajan *et al*., 2014). cFDA-SE labelled *S. aureus* 4s cells were then incubated in separate sets with equimolar concentrations of the ligands (8.0 µM, 16 µM and 32 µM) at 37ºC and 180 rpm for 6 h. Following incubation, cells were removed by centrifugation and leakage of carboxyfluorescein from treated MRSA cells was ascertained by measuring the fluorescence of the dye in the supernatant (Thiyagarajan *et al*., 2014). The cells were resuspended in sterile PBS and the fluorescence of the cell suspension was also measured at an excitation wavelength of 488 nm and emission wavelength of 518 nm. Fluorescence measurements were acquired from three independent experimental samples.

4.2.6. Potency of C2 against MRSA Biofilm

4.2.6.1. Crystal Violet Assay and cFDA-SE Assay

S. aureus 4s biofilm was grown in BHI media supplemented with 0.25% glucose in sterile 96 well microtiter plate in presence of varying concentrations of C2 (0.5 µM - 512 µM) and incubated for 48 h in a static and humid chamber at 37 ºC. Following incubation, media from the wells was carefully aspirated and the wells were washed with sterile PBS to remove non-adherent bacterial cells. Subsequently, the biofilm biomass and metabolic activity of biofilm cells were ascertained in separate sets by performing a crystal violet assay and MTT assay and the minimum biofilm inhibitory concentration (MBIC) of C2 was determined as described previously (Goswami *et al*., 2014).

4.2.6.2. FESEM and AFM Analysis

S. aureus 4s biofilm was grown on sterile glass cover slips by following an earlier described method (Goswami *et al*., 2014) in presence of 32 µM C2 for 48 h. Following incubation, the biofilm samples were subjected to FESEM and AFM analysis by following a previously described method (Goswami *et al*., 2014).

Table 4.1. Sequence of primers used in quantitative real-time PCR-based gene expression studies.

Sl. No.	Target Gene	Oligo Sequence (5' to 3')
1.	*agrC*	Forward: CCAGCTATAATTAGTGGTATTAAGTACAGTAAACT Reverse: AGGACGCGCTATCAAACATTTT
2.	*fnbA*	Forward: ACCAGTACCACCTGCCAAAG Reverse: ACCAATGAAGCAATCAGAAAACACT
3.	*cnbA*	Forward: AATAGAGGCGCCACGACCGT Reverse: GTGCCTTCCCAAACCTTTTGAGCA

4.2.7. Effect of C2 on agrC, fnbA and cnbA Gene Expression in MRSA

Cells of *S. aureus* 4s (~10^6 CFU/mL) were grown in separate sets in BHI media incorporated with C2 (8.0 μM and 16 μM) at 37 °C and 180 rpm for 9 h. Following treatment, the total RNA from MRSA cells was isolated using TRIzol™ Max™ Bacterial RNA Isolation Kit and 200 ng of RNA from each sample was used for quantitative real-time PCR under conditions described previously (Dey *et al*., 2020). The sequence of the primers for *agrC*, *fnbA* and *cnbA* gene used in qRT-PCR is depicted in Table 4.1. The fold change in the expression of the target genes was evaluated by the $\Delta\Delta C_T$ method (Livak, *et al*., 2001). Statistical analysis for fold change in target gene expression was performed by a one-way analysis of variance (ANOVA).

4.3. Results and Discussion

4.3.1. Design Rational of Quinoxaline-based Ligands (C1-C4)

Given the widely acknowledged resistance of MRSA against therapeutic antibiotics, deployment of small synthetic ligands that can breach the fundamental resistance mechanism and potentiate the bactericidal efficacy of an antibiotic will provide significant therapeutic dividend. In this regard, quinoxaline-based ligands (C1-C4) were synthesized having varying functional groups (Basak *et al*., 2021; Basak and Das, 2021; Ghosh *et al*., 2022; Appendix Chapter 4). The quinoxaline scaffold was selected based on previous reports on their antibacterial and other pharmacological attributes (Cheng *et al*., 2016; Shintre *et al*., 2017). The quinoxaline-based ligands C1-C4 (Figure 4.1) were planar in nature and possess H-bond acceptor/donor groups. To understand the

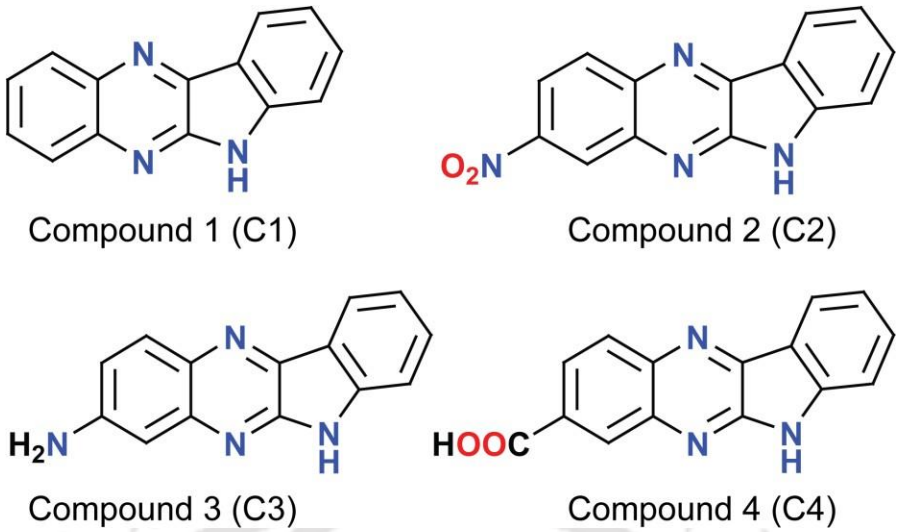

Figure 4.1. Structure of quinoxaline-based synthetic ligands (C1-C4).

role of the electronic nature of the ligands in bactericidal activity, three derivative molecules (C2 to C4) were synthesized. C2 was derivatized with the strong electron withdrawing -NO_2 group to make the scaffold electron deficient, whereas C3 and C4 were functionalized with electron donating basic (-NH_2) and acidic (-COOH) group.

4.3.2. Antibacterial Activity of Ligands

With regard to bactericidal activity against MRSA, it was observed that only C2 exhibited prominent antibacterial activity against the clinical MRSA strain *S. aureus* 4s (Figure 4.2B). This suggested that the presence of a strong electron-deficient group (-NO_2 group) perhaps contributes to the antibacterial activity of C2. The MIC of C2 against *S. aureus* 4s strain was determined to be 32 µM (Figure 4.2B), which was equivalent to that of CPX against the MRSA strain. The anti-MRSA activity of C2 was also captured in alamar blue dye assay, wherein reduction of resazurin, which can be considered as an index of the metabolic activity of live cells was dramatically reduced

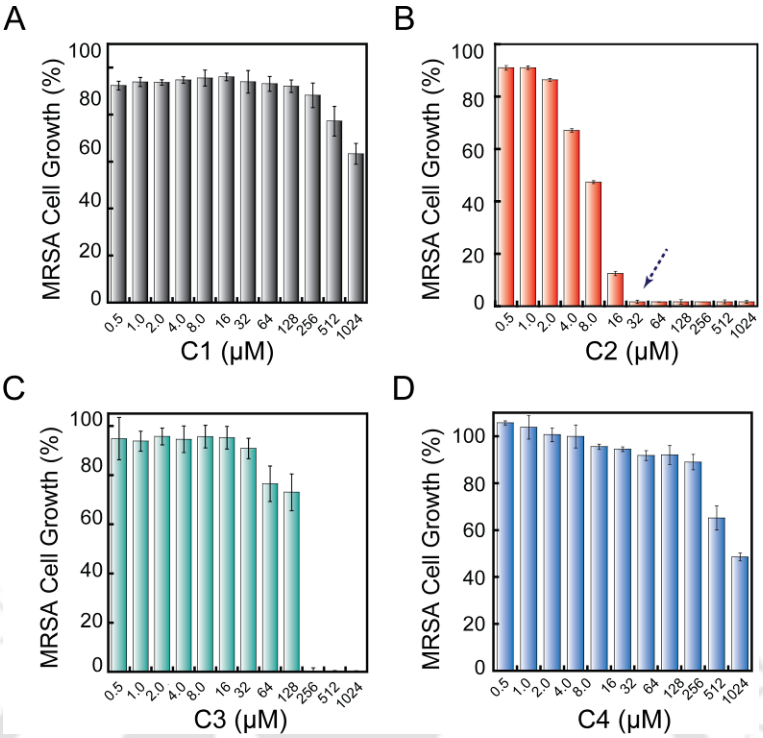

Figure 4.2. Bactericidal activity of quinoxaline-based ligands (C1-C4) determined against *S. aureus* 4s strain by microtiter well broth dilution assay. Dashed arrow in (B) indicates the MIC level of C2 (32 μM) against the target MRSA strain.

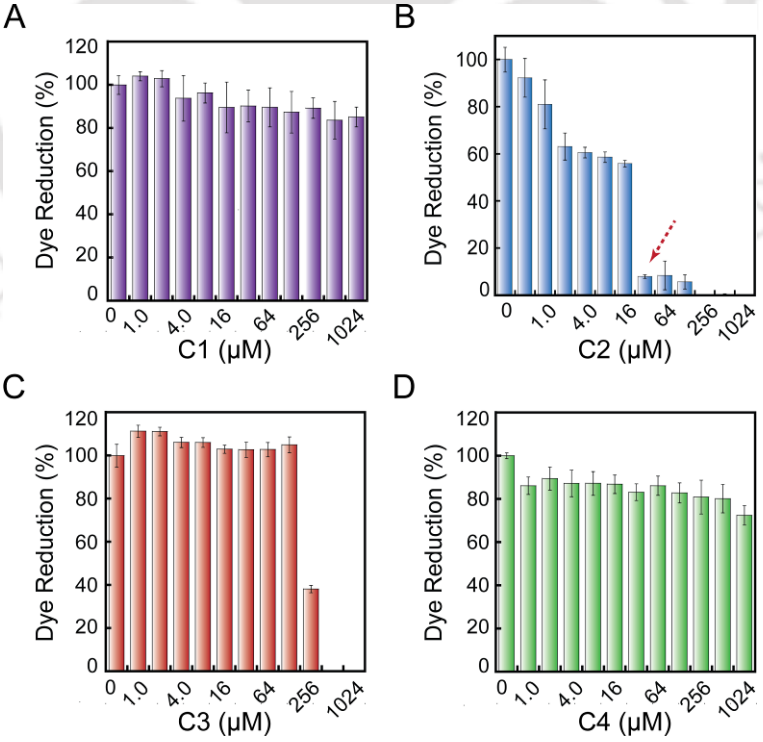

Figure 4.3. Bactericidal activity of quinoxaline-based ligands (C1-C4) determined against *S. aureus* 4s strain by alamar blue assay. Dashed arrow in (B) indicates the magnitude of dye reduction rendered by the target MRSA strain treated with 32 μM C2.

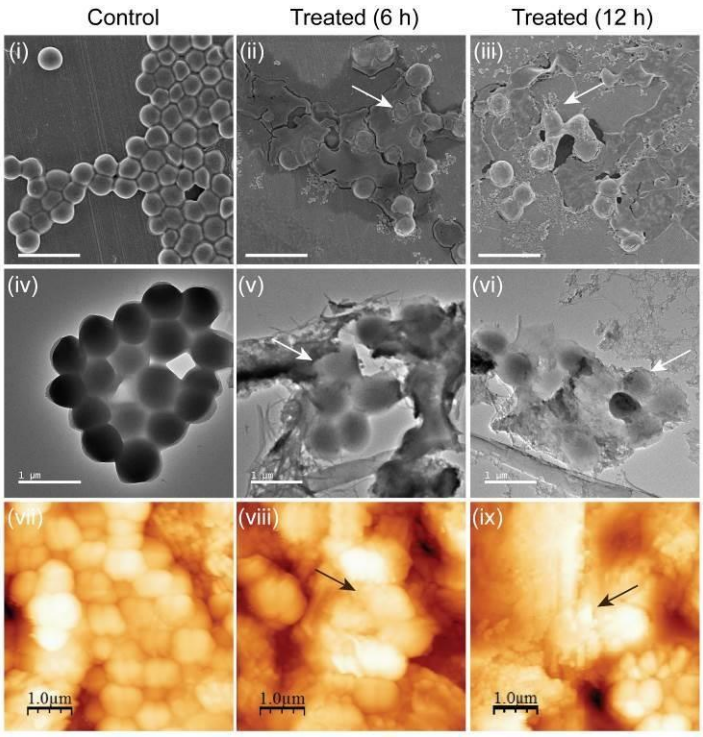

Figure 4.4. Bactericidal activity of C2 (32 µM) against *S. aureus* 4s cells ascertained by (i-iii) FESEM, (iv-vi) FETEM and (vii-ix) 2D AFM analysis. Scale bar for the images in (i-iii) is 1.0 µm. The arrows in panels ii, iii, v, vi, viii and ix indicate a loss of typical morphology in C2-treated MRSA cells.

upon treatment with C2 at a concentration of 32 µM and above (Figure 4.3B). The metabolic activity exhibited by the target MRSA strain remain virtually unaffected in presence of ligands C1 and C4 (Figure 4.3A-4.3D), while C3 could render a notable effect on the metabolic activity of MRSA only at very high concentrations of 256 µM and above (Figure 4.3C).

In order to substantiate the anti-MRSA activity of C2, microscopic analysis was pursued. In FESEM analysis, untreated cells of *S. aureus* 4s revealed a uniform margin and a morphology, characteristically associated with staphylococci (Figure 4.4, Panel i). However, cells treated with 32 µM of C2 exhibited a distorted shape and were shrunken, which suggested extensive cellular damage (Figure 4.4, Panels ii-iii). Further, the magnitude of cell damage was higher when MRSA cells were treated with C2 for a longer period of time (Figure 4.4, Panels ii-iii). A similar effect was also captured in FETEM analysis of C2-treated MRSA cells (Figure 4.4, Panels iv-vi). The effect of C2 on MRSA cells was also observed through AFM analysis, wherein the characteristic spherical morphology of MRSA cell clusters was severely affected due to large scale cell

disruption (Figure 4.4, Panels vii-ix). The extent of cell damage in MRSA was validated by analysis of average height profile, which was observed to reduce from ~ 460 nm for untreated cells to ~ 341 nm and ~ 298 nm in case of cells treated with C2 for 6 h and 12 h, respectively (Figure A4.5 in Appendix).

4.3.3. Membrane-Directed Activity of Ligands

Given the strong bactericidal activity exhibited by the antimicrobial C2, experiments were conducted with cFDA-SE labelled MRSA in order to determine the membrane-directed activity of this ligand against the target pathogen. cFDA-SE labeled cells were selected for the assay as the amine reactive fluorophore is known to conjugate with intracellular proteins and thereby prevent passive leakage of the dye from viable cells (Hoefel *et al*., 2003). The potency of a membrane-targeting bactericidal agent can then be ascertained quantitatively by measuring the extent of retention of the cell-associated dye following membrane damage and dye leakage from treated cells. In the present study, it was observed that there was a systematic increase in the leakage of cFDA from MRSA cellsupon treatment with an increasing concentration of C2. Herein, the extent of dye leakage from MRSA cells treated with 8.0 µM, 16 µM (0.5 × MIC) and 32 µM (equal to MIC level) was estimated to be ~20%, ~48% and ~80%, respectively (Figure 4.5A). Further, in case of untreated cells (control), the relative cell-associated cFDA-SE fluorescence intensity was high, which suggested the presence of a large population of viable cells (Figure 4.5B). Upon treatment with an increasing concentration of C2, there was a notable decrease in the cFDA-SE fluorescence intensity associated with MRSA cells, and apparently this phenomenon exhibited a dose-dependent effect (Figure 4.5B), akin to the earlier results obtained for dye leakage (Figure 4.5A). It can thus be conjectured that C2 displayed membrane-directed activity against MRSA wherein the ligand inducedmembrane damage and leakage of cFDA-SE dye from the affected cells. Consequently, the population of cFDA-SE labelled viable cells was also reduced significantly in a dose-dependent manner as captured in the assay (Figure 4.5B).

4.3.4. Antibiofilm Activity of C2 against MRSA

S. aureus is of serious healthcare concern in the clinics as it is known to form resilient biofilms, which pose considerable therapeutic challenge (Turner *et al*., 2019; Stoodley *et al*., 2011; Oliveira *et al*., 2018; Darouiche, 2004; Hall-Stoodley *et al*., 2004). Given

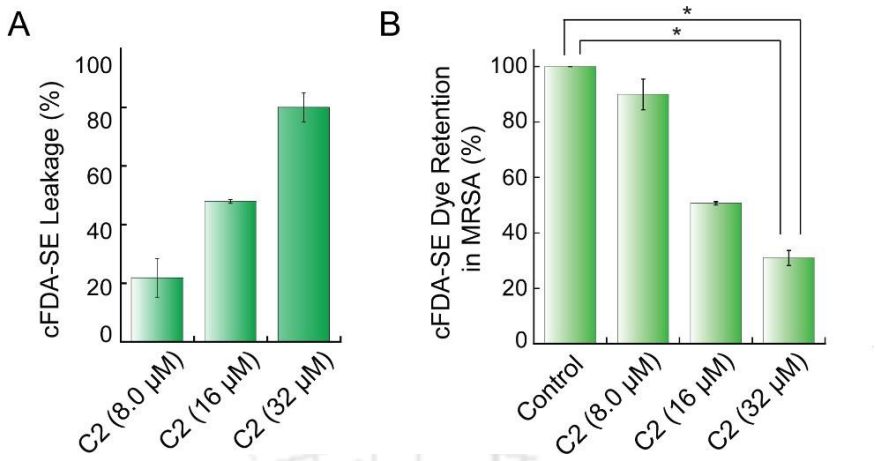

Figure 4.5. (A) Membrane disruption activity of C2 against *S. aureus* 4s cells ascertained by measuring (A) leakage of cFDA-SE dye and (B) retention of cFDA-SE dye in C2-treated cells. * in (B) indicates a *p*-value of <0.001 in one-way ANOVA.

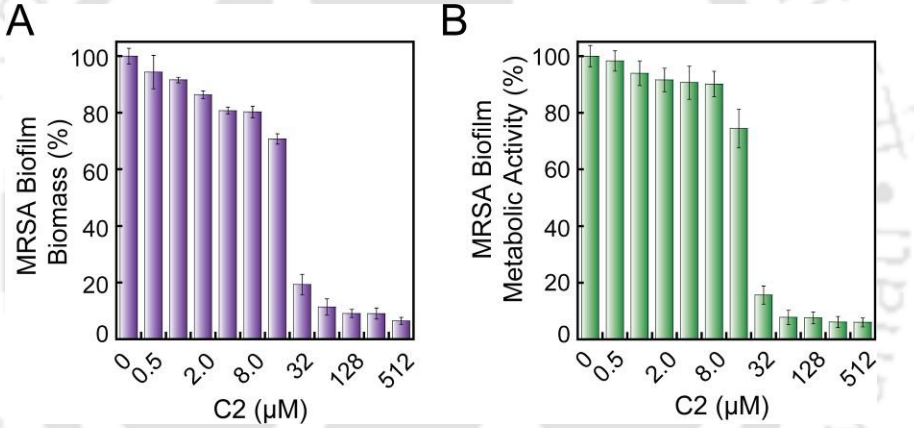

Figure 4.6. (A) Crystal violet assay to determine the effect of C2 on MRSA biofilm biomass. (B) MTT assay to ascertain the effect of C2 on MRSA biofilm metabolic activity.

that the antimicrobial C2 displayed significant bactericidal and membrane-directed activity, it was pertinent to ascertain the antagonistic effect of C2 against MRSA biofilm. To this end, solution-based assays based on crystal violet staining for biofilm biomass and MTTassay for biofilm metabolic activity revealed that C2 could impart a dose-dependent effect on the biomass as well as viability of MRSA biofilm (Figure 4.6A-4.6B). This observation indicated that the bactericidal effect of C2 against MRSA cells was retained even in the complex environment of a biofilm formed by the pathogen. It was also observed that the minimum biofilm inhibitory concentration (MBIC) of C2 against the tested MRSA strain *S. aureus* 4s was 32 µM, which also coincided with its MIC against the pathogen. The antagonistic effect of C2 on MRSA

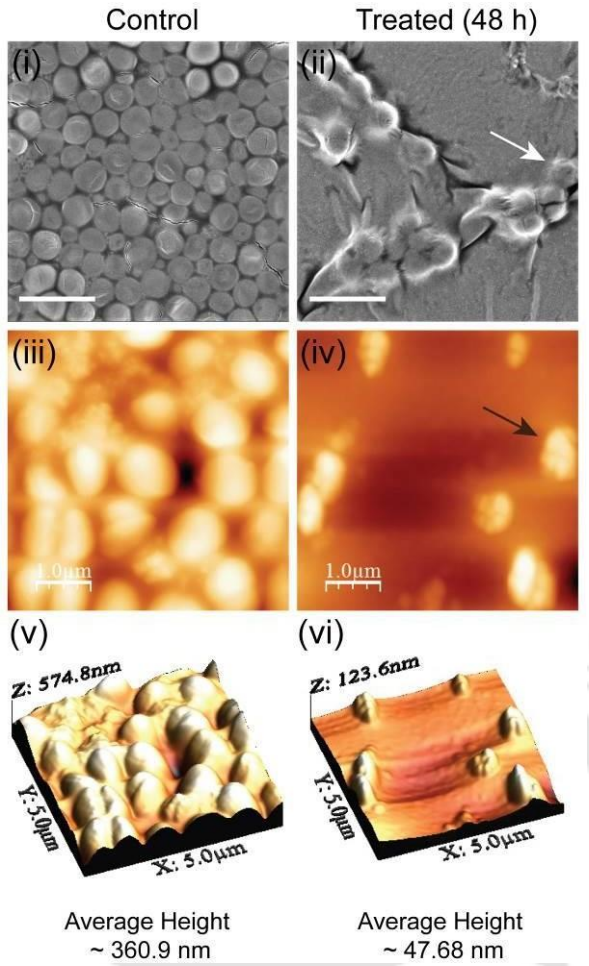

Figure 4.7. (i-ii) FESEM, (iii-iv) 2D-AFM and (v-vi) 3D-AFM analysis to evaluate the antibiofilm effect of C2 (32 µM) against *S. aureus* 4s biofilm treated for 48 h.

biofilm by C2 was also evident in FESEM analysis wherein the quintessential cell-cell adhesion associated with MRSA biofilm was breached (Figure 4.7. Panels i-ii). AFM analysis provided further evidence of the activity of C2 against MRSA biofilm, wherein the typical cell morphology was obliterated and the average height profile of treated biofilm was reduced significantly as against the control cells (Figure 4.7, Panels iii-vi).

4.3.5. Effect of C2 on the Expression of agrC, fnbA and cnbA Genes in MRSA

In the context of wound-site infections and biofilm formation on medical devices by staphylococci, expression of cell surface adhesins that are implicated in binding to host extracellular matrix such as collagen and fibronectin have a critical role (Lee *et al*., 2018; Aricola *et al*., 2012; Archer *et al*., 2011). In *S. aureus*, the accessory gene regulator (*agr*) locus is a key regulator, which governs the expression of several virulence factors such as enterotoxins, exfoliatin, cytotoxins, and the adhesins involved in binding to collagen,

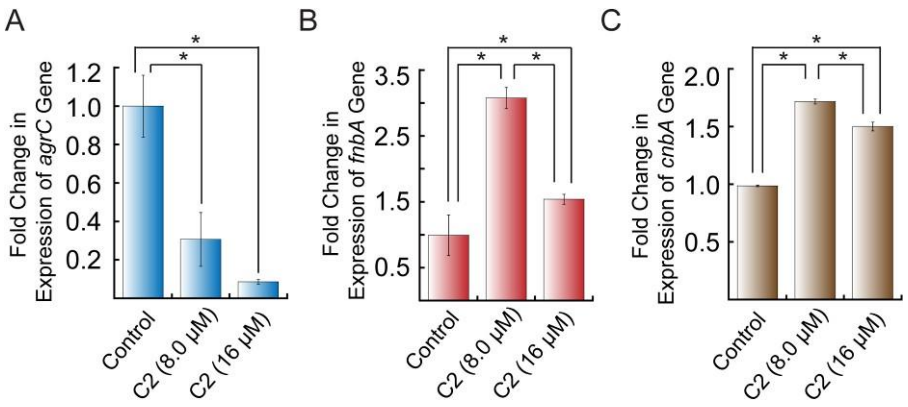

Figure 4.8. Evaluation of *agrC*, *fnbA* and *cnbA* gene expression in *S. aureus* 4s treated with C2. * indicates *p* value < 0.001 in one-way ANOVA.

fibronectin and fibrinogen (Novick, 2003; Jarraud *et al*., 2000; Aricola *et al*., 2012). It is also acknowledged that in *S. aureus*, *agr* is not involved significantly in early biofilm formation, while it accentuates biofilm dispersion (Aricola *et al*., 2012). However, following early biofilm development, there is an upregulation of the *agr* genes, which results in suppression of adhesins expression (Archer *et al*., 2011). In the current investigation, it was observed that the antimicrobial C2 displayed considerable activity against MRSA biofilm. Hence, it was conceived that it would be pertinent to conduct experiments and ascertain the effect of C2 on the expression of *agr* and the adhesin specific genes *fnbA* and *cnbA* coding for fibronectin binding protein and collagenbinding protein, respectively, in MRSA. A qRT-PCR analysis indicated that the expression of *agrC* gene (coding for histidine kinase element of the *agr* operon) in MRSA was significantly downregulated upon treatment with sub-MIC levels of C2 in a dose-dependent manner (Figure 4.8A). To this end, the fold change in the expression of*agrC* in MRSA upon treatment with 8.0 µM and 16 µM C2 was observed to be ~0.30 and ~0.09, respectively (Figure 4.8A). The ability of C2 to downregulate *agrC* augers well as suppression of *agr* expression is likely to lead to lower levels of toxin productionby MRSA, which in turn may reduce the risk of invasive as well as skin and soft tissue infections caused by the pathogen (Lee *et al*., 2018; Cheung *et al*., 2011). In case of the adhesin genes, it was observed that in presence of 8.0 µM C2, expression of *fnbA* and *cnbA* genes in the MRSA strain were elevated with the fold change in expression being ~3.0 and ~1.7, respectively (Figure 4.8B-4.8C). A suppressed level of expression of *agrC* observed earlier in presence of 8.0 µM C2 (Figure 4.8A) may account for the higher levels of *fnbA* and *cnbA* gene expression in MRSA, since it is known that *agr* can

negatively regulate adhesin gene expression *agr* genes, which results in suppression of adhesins expression (Archer *et al*., 2011). In comparison to the treatment with 8.0 µM C2, it was interesting to observe that in presence of 16 µM C2, which is equivalent to 0.5 × MIC against the tested MRSA strain, expression of both *fnbA* and *cnbA* genes were diminished with the fold change in expression being ~1.5 for both the genes (Figure 4.8B-4.8C). It is envisaged that the ability of C2 to dampen the expression levels of the adhesin genes *fnbA* and *cnbA* in a dose-dependent manner will be beneficial as a preventative therapeutic strategy against MRSA biofilm formation. To this end, it may be mentioned that in the current study, solution-based crystal violet and MTT assay have indeed revealed significant inhibition of MRSA biofilm formation when C2 was used at concentrations in excess of 16 µM (Figure 4.6). Based on its effect on the expression levels of the adhesin genes *fnbA* and *cnbA*, it is also envisioned that C2 can hold considerable potential as an anti-MRSA coating agent on catheters and other implanted medical devices as these adhesins are implicated in colonization of MRSA on medical devices and other abiotic surfaces (Lee *et al*., 2018; Aricola *et al*., 2012).

4.4. Significant Findings

The salient findings of the present study can be stated as follows:

1. Amongst a set of rationally designed quinoxaline-based synthetic ligands (C1-C4), the ligand C2 displayed strong bactericidal activity against the MRSA strain *S. aureus* 4s, with an MIC of 32 µM.

2. A cFDA-SE dye-based fluorescent assay revealed a dose-dependent membrane-directed activity rendered by C2 on MRSA cells.

3. A dose-dependent activity of C2 against MRSA biofilm was evidenced in solution-based crystal violet and MTT assay, wherein the minimum biofilm inhibitory concentration (MBIC) of C2 against *S. aureus* 4s biofilm was observed to be 32 µM.

4. A quantitative real-time PCR analysis indicated that the expression of the regulator element *agrC* and the adhesin genes *fnbA* and *cnbA*, which are implicated in biofilm formation were suppressed upon treatment with C2.

Based on the key leads obtained in this study, it is evident that the quinoxaline antimicrobial C2 may hold therapeutic potential as an antibacterial to mitigate MRSA infections. Besides,the membrane-directed activity of C2 can perhaps be leveraged in a combinatorial treatment regimen to heighten the activity of a conventional antibiotic for elimination of MRSA. To this end, in the following chapter, the adjuvant potential of C2 in enhancing the efficacy of CPX is ascertained against planktonic cells as well as biofilm of MRSA.

Chapter 5

Potential of Quinoxaline-based Antimicrobial (C2) in Combination Therapy for Mitigation of MRSA in an*In Vitro* Bone Cell Infection Model

This chapter evaluates the adjuvant potential of C2 in enhancing the efficacy of CPX against MRSA. The efficacy of the combination treatment of C2 and CPX in curbing MRSA invasion in an in vitro bone cell infection model is also presented in this chapter.

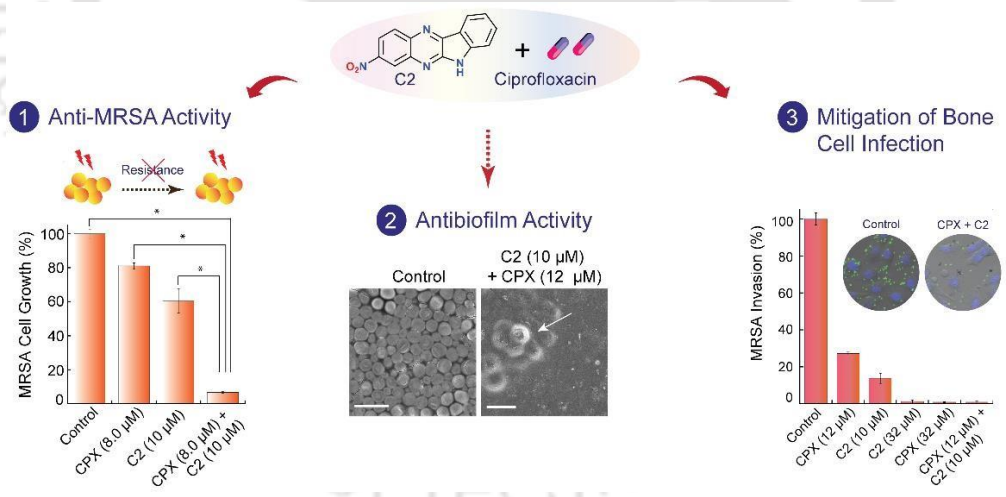

ABSTRACT

The present chapter illustrates the results of the studies performed to determine the adjuvant potential of C2 in enhancing the efficacy of CPX against MRSA. A checkerboard assay indicated that the MIC of CPX against *S. aureus* 4s was decreased to 8.0 µM (4-fold reduction) in combination with 10 µM, 12 µM and 16 µM C2, and in presence of 10 µM C2 and 8.0 µM CPX, growth of MRSA was significantly reduced (~ 7.0 % growth). Further, in case of the combinatorial treatment regimen, growth of the target MRSA cells was completely arrested till 360 generations as the membrane-targeting activity of C2 could effectively deter the emergence of ciprofloxacin resistance trait in MRSA cells. A combination of 10 µM C2 and 12 µM CPX rendered a prominent inhibition of MRSA biofilm formation, wherein the biofilm metabolic activity was reduced to only ~ 11%. Moreover, the MBIC of CPX against *S. aureus* 4s biofilm was 12.0 µM (~ 10-fold reduction) and a synergistic interaction was observed between C2 and CPX based on an estimation of the FIC index. Superior inhibition of MRSA biofilm in the combination treatment was also captured in FESEM and AFM analysis, which revealed extensive disruption of cell integrity and cell-cell adhesion. Based on the encouraging leads, the therapeutic potential of the combination treatment regimen was assessed in an *in vitro* bone cell infection model for MRSA. An adhesion assay indicated that only ~ 17% of MRSA cells adhered onto cultured MG-63 cells (human osteosarcoma cells) in case of the combinatorial treatment (12 µM CPX and 10 µM C2), which was significantly lower than that observed in case of treatment with either 12 µM CPX or 10 µMC2 alone. A similar trend was also observed in an invasion assay wherein in case of the combinatorial treatment regimen, the relative MRSA cell invasion onto MG-63 cells was estimated to be only ~ 0.37%. A dual-label fluorescence microscopic analysis provided additional evidence of the efficacy of the combinatorial treatment regimen in reducing MRSA cell invasion into MG-63 cells. The therapeutic benefit of the combinatorial treatment of C2 and CPX was evident as the viability of cultured MG-63 cells was observed to be ~ 91 %.

5.1. Introduction

The global healthcare burden of infections caused by MRSA in the clinics and the community setting has reached an epidemic proportion (Chambers and DeLeo, 2008; Tong *et al*., 2015; Lee *et al*., 2018; Turner *et al*., 2019; Craft *et al*., 2019). Therapeutic interventions against MRSA advocate the use of antibiotics such as vancomycin, daptomycin or linezolid (Lee *et al*., 2018; Liu *et al*., 2011), whereas other antibiotics such as ceftaroline, telavancin and delafloxacin are emerging in the pipeline for therapeutic use against MRSA (Lee *et al*., 2018). However, due to a rapid evolution of antimicrobial resistance traits in MRSA strains against critical antibiotics (Weigel *et al*., 2003; Rossi *et al*., 2014; Richter *et al*., 2011; Wuthrich *et al*., 2019), there is an urgent demand for alternate therapeutic intercessions that can curb MRSA infections. Moreover, MRSA is also known to readily form biofilms in tissues and implantable medical devices, wherein a matrix envelope can not only protect the embedded cells from the host immune system but can also act as a permeability barrier and impede the penetration of chemotherapeutic agents and antibiotics (Arciola *et al*., 2018; Stoodley *et al*., 2011; Oliveira *et al*., 2018; Hall and Mah, 2017; Craft *et al*., 2019).

The limitations and poor efficacy of antibiotic-mediated monotherapy combined with the protracted process of drug discovery against MRSA has further exacerbated the crisis in the clinics. In order to overcome this challenge, combination therapy has been perceived as a promising approach for alleviation of MRSA infections (Yu *et al*., 2020; Hawas *et al*., 2022; Cascioferro *et al*., 2021). For instance, studies have demonstrated that antibiotic combinations can be deployed for countering MRSA infections (Yu *et al*., 2020; Yan *et al*., 2018; Wang *et al*., 2020; Gidari *et al*., 2020). However, combination of antibiotics may often bear host-directed toxic implications. In this regard, the potential of small synthetic molecules to breach the resistance in target cells is worth exploring in restoring susceptibility of the pathogen to therapeutic antibiotics. To this end, some recent studies have indeed validated this premise and have demonstrated the use of various rationally designed polymeric as well as small molecules as adjuvants for rendering an efficient combination therapy directed against MRSA (Namivandi-Zangeneh *et al*., 2021; Wang *et al*., 2022; Vermote *et al*., 2017; Thappeta *et al*., 2020; Lee *et al*., 2022; Berndsen *et al*., 2022).

In case of a combination therapy directed against MRSA, small molecule adjuvants that can counter a core resistance barrier such as the membrane in target cells and thereby enhance antibiotic uptake can hold interesting prospect in re-establishing

susceptibility of the pathogen to antibiotics. Herein, membrane-targeting adjuvants emerge as potent candidate molecules that can increase the therapeutic efficacy of antibiotics in combination therapy (Dey *et al*., 2018; Kim *et al*., 2018; Kang *et al*., 2021; Thappeta *et al.*, 2020; Xiong *et al*., 2022). Based on this notion, in the current study, the potential of the membrane-acting quinoxaline antimicrobial C2 as an adjuvant to potentiate the efficacy of ciprofloxacin against MRSA planktonic cells as well as biofilm is investigated. Further, in this chapter, the therapeutic potential of the combination treatment regimen of C2 and ciprofloxacin against MRSA is also assessed in an *in vitro*bone cell infection model.

5.2. Materials and Methods

5.2.1. Materials

5 (and 6)-carboxyfluorescein diacetate succinimidyl ester (cFDA-SE), ciprofloxacin, Dulbecco's Modified Eagle Medium (DMEM), trypsin-EDTA and 3-(4,5-dimethyl-2-thiazolyl)-2,5-diphenyl-2H-tetrazolium bromide (MTT) were procured from Sigma-Aldrich (USA). Brain-Heart Infusion (BHI) broth was procured from HiMedia, Mumbai, India. Dimethyl sulfoxide (DMSO) was obtained from Merck, India. Fetal bovine serum (FBS) was obtained from PAA Laboratories, USA.

5.2.2. MRSA Growth Conditions

Staphylococcus aureus 4s strain was cultured in BHI broth at 37 ºC and 180 rpm for 12 h as mentioned previously in section 2.2.2.

5.2.3. Combinatorial Effect of C2 and Ciprofloxacin (CPX) on MRSA Cells

A checkerboard assay was performed in a sterile 96-well microtitre plate to ascertain the combination effect of C2 and ciprofloxacin on MRSA cells. In the assay, sub-MIC levels of C2 (8.0 µM, 10 µM, 12 µM and 16 µM) were selected in separate sets with every chosen concentration of CPX (1.0 µM - 16 µM). Following the combinatorial treatment at 37 ºC and 180 rpm for 12 h, growth of *S. aureus* 4s cells was recorded by measuring absorbance at 600 nm (Infinite M200, TECAN, Switzerland) and expressed as percentage growth as compared to untreated cells. In the combinatorial treatment regimen, the MIC of CPX in presence of C2 was determined and the fractional inhibitory concentration (FIC) index for the combination treatment was determined by following a previously described method (Giacometti *et al*., 2000). In a separate experiment, the

magnitude of dye leakage from cFDA-SE labelled *S. aureus* 4s cells subjected to treatment with 8.0 µM C8 and 8.0 µM CPX was also determined. Statistical analysis for cell growth and cFDA-SE dye leakage observed in MRSA cells upon combinatorial treatment (8.0 µM C8 and 8.0 µM CPX) as compared to cells treated with either 8.0 µM C8 or 8.0 µM CPX was performed by a one-way analysis of variance (ANOVA) using Sigma Plot version 11.0.

The potential of C2 in enhancing the potency of CPX against MRSA cells was also ascertained by FESEM analysis. Overnight grown cells of *S. aureus* 4s were recovered by centrifugation, washed twice with sterile PBS and resuspended in the same. The cells (~10^6 CFU/mL) were then incubated in separate sets with either 8.0 µM of C2 or 8.0 µM CPX or a combination of CPX (8.0 µM) and C8 (8.0 µM) for 12 h at 37 ºC and 180 rpm. Untreated cells (control) were also incubated in sterile PBS under the same conditions. Following incubation, untreated as well as treated cells were processed for FESEM analysis by essentially following the protocol described in section 2.2.8. The prepared samples were analyzed in a field emission scanning electron microscope (Zeiss Sigma, USA) at 3.0-5.0 kV and their images were recorded.

5.2.4. In Vitro Resistance Development in MRSA against CPX in Presence of C2

In vitro resistance development in *S. aureus* 4s cells against (a) 32 µM C2 and (b) a combination of 8.0 µM C2 and 8.0 µM CPX was ascertained by measuring MRSA cell growth in sequential cycles of growth as described in section 2.2.10. The experiment was conducted for a total of 360 generations of *S. aureus* 4s cell growth.

5.2.5. Effect of the Combinatorial Treatment of C2 and CPX on MRSA Biofilm

S. aureus 4s biofilm was grown in BHI media supplemented with 0.25% glucose in a sterile 96 well microtiter plate in presence of varying concentrations of C2 and CPX for 48 h in a static and humid chamber at 37 ºC. MRSA biofilm was grown in separate sets wherein varying levels of C2 (8.0 µM or 10 µM) were selected for every chosen concentration of CPX (8.0 µM or 12 µM). Following incubation for 48 h, the spent media from the wells was carefully aspirated and the wells were washed with sterile PBS to remove non-adherent cells. Subsequently, estimation of metabolic activity of biofilm cells and microscopic analysis of biofilm cells (FESEM and AFM analysis) was accomplished by following methods similar to that of C2 alone against MRSA biofilm as described earlier in section 4.2.6. The minimum biofilm inhibitory concentration of

CPX and the FIC index for the combination treatment was determined by following a previously described method (Thiyagarajan *et al*., 2017).

5.2.6. In Vitro Bone Cell Infection Model

Prior to the bone cell infection experiment, the cytotoxic potential of 10 µM C2, 12 µM CPX and a combination of both (10 µM C2 and 12 µM CPX) against cultured MG-63 cells was ascertained by performing an MTT assay. The growth conditions for MG-63 cells and the basic protocol of the MTT assay was similar to an earlier described method (Mullick *et al*., 2021). Studies to evaluate the ability of C2 in combination with CPX to mitigate MRSA infection in bone cells were conducted in a cell culture model by essentially following a protocol described earlier for a bacterial infection model in cancer cells (Singh *et al*., 2019). Initially, MG-63 cells (human osteosarcoma cells) were seeded in 96-well microtitre plate (~10^4 cells/well) and grown in DMEM medium supplemented with 10% FBS, penicillin (100 µg/mL) and streptomycin (100 µg/mL) at 37 °C under a humidified atmosphere of 5% CO_2 for 24 h. The MG-63 cells were then washed twice with sterile PBS and overnight grown cells of *S. aureus* 4s suspended in antibiotic-free DMEM medium were then added to MG-63 cells at a MOI (multiplicity of infection) of 100:1. Subsequently, in separate sets, the following were added to MRSA infected MG-63 cells: (a) CPX (12 µM), (b) C2 (12 µM), (c) C2 (32 µM), (d) CPX (32 µM) and (e) a combination of CPX (12 µM) and C2 (12 µM). In one set, MRSA-infected MG-63 cells subjected to the aforementioned treatment sets were then incubated under 5% CO_2 for 2 h, washed with sterile PBS to remove excess MRSA, lysed with 0.1% Triton X-100 and plated in BHI agar to enumerate MRSA cells. The cell numbers obtained for control sample (MG-63 cells infected with MRSA and devoid of any treatment with either C2 or CPX) was considered as a reference for MRSA cell adhesion (100% adhesion) and adhesion for other treated samples were expressed relative to the control. In another set, MRSA-infected MG-63 cells subjected to various treatment and incubated under 5% CO_2 for 2 h were washed with sterile PBS to remove excess MRSA and then incubated again in DMEM medium for another 2 h under 5% CO_2 to allow MRSA cell invasion. The cells were then lysed with 0.1% Triton X-100 and plated in BHI agar to enumerate MRSA cells. As described earlier for cell adhesion, the cell numbers obtained for control sample was considered as a reference for MRSA cell invasion (100% invasion) and invasion for other treated samples were expressed relative to the control. In case of imaging studies,

S. aureus 4s cells were labelled with cFDA-SE (Singh *et al*., 2012) and MG-63 cells were labelled with DAPI (Mukherjee and Ramesh, 2017). The labelled cells were then used in performing the infection experiment as outlined before. Herein, MG- 63 cells were seeded into confocal dish (20 mm diameter) instead of 96-well microtitre plate. MRSA-infected MG-63 cells subjected to various treatment regimen were washedthrice with sterile PBS and their images were captured using a confocal microscope (Zeiss LSM 880, Germany). During cell imaging, the excitation wavelength used for the laser was 405 nm for blue emission and 488 nm for green emission.

5.3. Results and Discussion

5.3.1. Combinatorial Effect of C2 and Ciprofloxacin (CPX) on MRSA Cells

In an earlier study it was observed that the MIC of CPX against the MRSA strain *S. aureus* 4s was 32 µM (Thiyagarajan *et al*., 2017). Interestingly, a checkerboard assay performed in the present study revealed that the MIC of CPX against *S. aureus* 4s was decreased in presence of an increasing concentration of C2 (Table 5.1). For instance, the MIC of CPX against the MRSA strain was reduced to 8.0 µM (4-fold reduction) in combination with 10 µM, 12 µM and 16 µM C2 (Table 5.1). In a control experiment, it was observed that MRSA cell growth was substantial in presence of 8.0 µM CPX alone (~ 81% growth) (Figure 5.1A). On the other hand, MRSA cell growth was also notable in presence of 10 µM C2 alone (~ 60% growth) (Figure 5.1A). Interestingly, in presence of 10 µM C2 and 8.0 µM CPX, growth of MRSA was significantly reduced (~ 7.0 % growth) (Figure 5.1A). It may also be mentioned here that for this combination (10 µM C2 and 8.0 µM CPX), an additive effect was observed based on the estimation of theFIC index. The potency of the combinatorial treatment regimen against MRSA was also captured in a cFDA-SE leakage assay, which indicated considerably higher degree of membrane damage in the target cells (Figure 5.1B). Herein, the extent of dye leakage from MRSA cells treated with 8.0 µM CPX or 8.0 µM C2 singularly was estimated to be ~ 22% and ~ 48%, respectively (Figure 5.1B). However, the dye leakage from MRSA cells subjected to the combinatorial treatment (10 µM C2 and 8.0 µM CPX) was estimated to be ~ 80%, which was equivalent to the magnitude of dye leakage observedin case of MRSA cells treated with MIC level (32 µM) of either C2 or CPX alone (Figure 5.1B). These results suggest that in the combinatorial treatment, C2 could perhaps breachthe membrane barrier and enhance CPX uptake in MRSA cells.

Table 5.1. Absorbance values (A_{600} ± standard deviation) obtained in the checkerboard assay for *S. aureus* 4s cells treated with a combination of C2 and ciprofloxacin.

C2 (µM)	Ciprofloxacin (µM)				
	1.0	**2.0**	**4.0**	**8.0**	**16**
0	1.076 ± 0.005	0.992 ± 0.036	0.927 ± 0.029	0.816 ± 0.016	0.514 ± 0.016
8.0	0.389 ± 0.020	0.351 ± 0.012	0.356 ± 0.008	0.162 ± 0.001	0.051 ± 0.001*
10	0.339 ± 0.010	0.339 ± 0.011	0.290 ± 0.001	0.094 ± 0.002*	0.050 ± 0.001
12	0.325 ± 0.016	0.327 ± 0.013	0.268 ± 0.007	0.062 ± 0.002*	0.048 ± 0.001
16	0.278 ± 0.012	0.155 ± 0.005	0.108 ± 0.014	0.055 ± 0.003*	0.068 ± 0.023

* Indicates minimum inhibitory concentration (MIC) of ciprofloxacin (CPX) obtained in the checkerboard assay. MIC of CPX was assigned as the lowest concentration of the antibiotic, which resulted in A_{600} value of <0.1 in the checkerboard assay.

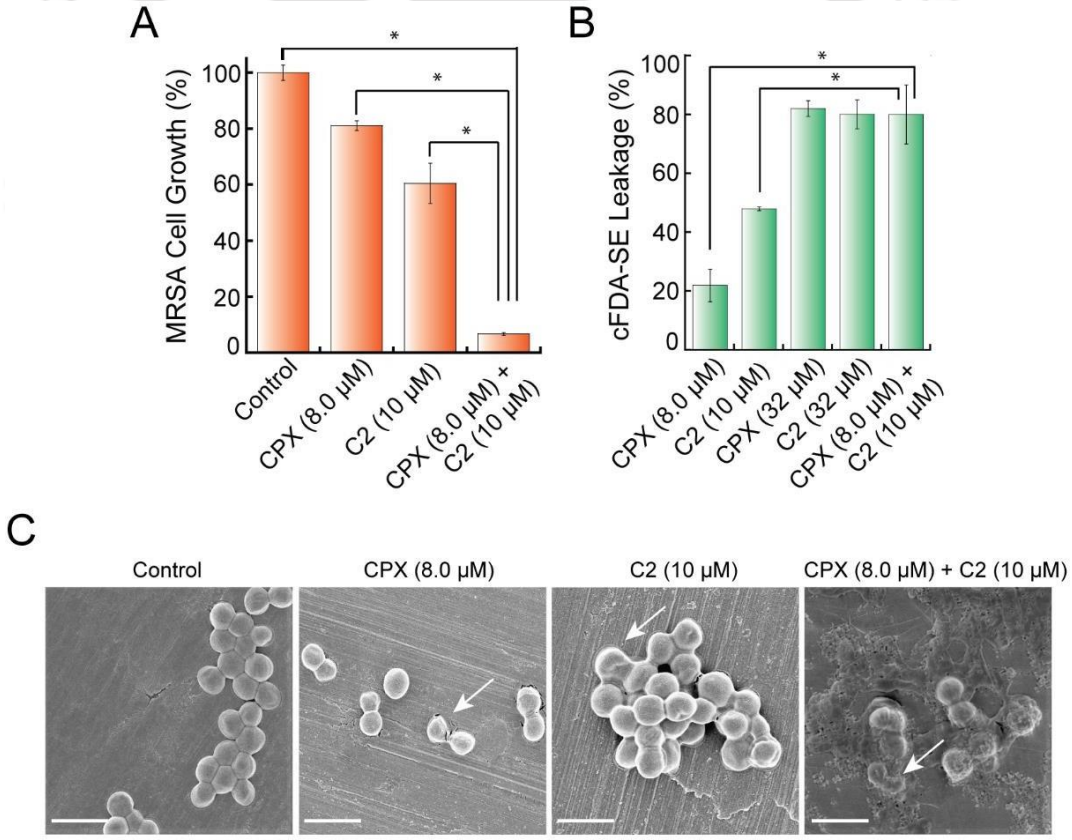

Figure 5.1. (A) Effect of the combinatorial treatment of C2 and CPX on the growth of *S. aureus* 4s. (B) Analysis of membrane-directed activity for the combinatorial treatment regimen by CFDA-SE leakage assay (C) FESEM analysis to ascertain the effect of combinatorial treatment with C2 and CPX on *S. aureus* 4s cells. Scale bar for the images is 1.0 µm.

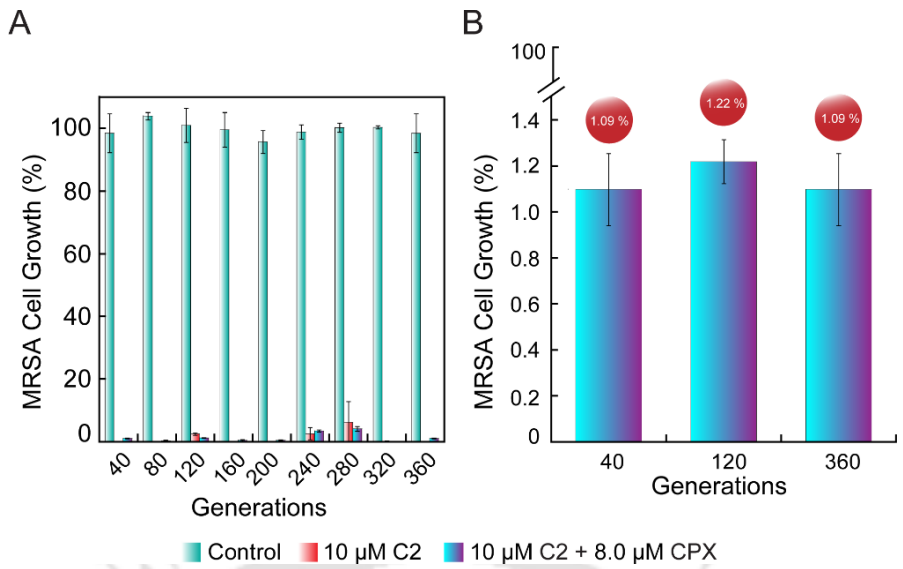

Figure 5.2. (A) Estimation of *S. aureus* 4s cell growth propagated for multiple generations either in presence of 32 µM C2 or a combination of 8.0 µM C2 and 8.0 µM CPX. (B) Magnified view of (A) indicating the percentage growth of MRSA cells attained over several generations.

The tandem effect of C2 and CPX thus resulted in significant cell death and membrane damage as evident from the high degree of dye leakage (~ 80%) observed in the treated cells (Figure 5.1B). FESEM analysis provided additional evidence of heightened cellular damage in MRSA following treatment with CPX and C2 in combination (Figure 5.1C), in contrast to the partial morphological distortion in MRSA cells treated with 8.0 µM CPX or 10 µM C2 singularly or the typical spherical morphology observed in case of untreated control cells (Figure 5.1C).

5.3.2. Potential of C2 in Preventing Development of Ciprofloxacin Resistance in MRSA

In order to ascertain the merit of C2 as an adjuvant in combination therapy against MRSA, it was pertinent to probe whether C2 could preventing development of CPX-resistance in MRSA cells when subjected to a combination treatment with C2 and CPX. To this end, *S. aureus* 4s cells were treated for 360 generations in separate sets with either 32 µM C2 (equal to MIC of C2 against *S. aureus* 4s) or with a combination of 10 µM C2 and 8.0 µM CPX. In presence of 32 µM C2 alone (MIC level) growth of *S. aureus* 4s cells was remarkably arrested till 360 generations (Figure 5.2A). This suggested the inability of MRSA cells to develop any resistance against the action of the ligand C2 over multiple generations of growth. With regard to CPX, an earlier study had indicated that *S. aureus* 4s cells displayed a propensity to develop high resistance against the antibiotic,

especially when MRSA cells were grown beyond 40 generations (Figure 2.8A-2.8B). Interestingly, in the current study, when *S. aureus* 4s cells were treated with a combination of 10 μM C2 and 8.0 μM CPX (four-fold lower concentrations than MIC of CPX against *S. aureus* 4s), cell growth was completely subdued (only ~ 1.0 growth) till 360 generations (Figure 5.2A-5.2B). This implied that even in presence of low concentrations of C2 and CPX, development of CPX resistance in the target cells was prevented. Thus, in the combination treatment regimen, the ligand C2 holds considerable potential to breach the membrane-associated resistance mechanism and mediate elimination of MRSA by low levels of CPX in a therapeutic cycle extending over several generations of cell growth.

5.3.3. Combinatorial Effect of C2 and Ciprofloxacin (CPX) on MRSA Biofilm

MRSA biofilm is resistant to conventional antibiotic therapy and is implicated in a large number of tissue- as well as implant-based infections (Turner *et al*., 2019; Lee *et al*., 2018; Oliveira *et al*., 2018; Stoodley *et al*., 2011). In order to hinder MRSA biofilms, combination of antimicrobials has been advocated as an effective therapeutic strategy. For instance, studies have demonstrated the feasibility of using anti-biofilm agents in combination with antibiotics or using multiple antibiotics in tandem in order to effectively curb MRSA biofilm (Cascioferro *et al*., 2021; Feldman *et al*., 2020; Lam *et al*., 2020; Thappeta *et al*., 2020). In the present investigation, it was observed that the ligand C2 could hinder MRSA biofilm formation and the MBIC of C2 against *S. aureus* 4s biofilm was 32 μM (Figure 4.6 in Chapter 4). Further, it was envisaged that the potent membrane-directed activity of C2 against MRSA (Figure 4.6 in Chapter 4) can perhaps be leveraged to breach the membrane in the matrix encased cells of MRSA biofilm and restore their susceptibility to the action of antibiotics in combination therapy. To this end, antibiofilm assay was performed in presence of C2 and CPX used at various concentrations. When 8.0 μM C2 was used in conjunction with either 8.0 μM CPX or 12 μM CPX, a dose-dependent effect on MRSA biofilm was evident through estimation of biofilm metabolic activity (Table 5.2). For instance, *S. aureus* 4s biofilm metabolic activity was estimated to be ~ 50% and ~ 42% in presence of a combination of either 8.0 μM C2 and 8.0 μM CPX or 8.0 μM C2 and 10 μM CPX, respectively (Table 5.2). This dose-dependent effect of the combination therapy on MRSA biofilm was unequivocal and was also captured when 10 μM C2 was used in conjunction with either 8.0 μM CPX or 12 μM CPX (Table 5.2). Interestingly, the inhibition of MRSA

Table 5.2. Determination of *S. aureus* 4s biofilm biomass and metabolic activity obtained in presence of a combination treatment with C2 and ciprofloxacin.

Combination Treatment	MRSA Biofilm Metabolic Activity (% ± Standard Deviation)
C2 (8.0 µM) + CPX (8.0 µM)	50.56 ± 2.22
C2 (8.0 µM) + CPX (12 µM)	42.34 ± 1.97
C2 (10 µM) + CPX (8.0 µM)	38.65 ± 1.79
C2 (10 µM) + CPX (12 µM)	11.22 ± 1.33

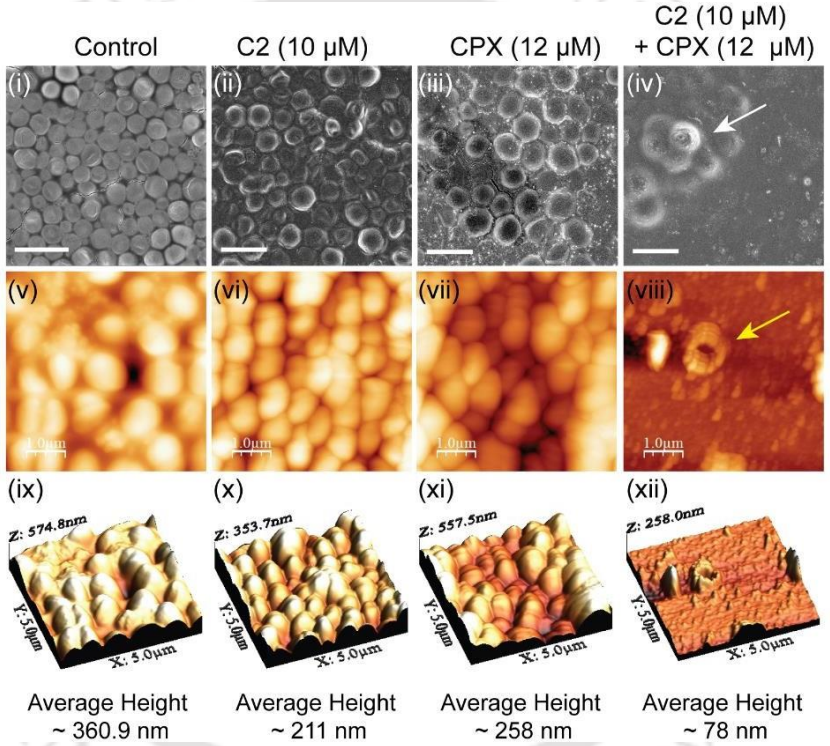

Figure 5.3. Effect of combinatorial treatment of C2 and CPX on *S. aureus* 4s biofilm ascertained by (i-iv) FESEM, (v-viii) AFM 2D and (ix-xii) AFM 3D image analysis. White arrow in panel (iv) and yellow arrow in panel (viii) indicate distorted morphology of MRSA cell subjected to the combinatorial treatment. Scale bar for the images in (i-iv) is 1.0 µm.

biofilm formation was remarkable in presence of 10 µM C2 and 12 µM CPX, wherein the biofilm metabolic activity was reduced to ~ 11%, (Table 5.2). It may be mentioned here that in presence of 10 µM C2, the MBIC of CPX against *S. aureus* 4s biofilm was

12.0 μM (~ 10-fold reduction in MBIC), whereas the estimation of the FIC index suggested that a synergistic interaction was achieved between C2 and CPX.

Inhibition of MRSA biofilm in the presence of 10 μM C2 and 12 μM CPX was further substantiated by microscopic analysis. FESEM analysis revealed that in case of control MRSA biofilm (untreated), the typical spherical shape of *S. aureus* cells and the characteristic cell-cell adhesion associated with biofilm formation was apparent (Figure 5.3, Panel i). A marginal distortion of both the cell morphology as well as the cell-cell adhesion was observed when *S. aureus* 4s biofilm was grown in presence of either 10 μM C2 or 12 μM CPX alone (Figure 5.3, Panels ii-iii). However, in case of the combination treatment (10 μM C2 and 12 μM CPX), there was a prominent disruption of cell-cell adhesion and the biofilm associated MRSA cells were largely disintegrated (Figure 5.3, Panel iv). AFM analysis further provided evidence of the potential of the combination treatment for mitigation of MRSA biofilm (Figure 5.3, Panels v-xii). Herein, a 3D topography image analysis revealed that the height profile reduced significantly from ~ 360 nm for untreated MRSA biofilm to ~ 78 nm in case of MRSA biofilm treated with 10 μM C2 and 12 μM CPX for 48 h (Figure 5.3, Panels ix-xii). Collectively, the results of the combination treatment experiments indicated that the membrane-directed activity and the antibiofilm activity displayed by ligand C2 against MRSA planktonic cells, which was determined in earlier studies (Figure 4.5-4.7 in Chapter 4) could be leveraged to potentiate the efficacy of CPX and thereby curb MRSA biofilm formation effectively. The results also reinforce the utility of deploying a membrane-acting agent in combination therapy for mitigation of MRSA biofilm as reported in earlier studies (Guo *et al*., 2021; Kim *et al*., 2019; Thiyagarajan *et al*., 2017; Goswami *et al*., 2014; Xiong *et al*., 2022; Kang *et al*., 2021; Thappeta *et al*., 2020).

5.3.4. Potential of Combination Therapy with C2 and CPX in an In vitro Bone Cell Infection Model

MRSA has been largely implicated in chronic bone infections like osteomyelitis and prosthetic joint infections (Lee *et al*., 2018; Turner *et al*., 2019; Tong *et al*., 2015). Studies on the interaction of *S. aureus* with osteoblasts suggest that the capability of the pathogen to invade and internalize into osteoblasts is critical in the pathogenesis of osteomyelitis and persistence of the pathogen and is also an underlying reason for antibiotic-refractive infections (Musso *et al*., 2021; Bongiorno *et al*., 2020; Sinha and Fraunholz, 2010; Horn *et al*., 2018; Ellington *et al*., 2006; Jevon *et al*., 1999;

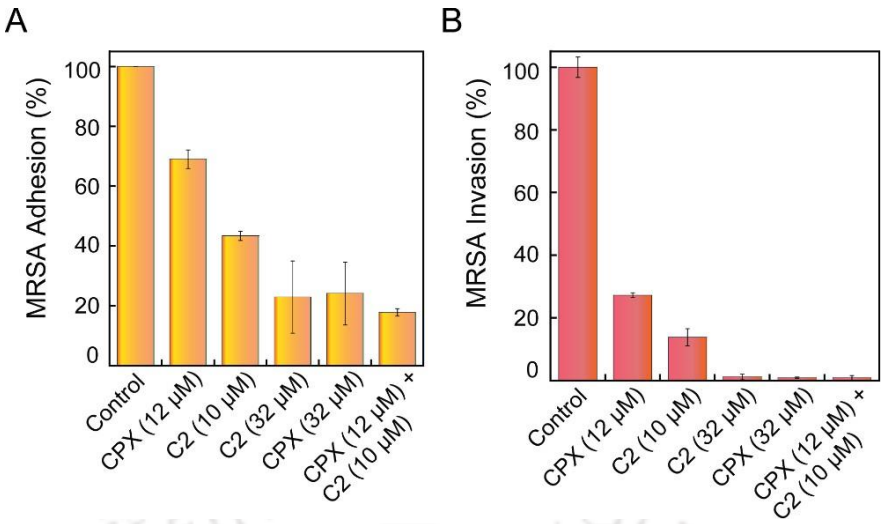

Figure 5.4. Estimation of (A) MRSA cell adhesion and (B) MRSA cell invasion in cultured MG-63 cells in presence of various treatment regimen.

Tuchscherr *et al.*, 2011). In the context of the interaction between *S. aureus* and osteoblasts, the phenomenon of pathogen adhesion and invasion hold the key to efficient internalization. Hence, it can be conceived that an antibacterial therapeutic which can deter the process of MRSA adhesion or invasion onto osteoblast is likely to hold considerable promise as an effective intervention to prevent bone cell infection by the pathogen. Based on this notion, experiments were conducted to assess the potential of a combinatorial treatment regimen encompassing 10 µM C2 and 12 µM CPX on curbing the adhesion and invasion of MRSA cells onto cultured osteoblast like MG-63 cells. It may be mentioned here that in these experiments, treatment with 10 µM C2 and 12 µM CPX was based on the results of earlier studies that revealed the potency of this combinatorial treatment against MRSA biofilm (Table 5.2, Figure 5.3). Prior to the bone cell infection experiment, the cytotoxic potential of 10 µM C2, 12 µM CPX and a combination of both (10 µM C2 and 12 µM CPX) against cultured MG-63 cells was ascertained by performing an MTT assay. Interestingly, it was observed that the viability of MG-63 cells subjected to treatment with 10 µM C2, 12 µM CPX and a combination of both (10 µM C2 and 12 µM CPX) was estimated to be ~ 89%, ~ 99.9% and ~ 91%, respectively (Table A5.1 in Appendix). This suggested that the concentration of C2 or CPX used in the bone cell infection experiments either singularly or in combination were not detrimental to the growth of MG-63 cells. In the bone cell adhesion experiment, an essential observation was the decrease in the magnitude of MRSA cell adhesion across every treatment regimen in comparison to the untreated control sample (Figure 5.4A).

Herein, the extent of MRSA cell adhesion onto MG-63 cells was estimated to be ~ 69% and ~ 43% when subjected to treatment with 12 µM CPX and 10 µM C2, respectively (Figure 5.4A). Interestingly, treatment with a combination of 12 µM CPX and 10 µM C2 led to a dramatic reduction in the magnitude of adhered MRSA cells, which amounted to only ~ 17% (Figure 5.4A). It can be conjectured that during the combination treatment with 12 µM CPX and 10 µM C2, the membrane-acting ligand C2 is likely to induce significant membrane damage in MRSA cells and concomitantly render enhanced killing of the pathogen by potentiating the activity of CPX. It can be presumed that membrane-compromised cells and non-viable disintegrated cells resulting from the combination treatment would fail to adhere onto MG-63 cells. Consequently, there will be a considerable reduction in the extent of MRSA cells adhered onto MG-63 cells, when subjected to the combinatorial treatment regimen.

In the bone cell invasion experiment, the extent of MRSA cell invasion across every treatment regimen was again considerably less as compared to the untreated control sample (Figure 5.4B). It may be noted here that following cell adhesion and washing of the loosely adhered cells, MG-63 cell-*S. aureus* 4s co-cultures were further incubated for 2 h to facilitate cell invasion. The 2 h co-culture time period chosen in the current study conformed with previous studies that ascertained uptake of model bacterial pathogens by mammalian cells in a cell culture model (Jevon *et al*., 1999; Rasigade *et al*., 2013; Singh *et al*., 2019). In the current study, the relative MRSA cell invasion onto MG-63 cells was estimated to be ~ 27% and ~ 11% when subjected to treatment with 12 µM CPX and 10 µM C2, respectively (Figure 5.4B). Treatment with a combination of 12 µM CPX and 10 µM C2 resulted in a remarkable reduction in the quantum of MRSA cell invasion, which was estimated to be only ~ 0.37% (Figure 5.4B). Further, it was also observed thatthe efficacy of the combinatorial treatment regimen in curbing MRSA cell invasion onto MG-63 cells was on par with that observed in case of treatment with either CPX or C2 alone at MIC level (32 µM each). The degree of cell invasion would largely depend on the initial population of MRSA cells adhered onto MG-63 cells. Prior results seem to suggest that the population of MRSA cells adhered onto MG-63 cells in the combinatorial treatment (~ 17%) was significantly lower than the untreated sample (Figure 5.4A). Further, when a low population of adhered MRSA cells are further subjected to an invasion assay for an additional 2 h, it is likely that the MRSA cells, which are still adhered onto the surface

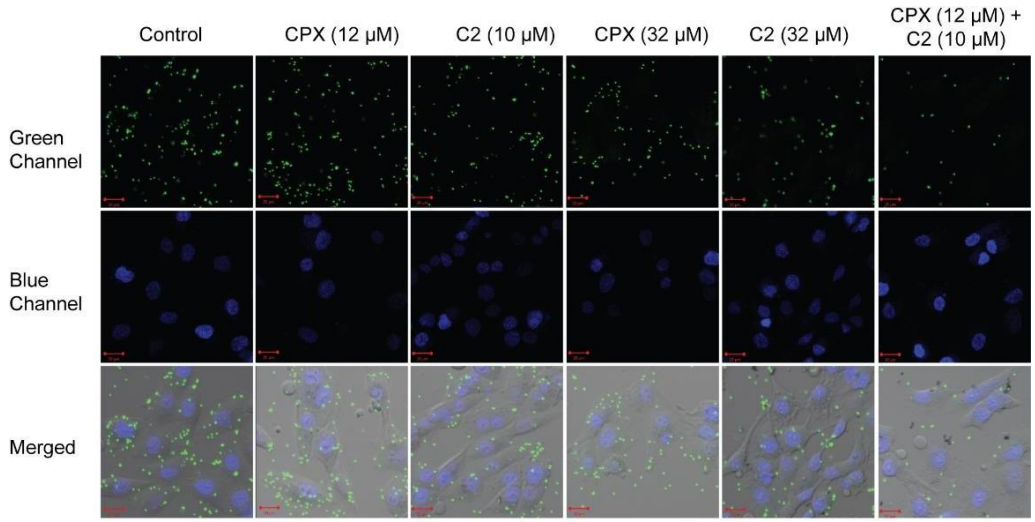

Figure 5.5. Fluorescence microscope analysis to ascertain MRSA cell invasion in cultured MG-63 cells in presence of various treatment regimen.

of MG-63 cells are vulnerable to the combinatorial treatment of CPX and C2, which consequently leads to a significant decrease in the fraction of MRSA invading MG-63 cells. The results obtained in the invasion assay in case of combination treatment with 12 µM CPX and 10 µM C2 was further substantiated by fluorescence microscope analysis wherein the number of cFDA-SE labelled *S. aureus* 4s cells invading DAPI-stained MG-63 cells were distinctly less than that observed in case of untreated cells as well as cells treated singularly with either 12 µM CPX or 10 µM C2 (Figure 5.5). Collectively, the leads obtained from the combinatorial treatment experiments are encouraging as they seem to suggest that the membrane-targeting ligand C2 in conjunction with CPX was able to effectively hinder MRSA infection in cultured osteoblast like bone cells. Considering the ramifications of MRSA-mediated bone infection and the challenges associated with antibiotic-refractory therapy, the ligand C2 emerges as a potential adjuvant that can restore the susceptibility of the pathogen to CPX and offer a possible therapeutic strategy to mitigate bone cell infection. In future, these results can be further strengthened through rigorous animal model experiments.

5.4. Significant Findings

The essential findings of the present study can be stated as follows:

1. On the basis of a checkerboard assay. it was evident that the MIC of CPX against *S. aureus* 4s cells was decreased 4-fold (8.0 µM) in combination with 10 µM, 12 µM and 16 µM C2.

2. In presence case of the combinatorial treatment regimen (10 μM C2 and 8.0 μM CPX), growth of the target MRSA cells was completely subdued till 360 generations.
3. A significant inhibition of MRSA biofilm formation was observed in presence of a combination of 10 μM C2 and 12 μM CPX, with the biofilm metabolic activity estimated to be only ~ 11%. The MBIC of CPX against *S. aureus* 4s biofilm was reduced ~ 10-fold (12.0 μM) and a synergistic interaction ensued between C2 and CPX.
4. In an *in vitro* bone cell infection model for MRSA, only ~ 17% cells adhered onto cultured MG-63 cells in presence of 12 μM CPX and 10 μM C2), which was significantly lower as compared to treatment with either 12 μM CPX or 10 μM C2 alone.
5. An analogous trend was also observed in an invasion assay wherein the relative MRSA cell invasion onto MG-63 cells was only ~ 0.37% in case of the combinatorial treatment regimen.
6. A dual-label fluorescence microscopic analysis corroborated the efficacy of the combinatorial treatment regimen in reducing MRSA cell invasion into MG-63 cells.
7. The therapeutic merit of the combinatorial treatment with 10 μM C2 and 12 μM CPX was evident as the growth characteristic of cultured MG-63 cells subjected to the treatment was not adversely affected, wherein the cell viability was estimated to be ~ 91 %.

Based on the salient results obtained in this study, it is evident that the membrane-targeting quinoxaline antimicrobial C2 could be harnessed in a combinatorial treatment regimen to heighten the activity of ciprofloxacin for effective elimination of MRSA planktonic cells and prevention of biofilm formation. Moreover, the therapeutic potential of the combinatorial treatment regimen was also evident in an *in vitro* bone cell infection model, wherein MRSA adhesion and invasion into cultured MG-63 cells could be hindered to a significant extent. However, to leverage the adjuvant potential of C2, development of a non-toxic cargo, which will render sustained release of the molecule is critical. To this end, generation of a C2-loaded nanocarrier for potential therapeutic applications against MRSA is described in the next chapter.

भारतीय प्रौद्योगिकी संस्थान गुवाहाटी
Indian Institute of Technology Guwahati

Chapter 6

Development of a Quinoxaline Ligand-loaded Nanocomposite for Anti-MRSA therapy and Alleviation of MRSA invasion in an Orthopaedic Implant

This chapter evaluates the anti-MRSA activity of C2-loaded HSA nanocarrier (C2-HNC). The potential of the combination treatment of C2-HNC and CPX in mitigation of MRSA invasion onto an orthopaedic titanium wire is also illustrated in thischapter.

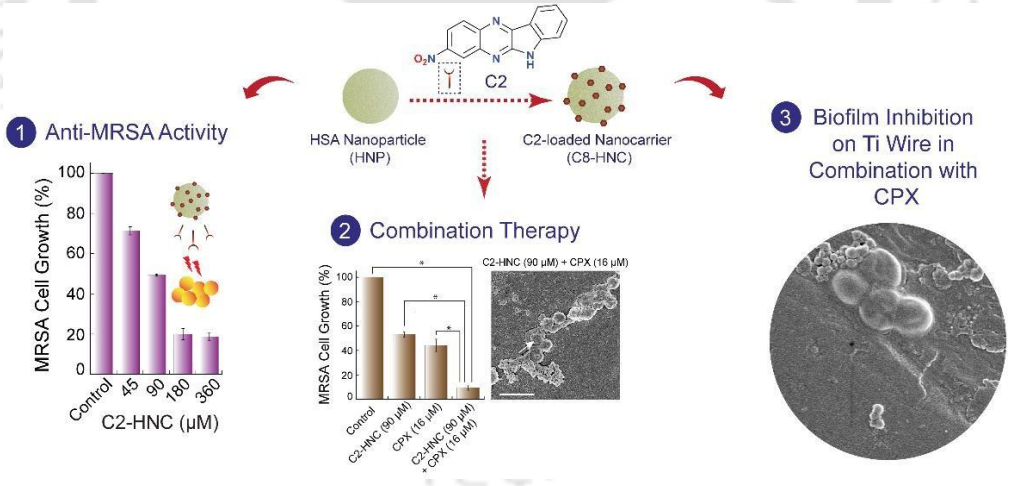

ABSTRACT

This study describes the therapeutic potential of C2-loaded HSA nanocarrier (C2-HNC) for mitigation of MRSA biofilm in an orthopaedic implant. Initially, HSA nanoparticle (HNP) was prepared by a desolvation method. C2-HNC was generated by incubating HNPs with varying concentration of C2. FETEM analysis revealed that C2-HNC was spherical with an average particle size of ~197 nm. The loading efficiency (LE) for the nanocarrier reached a saturation level of ~ 82% at a loading concentration of 375 µM C2. At pH 3.0, release of C2 was ~ 52% in 24 h, while at higher pH of HEPES buffer and simulated body fluid (SBF), the release of C2 was sustained and reached ~ 90% and ~ 81%, respectively, after 24 h. C2-HNC displayed a dose-dependent anti-MRSA activity, wherein the growth for *S. aureus* 4s cells treated with C2-HNC loaded with 45 µM, 90 µM, 180 µM and 360 µM C2 was estimated to be ~ 71%, ~ 49%, ~ 20% and ~ 18%, respectively. A combinatorial treatment with C2-HNC (loaded with 90 µM C2) and CPX (16 µM) resulted in a remarkable growth inhibition in MRSA cells (~ 9.0 % growth) and the nanocarrier was non-toxic to cultured MG-63 cells upto a loading concentration of 360 µM C2. A Ti wire was coated with collagen type I solution containing 128 µM C2 by a standard dip coating method and characterized by FESEM, EDX, FETEM-based mapping and FTIR analysis, which supported the presence of collagen and C2 in coated Ti wire. FESEM analysis indicated that C2-incorporation could significantly hinder MRSA biofilm formation on collagen-coated Ti wire. Interestingly, the eluates from the Ti wire samples were non-toxic to cultured MG-63 cells indicating that the coated Ti wires were biocompatible. In presence of a combinatorial treatment with C2-HNC (loaded with 90 µM C2) and CPX (16 µM), sparse adhesion of MRSA cells was observed on collagen-coated Ti wire upon, which suggested that the developed payload nanocarrier could impart a bactericidal as well as adjuvant effect and effectively thwart MRSA invasion in the implant.

1. Introduction

Methicillin-resistant *Staphylococcus aureus* is implicated in a large number of clinical infections such as bacteremia, endocarditis, periprosthetic joint infections (PJIs), osteomyelitis, skin and soft tissue, pulmonary and device-related infections (Chambers and DeLeo, 2008; Tong *et al*., 2015; Lee *et al*., 2018; Turner *et al*., 2019; Craft *et al*., 2019). Therapeutic interventions against MRSA are challenging since the pathogen displays a unique physiological adaptation and can form resilient biofilms in tissues and in medical implant (Arciola *et al*., 2018; Stoodley *et al*., 2011; Oliveira *et al*., 2018; Darouiche, 2004; Ribeiro *et al*., 2012). The biofilm-associated cells are embedded in a matrix, that can shield the cells from the host immune response and also present a permeability barrier to antibiotics (Hall and Mah, 2017; Fuente-Nunez *et al*., 2013; Otto, 2008). Hence, in medical implants, colonization by a robust biofilm can trigger the infection process, lead to high rates of implant failure and even cause osteomyelitis in case of orthopaedic devices. In case of PJIs, the associated complications are even more as a revision surgery may be required to remove the infected implant and insert a new implant.

Invasion of implantable medical devices by MRSA biofilm can perhaps be forestalled by accomplishing a surface modification of the device and reduce attachment of cells, or by incorporating antibacterials in the device, which can either kill the planktonic cells or perturb the initial events of biofilm formation (Visperas *et al*., 2022; Ghimire and Song, 2021). Notwithstanding the studies which illustrate the demonstration of such approaches, the beneficial outcome has been rather limited (Hetrick and Schoenfisch, 2006; Aricola *et al*., 2012). In case of implant infection, a fundamental problem is that the implant colonization may encompass the deposition of host macromolecules like collagen and fibronectin onto the surface of the implant. It is acknowledged that collagen adhesion is implicated in the pathogenesis of *S. aureus* (Kouidhi *et al*., 2010) and thus bone, cartilage and skin tissues, which are collagen-rich are prone to *S. aureus* infections. Moreover, the high propensity of *S. aureus* to adhere onto collagen can also facilitate formation of recalcitrant biofilm and subsequent infection of the implant. Hence, there is a need to discover potential drug candidates that can hinder MRSA biofilm formation on collagen and thereby minimize the risk of device-related infections.

Titanium (Ti)-based devices possess favorable traits such as high biocompatibility, anti-corrosive property and superior mechanical attributes and thus

render a high degree of osseointegration as an orthopaedic implant (Gulati *et al*., 2018). However, to achieve the desired clinical outcome as an orthopaedic implant, it is critical that the Ti implants display significant bactericidal property. In this regard, there are studies which demonstrate the functionalization of Ti-based implants for rendering high bactericidal activity and minimizing the risk of pathogen colonization (Hu *et al*., 2012; Bakhshandeh *et al*., 2017; Zhao *et al*., 2019). In order to generate a Ti implant displaying bactericidal property, a critical parameter which needs to be considered is that an implant coating should be a potent molecule and should be released adequately in order to in kill the invading pathogen in large numbers and thereby prevent adhesion of the pathogen on the implant surface. Based on the aforementioned rational, the current study describes the generation of a Ti wire coated with the anti-MRSA quinoxaline antimicrobial C2, which could effectively deter colonization of the model implant by the pathogen. The study also illustrates the generation of HSA nanocarrier-loaded with ligand C2 and explores the feasibility of deploying the nanocarrier in a combinatorial therapy regimen with ciprofloxacin in order to prevent MRSA adhesion onto a model Ti-based orthopaedic implant.

6.2. Materials and Methods

6.2.1. Materials

5 (and 6)-carboxyfluorescein diacetate succinimidyl ester (cFDA-SE), ciprofloxacin, Dulbecco's Modified Eagle Medium (DMEM), trypsin-EDTA and 3-(4,5-dimethyl-2-thiazolyl)-2,5-diphenyl-2H-tetrazolium bromide (MTT), potassium bromide, paraformaldehyde, titanium wire (0.25 mm diameter), pepsin, pancreatin and collagen type I were procured from Sigma-Aldrich (USA). Brain-Heart Infusion (BHI) broth was procured from HiMedia, Mumbai, India. Dimethyl sulfoxide (DMSO) and methanol was obtained from Merck, India. Fetal bovine serum (FBS) was obtained from PAA Laboratories, USA.

6.2.2. MRSA Growth Conditions

Staphylococcus aureus 4s strain was cultured in BHI broth at 37 ºC and 180 rpm for 12 h as mentioned previously in section 2.2.2.

6.2.3. C2-loaded HSA Nanocarrier (C2-HNC)

HSA nanoparticles (HNPs) were initially generated by following a previously described desolvation method (Langer *et al*., 2003). For generation of C2-loaded HSA nanocarrier (C2-HNC), HNPs (1.0 mg/mL in sterile MilliQ water) were incubated in separate sets overnight under rocking condition at room temperature with C2 (25 µM - 1254 µM). Subsequently, C2-HNC was recovered by centrifugation at 10000 rpm for 5.0 min and stored in -20 ºC till further use.

6.2.4. Characterization of HNP and C2-HNC

A 10 µL aliquot each of HNP (1.0 mg/mL in sterile MilliQ water) and C2-HNC 1.0 mg/mL HNP having a loading concentration of 360 µM C2) was separately drop-casted onto aluminium foil. The sample was then dried overnight in a laminar hood, visualized in a field emission scanning electron microscope (Zeiss Sigma, USA) and the obtained images were recorded. In case of AFM analysis, a 10 µL aliquot of HNP (1.0 mg/mL in sterile MilliQ water) and C2-HNC (1.0 mg/mL HNP having a loading concentration of 360 µM C2) was separately spotted onto a sterile glass cover slip (18 mm × 18 mm). The cover slip was then air dried overnight in a laminar hood. AFM images were acquired in non-contact mode over a 10 µm × 10 µm area at a scan rate of 0.5-1.0 line/s (Oxford Instruments plc, U.K). Cantilevers made up of silicon nitride were used having a resonant frequency of ca. 150 to 200 kHz. Analysis of the amplitude channel and topographic images was accomplished by using the WSxM v5.0 Develop 6.5 image viewer software. For estimation of particle size, HNPs were resuspended in sterile MilliQ water (1.0 mg/ml) and 0.2 ml aliquot of the sample was further dispersed in 0.8 ml sterile MilliQ and subjected to DLS analysis (Zetasizer, Malvern, UK). In a separate set, C2-HNC ((1.0 mg/mL HNP having a loading concentration of 360 µM C2) was dispersed in sterile MilliQ water (final volume of 1.0 mL). A 0.1 mL aliquot of this solution was further diluted in sterile MilliQ water to a final volume of 1.0 mL and subjected to particle size estimation by DLS. The DLS experiments were performed in three independent sets and every set consisted of three replicates.

6.2.5. Estimation of Loading Efficiency (LE) and Cumulative Release Kinetics

Initially, a UV-visible absorbance spectrum of varying concentrations of C2 (10 µM - 1000 µM) was recorded at 280 nm in a spectrophotometer (Lambda 25, Perkin-Elmer).

The absorbance maxima of C2 at 280 nm was recorded to generate a standard curve, which was subsequently used for estimation of loading efficiency (LE) of C2. For estimation of LE, HNPs (1.0 mg/mL in sterile MilliQ water) were incubated with varying concentrations of C2 (100 µM - 500 µM) for 12 h on a rocker at room temperature. Following incubation, the solution was centrifuged at 10000 rpm for 5 min. The pellet, which represents C2-HNC was resuspended in sterile MilliQ water. The concentration of free C2 in the supernatant was determined from the previously generated calibration curve for the ligand. LE was determined using a standard calculation as described previously in section 3.2.4. All the experiments were performed in three independent sets and every set consisted of three replicates. Data analysis and calculation of standard deviation was performed with Microsoft Excel 2010 (Microsoft Corporation, USA).

In order to ascertain the *in vitro* release kinetics, C2-HNC (1.0 mg/mL HNPs loaded with a final concentration of 325 µM C2) was dispersed in separate sets in 1.0 mL each of 10 mM HEPES buffer (pH 7.4), 10 mM citrate buffer (pH 3.0) and simulated body fluid (SBF, pH 8.0). The composition of SBF was as described earlier (Kokubo *et al.*, 1990). The samples were incubated in an orbital shaker at 120 rpm and 37 ºC. Samples were withdrawn at regular intervals (0.5 h, 1 h, 2 h, 6 h, 12 h and 24 h) and centrifuged at 10000 rpm for 3.0 min. The supernatant from each sample was transferred into a fresh microcentrifuge tube and absorption spectra of the solution was measured at 280 nm in a spectrophotometer. A previously generated calibration curve for C2 was used to quantify the release of C2 from C2-HNC at various time periods and expressed as % cumulative release. All the experiments were performed in three independent sets and every set consisted of three replicates.

6.2.6. Anti-MRSA Activity and Cytotoxic Potential of C2-HNC

In a 96-well microtitre plate, *S. aureus* 4s (~10^6 CFU in BHI medium) was grown in separate sets in presence of varying concentration of C2-HNC (loaded with 45 µM, 90 µM, 180 µM and 360 µM C2) at 37 ºC and 180 rpm for 12 h. Following incubation, the growth of MRSA cells was ascertained by recording the absorbance of the culture at 600 nm in a microtitre plate reader (Infinite M200, TECAN, Switzerland) and expressed as percentage growth compared to untreated cells. An MTT-based assay was conducted to ascertain the cytotoxic potential of C2-HNC (loaded with 45 µM, 90 µM, 180 µM and 360 µM C2) against MG-63 cells (human osteosarcoma cells). The growth conditions for

MG-63 cells and the protocol for conducting the MTT assay was similar to the method described in an earlier study (Mullick *et al*., 2021).

6.2.7. Effect of the Combinatorial Treatment of C2-HNC and CPX on MRSA

A 10 µL aliquot of *S. aureus* 4s cell suspension (~10^6 CFU suspended in BHI) was inoculated into a sterile 96-well microtitre plate containing 100 µL BHI medium supplemented in separate sets with 4.0 µM, 8.0 µM and 16 µM CPX. For combination treatment sets, C2-HNC (loaded with 45 µM, 90 µM and 180 µM C2) was used in separate sets with every chosen concentration of CPX. The treatment of cells was accomplished at 37 ºC and 180 rpm for 12 h. Cell growth was ascertained by measuring absorbance at 600 nm (Infinite M200, TECAN, Switzerland) and expressed as percentage growth compared to untreated cells. The magnitude of decrease in MIC of CPX in presence of C2-HNC was also determined. Statistical analysis for MRSA cell growth upon combinatorial treatment (90 µM C2-HNC and 16 µM CPX) as compared to cells treated with either 90 µM C2-HNC or 16 µM CPX was performed by a one-way analysis of variance (ANOVA) using Sigma Plot version 11.0. The adjuvant potential of C2-HNC was also ascertained by FESEM and TEM analysis.

6.2.8. Titanium Wire Coated with C2-Incorporated Collagen (C2-Co-TW)

Titanium (Ti) wire was cut into multiple pieces of 1.5 cm length each. The wire surface was cleaned, sterilized and then subjected to dip-coating in separate wells of a 6-well tissue culture plate with either type I collagen alone (1.0 mg/mL in sterile tissue culture grade water) or varying concentrations of C2 (128 µM or 512 µM) added to type I collagen solution (1.0 mg/mL in sterile tissue culture grade water). The essential steps of process of cleaning, sterilization and dip-coating of the Ti wires was based an earlier described procedure (Mullick *et al*., 2022). The coating was accomplished at 37°C in static condition overnight. Subsequently, the coating solutions were removed and the collagen-coated Ti wire (Co-TW) and C2-incorporated collagen-coated Ti wire (C2-Co-TW) were dried overnight in a laminar hood. The coated as well as bare Ti wire (TW) was characterized by FESEM (Zeiss, Germany), EDX analysis and FTIR spectra by following the procedure described previously (Mullick *et al*., 2022). The Ti wires were also visualized by FETEM mapping studies (INCA, JEOL JEM 2100F, Japan).

6.2.9. Anti-MRSA Activity and Cytotoxic Potential of C2-Co-TW

S. aureus 4s cells were inoculated at 1% level in BHI medium and grown overnight at 37 ºC and 180 rpm. Subsequently, 12-well tissue culture plates were inoculated with the grown MRSA culture (~ 10^6 CFU/mL) in BHI media having 0.25% glucose and Co-TW as well as C2-Co-TW having varying coating concentrations of C2 (128 µM or 512 µM) were introduced into the wells in separate sets. The plate was then incubated at 37 ºC under static condition in separate sets for 6 h and 12 h. Following incubation, the spent media was carefully aspirated and the wires containing the grown MRSA were removed, dried under sterile laminar air flow and then visualized under FESEM. In order to evaluate the cytotoxic potential of the coated Ti wires, Co-TW as well as C2-Co-TW having varying coating concentrations of C2 (128 µM or 512 µM) were incubated overnight in separate tubes containing DMEM media at 37 ºC and 180 rpm for elution of C2 into the media. The eluates were now added to MG-63 cells grown to 80% confluency and a standard MTT assay was performed to ascertain the cell viability. The basic protocol for MTT assay was similar to the procedure described earlier (Mullick *et al*., 2021).

6.2.10. Effect of the Combinatorial Treatment of C2-HNC and CPX on Adhesion of MRSA onto Collagen-coated Titanium Wire

Initially, 1.5 cm pieces of collagen-coated Ti wire (Co-TW) was placed in separate wells of a 12-well tissue culture plate having BHI media incorporated with 0.25% glucose. Overnight grown *S. aureus* 4s cells were inoculated into 12 well tissue culture and incubated at 37 ºC under static condition for 24 h in presence of C2-HNC (loading concentration of 90 µM C2) and 16 µM CPX (0.5 × MIC). Following incubation, the spent media was gently removed and the Ti wires containing the grown MRSA biofilm were removed, dried under sterile laminar air flow and visualized under FESEM.

6.3. Results and Discussion

6.3.1. Generation of C2-HNC

Earlier studies had established the potential of the quinoxaline-based ligand C2 as an adjuvant for combination therapy against MRSA (Chapter 5). However, to harness the therapeutic prospect of C2, it is critical to develop a biocompatible delivery vehicle, which will support slow release of the ligand. To this end, HSA nanoparticle (HNP) was generated by a desolvation method (Langer *et al*., 2003) and tested as a deliver

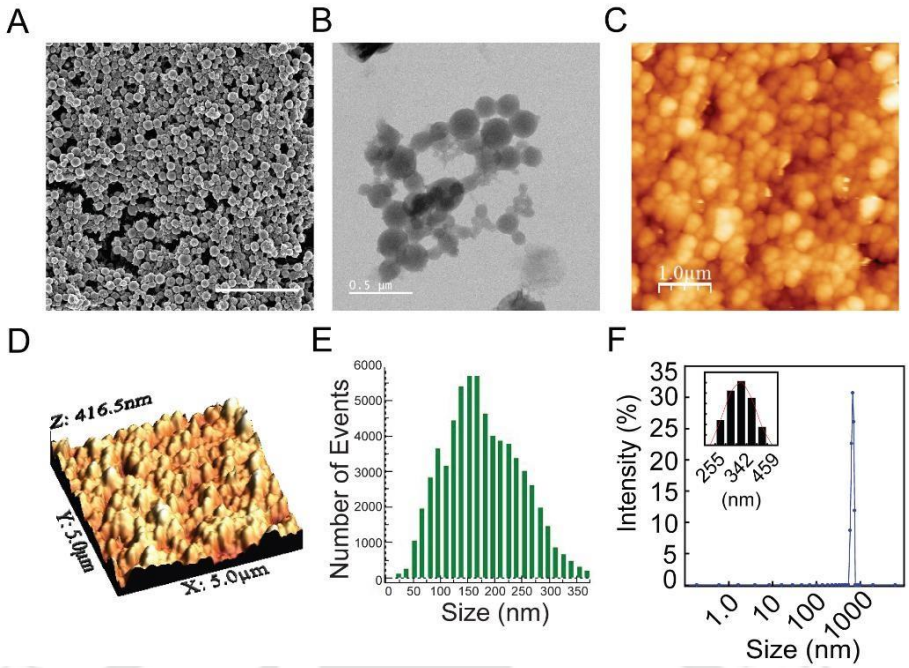

Figure 6.1. Characterization of HSA nanoparticle (HNP) by (A) FESEM, (B) TEM, (C-E) AFM analysis Scale bar in (A) is 1.0 µm. (C) and (D) indicate 2D and 3D topography AFM image of HNP, respectively. (E) Height profile of HNPs determined by analysis of the image in (D). (F) Estimation of hydrodynamic radius of HNP by DLS. Inset depicts size distribution histogram.

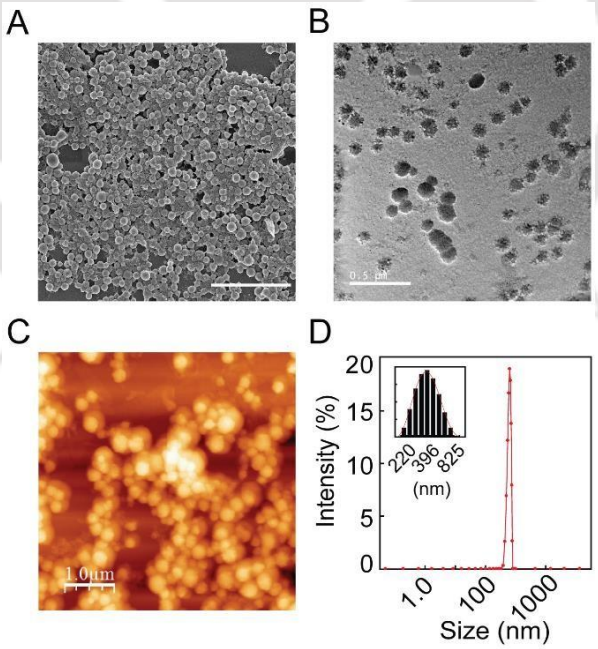

Figure 6.2. Characterization of C2-loaded HSA nanocarrier (C2-HNC) by (A) FESEM, (B) TEM, (C) AFM analysis. Scale bar in (A) is 1.0 µm. (D) Estimation of hydrodynamic radius of C2-HNC by DLS. Inset depicts size distribution histogram.

Table 6.1. Estimation of the loading efficiency (LE) of C2 in HSA nanoparticle.

Loading Concentration of C2 (µM)	Loading Efficiency (%)
100	25.37
125	40.31
190	57.01
250	75.30
375	82.55
500	82.81

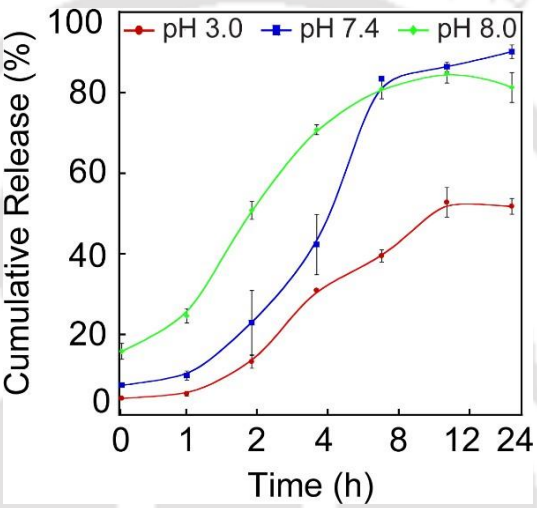

Figure 6.3. Estimation of the cumulative release of C2 from C2-HNC incubated in various buffer systems.

agent. FESEM analysis revealed that HNPs were spherical in shape with an average particle size of ~ 182 nm (Figure 6.1A). The spherical shape of HNPs was also observed in TEM and AFM analysis (Figure 6.1A-6.1B). The average hydrodynamic radius of HNP assessed by DLS was ~ 342 nm (Figure 6.1F). With regard to C2-HNC, FESEM and FETEM analysis indicated that the nanocarrier was also spherical in shape (Figure 6.2A-6.2B), albeit larger in size (average particle size ~ 197 nm) as compared to HNPs (average particle size of ~ 182 nm). The spherical shape of C2-HNC was also captured in AFM analysis (Figure 6.2C). The average hydrodynamic radius of C2-HNC was ~ 396 nm (Figure 6.2D).

With regard to the loading efficiency (LE) of C2, it was observed that there was an increase in the quantum of LE as a function of the concentration of C2 and at

~ 375 µM of C2, a saturation effect was observed (Table 6.1). Further, in presence of 500 µM C2 (maximum loading concentration of C2), LE was ~ 82% (Table 6.1). For ascertaining the release kinetics, C2-HNC loaded with 325 µM C2 was used. Following incubation for 24 h in an acidic buffer (pH 3.0), the cumulative release of C2 was ~ 52% (Figure 6.3). On the other hand, in HEPES buffer (pH of 7.4) and SBF (pH 8.0), a sustained release profile for C2 was observed and the extent of cumulative release of C2 was apparently higher than that observed in citrate buffer (Figure 6.3). Quantitative estimation indicated that the cumulative release of C2 in HEPES buffer and SBF was ~ 90% and ~ 81%, respectively, after 24 h of incubation (Figure 6.3). It may be mentioned here that the concentration of C2 released in the physiologically relevant HEPES buffer and SBF was significantly higher than effective dose of the ligand required for bactericidal activity against the MRSA strain *S. aureus*. Based on these results, it was thus evident that C2-HNC supported a favorable release profile of C2, which is amicable for therapeutic applications against the MRSA strain.

6.3.2. Anti-MRSA Activity and Cytotoxic Potential of C2-HNC

Based on the favorable release profile of C2 in physiologically relevant buffer system, the subsequent aim of the study was to ascertain the anti-MRSA activity of the developed nanocarrier. To this end, a distinct growth inhibition for *S. aureus* 4s cells was noted upon treatment with C2-HNC (Figure 6.4A). Further, a dose-dependent effect was observed when the MRSA cells were treated with C2-HNC loaded with an increasing concentration of the ligand. For instance, the growth for *S. aureus* 4s cells treated with C2-HNC loaded with 45 µM, 90 µM, 180 µM and 360 µM C2 was estimated to be ~ 71%, ~ 49%, ~ 20% and ~ 18%, respectively (Figure 6.4A). These results are encouraging as they seem to suggest that the potent bactericidal activity of C2 against the tested MRSA strain was conserved even after encapsulation in the HSA nanocarrier. In the current study, a key objective was to develop a C2-loaded nanocarrier, which can be leveraged for mitigation of MRSA invasion into orthopaedic implant. To this end, it was also critical that the developed nanocarrier was biocompatible and non-toxic to cultured bone cells. In order to ascertain this premise, the cytotoxic potential of C2-HNC was assessed against cultured osteoblast like MG-63 cells. A standard MTT assay indicated that C2-HNC loaded with varying concentrations of the ligand (45 µM - 360 µM) was non-toxic to MG-63 cells as the cell viability was in excess of ~ 90% (Figure 6.4B). Collectively, the prominent

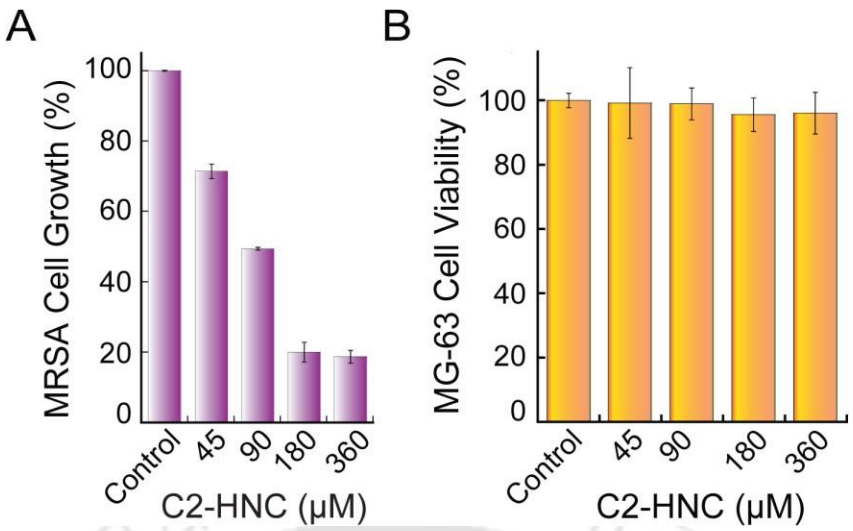

Figure 6.4. (A) Estimation of MRSA cell growth in presence of C2-HNC loaded with varying concentrations of C2. (B) MTT assay-based estimation of the cytotoxic effect rendered by C2-HNC on cultured MG-63 cells. The loading concentration of C2 is shown in the figure. Data point obtained from six experimental samples were used to ascertain mean ± standard deviation.

anti-MRSA activity and the non-toxic nature observed for C2-HNC were encouraging and suggested that the nanocarrier may hold interesting therapeutic prospects in alleviation of MRSA infection in orthopaedic implants.

6.3.3. Effect of Combinatorial Treatment of C2-HNC and CPX on MRSA

The significant anti-MRSA activity exhibited by C2-HNC in conjunction with its biocompatible nature were interesting leads. The subsequent aim of the investigation was to ascertain whether C2-HNC could potentiate the activity of CPX against MRSA, analogous to the free ligand alone. To this end, a checkerboard assay was set up to ascertain MRSA cell growth in separate sets upon treatment with C2-HNC (loaded with 45 μM, 90 μM and 180 μM C2) in conjunction with 4.0 μM, 8.0 μM or 16 μM CPX. In presence of C2-HNC (loaded with 90 μM C2), MRSA cell growth was estimated to be ~ 49% (Figure 6.5). Further, it was observed that *S. aureus* 4s displayed ~ 44% growth upon treatment with 16 μM CPX (0.5 × MIC) (Figure 6.5). Interestingly, a significant growth inhibition (only ~ 9.0 % growth) was observed when MRSA cells were grown in presence of both C2-HNC (loaded with 90 μM C2) and CPX (16 μM) (Figure 6.5). Notably, the growth inhibition observed in presence of C2-HNC in combination with CPX was comparable to that observed for CPX alone used at MIC level (32 μM).

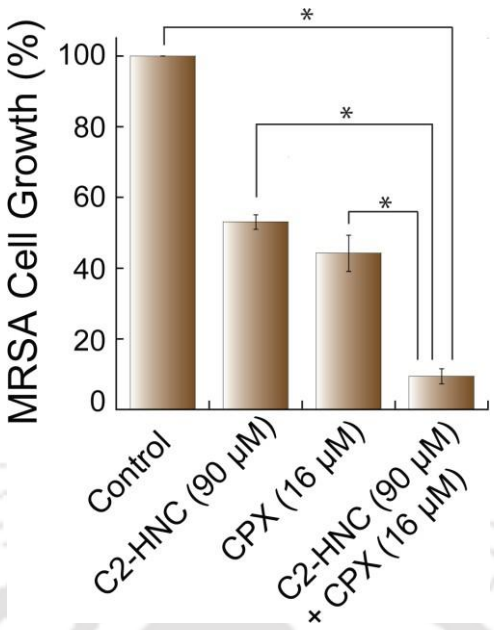

Figure 6.5. Estimation of MRSA cell growth in presence of C2-HNC (loaded with 90 µM C2) and CPX (16 µM). * represents *p* value < 0.001 in one-way ANOVA.

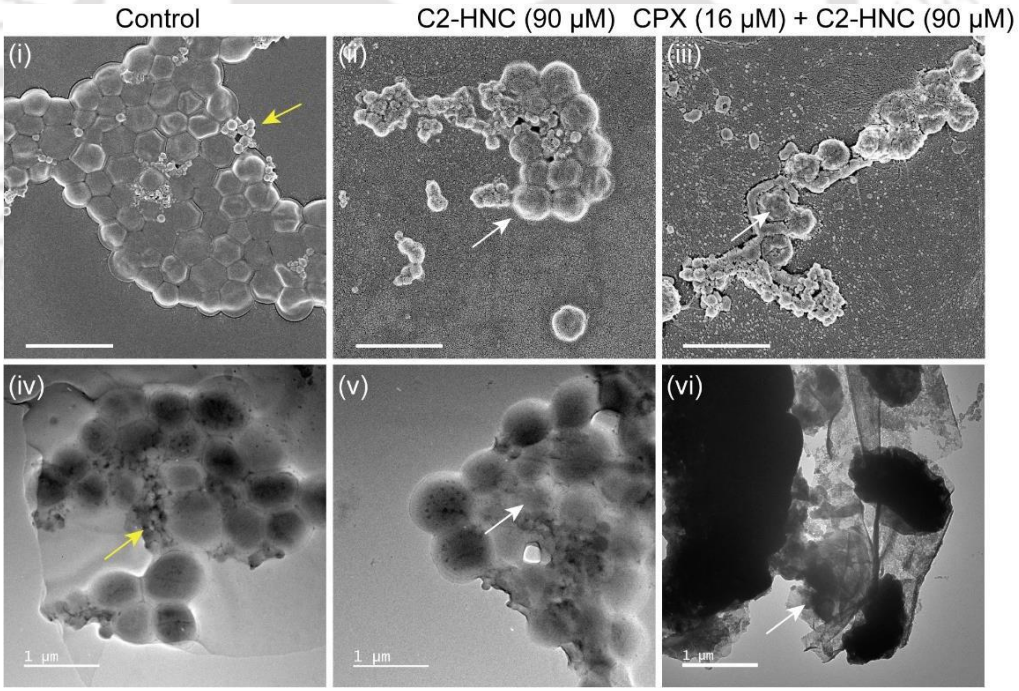

Figure 6.6. Effect of combinatorial treatment of C2-HNC and CPX on S. aureus 4s cells ascertained by (i-iii) FESEM analysis and (iv-vi) TEM analysis. Yellow arrow in panels (i) and (iv) indicate nanocarrier attached onto MRSA cells. White arrow in panels (ii), (iii), (v) and (vi) indicate damaged MRSA cells. Scale bar for panels (i-iii) is 1.0 µm.

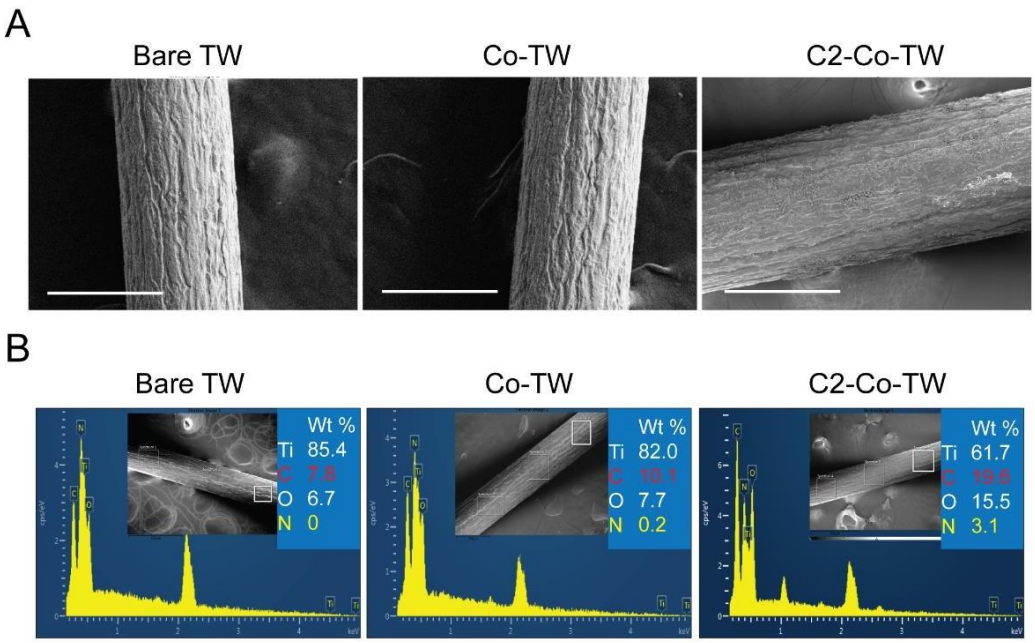

Figure 6.7. Characterization of bare Ti wire, Ti wire coated with collagen type I solution (Co-TW) and Ti wire coated with collagen type I solution containing 128 µM C2 (C2-Co-TW) by (A) FESEM analysis and (B) EDX analysis. Scale bar for the images in (A) is 100 µm.

The antagonistic effect of the combination treatment on MRSA cells was also evident in FESEM and TEM analysis. Herein, the HNPs could be observed adhering onto intact target cells of MRSA in case of the control samples (Figure 6.6, Panels i and iv). A partial disintegration of cells could be noted for MRSA cells treated with C2-HNC alone (Figure 6.6, Panels ii and v). For the combinatorial treatment regimen, a significant distortion of MRSA cell morphology was evident in comparison to control cells (Figure 6.6, Panels iii and vi).

6.3.4. Titanium Wire Coated with C2-Incorporated Collagen (C2-Co-TW)

Titanium (Ti) wire is a widely acknowledged orthopaedic implant material having a wide range of bone repair and tissue engineering applications (Geetha *et al*., 2009; Spriano *et al*., 2018). However, Ti implants require functionalization as they are essentially bioinert in nature. Based on this premise, in the current study the Ti wire was coated with collagen type I solution containing varying concentrations of C2 (128 µM or 512 µM). In FESEM analysis, the bare titanium wire (TW) revealed a somewhat rough surface (Figure 6.7A), whereas a thick corrugated surface was manifested in case of Co-TW as well as C2-Co-TW (Figure 6.7A). FESEM-EDX analysis of Co-TW and C2-Co-TW indicated a notable increase in the wt% of C and O

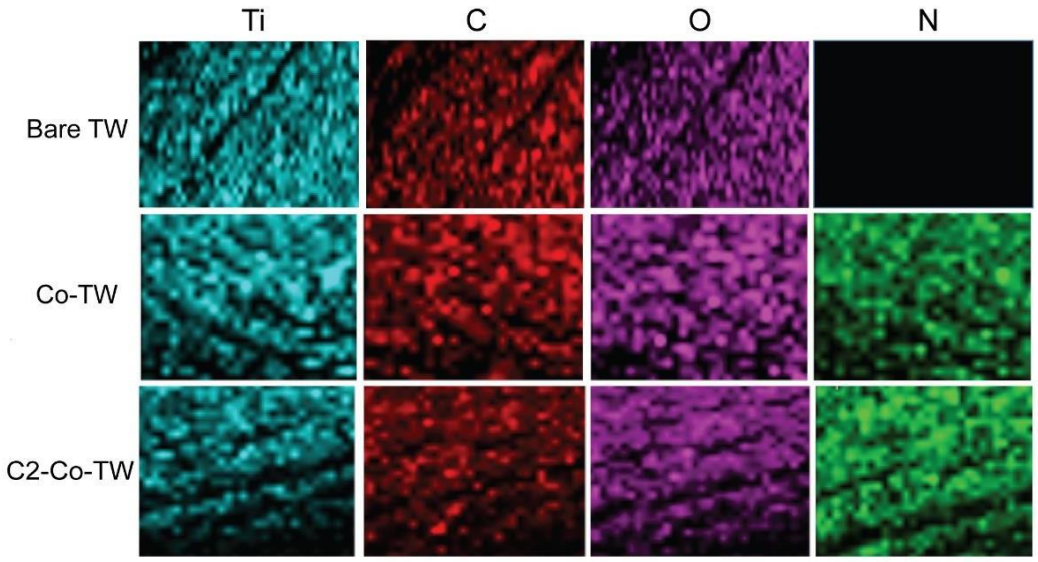

Figure 6.8. Characterization of bare Ti wire, Ti wire coated with collagen type I solution (Co-TW) and Ti wire coated with collagen type I solution containing 128 µM C2 (C2-Co-TW) by FETEM-based mapping analysis.

as compared to bare Ti wire (Figure 6.7B). This indicated the deposition of collagen and C2 upon the surface of Ti wire (Figure 6.7B). Elemental mapping analysis, which revealed a distinct signal for elemental N also supported the coating of collagen and C2 upon the surface of Ti wire (Figure 6.8). Further, FTIR analysis also indicated the presence of the signature stretching frequencies of C2 in C2-Co-TW (Figure A6.1).

6.3.5. Anti-MRSA Activity of C2-Co-TW

Orthopaedic implants are highly prone to staphylococcal infections. In order to address this problem, coating of the implant with a potent bactericidal agent is a viable solution. Based on this tenet, in the present study, the quinoxaline antimicrobial C2, which displayed high anti-MRSA activity was tested as an antibacterial coating on orthopedic Ti wire. The antagonistic activity of C2-incorporated collagen-coated Ti wire (C2-Co-TW) was studied by FESEM. In case of the collagen-coated Ti wire (Co-TW), a dense population of MRSA cells organized as a surface biofilm could be observed (Figure 6.9, panels i and iv). Further, the typical cell-cell adhesion associated with MRSA biofilm was evident on the surface of the Ti wire (Figure 6.9, panel iv). In case of C2- coated Ti wire, a scanty population of MRSA cells were observed to adhere on the surface of the Ti wire (Figure 6.9, panels ii and v) following 6 h of incubation. Moreover, the attached MRSA cells appeared shriveled and lost their structural integrity (Figure 6.9, panel v). The anti-MRSA activity rendered by C2-coating over Ti wire was even more

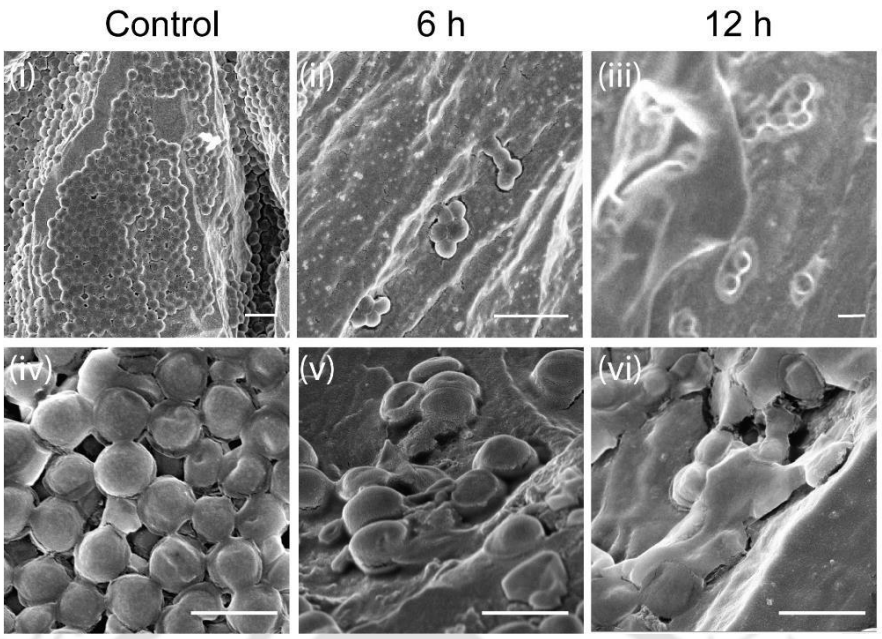

Figure 6.9. FESEM images of *S. aureus* 4s cells grown on collagen-coated Ti wire (control) and C2-incorporated collagen coated Ti wire (C2-Co-TW) for 6 h and 12 h. Scale bar for images in panel (i-iii) is 2.0 µm. Magnification for images in panels i, ii and iii is 5.0 KX, 10 KX and 5.0 KX, respectively. Scale bar and magnification for images in panel (iv-vi) is 200 nm and 50 KX, respectively.

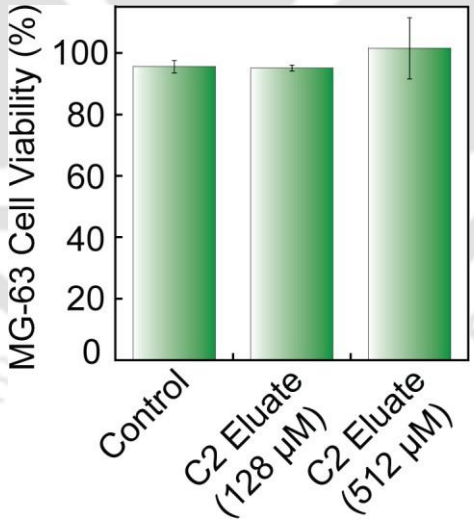

Figure 6.10. MTT assay-based assessment of the cytotoxic potential of C2-HNC on cultured MG-63 cells. The loading concentration of C2 is shown in parenthesis. Data point obtained from six experimental samples were used to ascertain mean ± standard deviation.

pronounced in case of an incubation period of 12 h (Figure 6.9, panels iii and vi). Herein, the number of MRSA cells adhered onto the coated Ti wire were diminished

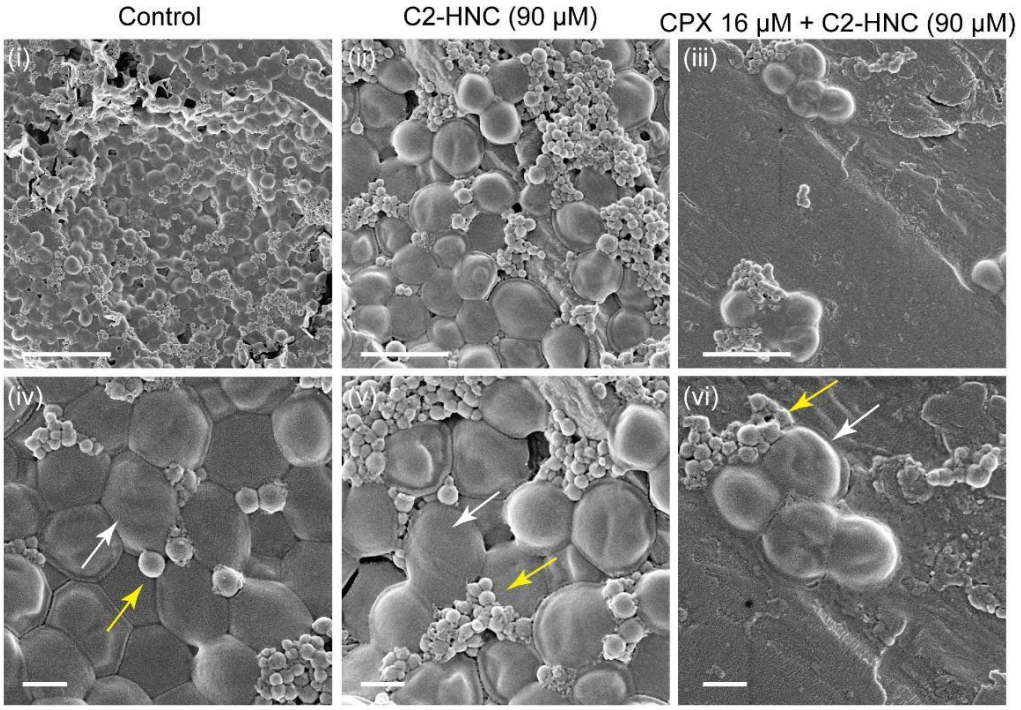

Figure 6.11. FESEM analysis to ascertain the effect of combinatorial treatment with C2-HNC (loaded with 90 µM C2) and CPX (16 µM) on *S. aureus* 4s cells. Scale bar for (i), (ii) and (iii) is 2.0 µm, 1.0 µm and 1.0 µm, respectively. Scale bar for the images in (iv-vi) is 500 nm. Magnification for images in panels i, ii and iii is 10 KX, 25 kX and 25 KX, respectively. Magnification for images in panel (iv-vi) is 50 KX. Yellow arrow in panels (iv), (v) and (vi) indicate nanocarrier attached onto MRSA cells. White arrow in panels (iv), (v) and (vi) indicate MRSA cells.

further and the morphological distortion observed in the cells was also more profound (Figure 6.9, panels iii and vi). Collectively, the results seem to imply that a sustained release of the antibacterial ligand C2 from the coated Ti wire could not only eliminate MRSA cells in the vicinity and thereby reduce large scale adhesion of the pathogen onto Ti wire but could also annihilate the fraction of the adhered MRSA cells by a contact killing effect. In order to test the therapeutic utility of the C2-coated Ti wire as an orthopaedic implant, it was pertinent to evaluate its toxic potential. To this end, eluates from the C2-coated Ti wires (coated with 128 µM and 512 µM C2) were non-toxic to cultured MG-63 cells (Figure 6.10).

6.3.6. Effect of the Combinatorial Treatment of C2-HNC and CPX on Adhesion of MRSA onto Collagen-coated Titanium Wire

Colonization of implantable medical devices by MRSA biofilm is a significant problem in the clinics. Deposition of human matrix protein such as collagen on the surface of an implant can be a trigger point since collagen adhesion by plays a potential role in pathogenesis and the infection process. In order to address this challenge, there is a need for a therapeutic intervention that can that can either annihilate MRSA in the vicinity of the implant and thereby minimize the extent of device-related infections or deter colonization on the implant by the pathogen. Based on the potent anti-MRSA activity and non-toxic attribute of C2-HNC towards cultured bone cells and the efficacy of a combinatorial treatment regimen (90 µM C2-HNC and 16 µM CPX) in eliminating MRSA (Figure 6.4-6.6), it was envisaged that the combination treatment regimen can perhaps be leveraged to hinder MRSA invasion onto an orthopaedic Ti wire. In case of treatment with only HNP (control), FESEM analysis of Ti wire indicated that MRSA could profusely colonize the surface of the implant (Figure 6.11, panel i) and certain fraction of HSA nanoparticle was observed to adhere onto MRSA biofilm formed on the surface of Ti wire (Figure 6.11, panel iv). Colonization of MRSA on Ti wire was also evident in case of treatment with 90 µM C2-HNC alone (Figure 6.11, panel ii and v). However, in this case, the extent of colonization was slightly lower as compared to the control sample and the cell integrity in some of the adhered MRSA cells was also compromised (Figure 6.11, panel ii and v). Interestingly, FESEM analysis clearly indicated that the combination treatment with 90 µM C2-HNC and 16 µM CPX was able to significantly curb MRSA cell adhesion onto Ti wire and the few adhered cells of the pathogen appeared quite distorted, indicating a significant loss of cell integrity. Based on these results, it was apparent that the combinatorial treatment regimen (90 µM C2-HNC and 16 µM CPX) holds considerable potential as a therapeutic intervention to deter MRSA-mediated infection of an orthopaedic implant.

6.4. Significant Findings

The key findings of the present study can be stated as follows:

1. C2-loaded HSA nanocarrier (C2-HNC) was generated which was spherical in shape with an average particle size of ~197 nm. The loading efficiency (LE) for the nanocarrier reached a saturation level of ~ 82% at a loading concentration of 375 µM C2.

2. At a physiologically relevant pH of HEPES buffer and simulated body fluid (SBF), the release of C2 was sustained and reached high levels amounting to ~ 90% and ~ 81%, respectively, after 24 h.
3. C2-HNC exhibited potent bactericidal activity against MRSA wherein the growth for *S. aureus* 4s cells treated with C2-HNC loaded with 45 µM, 90 µM, 180 µM and 360 µM C2 was estimated to be ~ 71%, ~ 49%, ~ 20% and ~ 18%, respectively.
4. A combinatorial treatment with C2-HNC (loaded with 90 µM C2) and CPX (16 µM) could effectively suppress the growth of MRSA cells (~ 9.0 % growth) and the nanocarrier was non-toxic to cultured MG-63 cells.
5. C2-coated Ti wire could significantly prevent MRSA biofilm formation on the wire surface and the eluates from the Ti wire samples were non-toxic to cultured MG-63 cells suggesting that the coated Ti wires were biocompatible.
6. A combinatorial treatment with C2-HNC (loaded with 90 µM C2) and CPX (16 µM) could effectively thwart adhesion of MRSA cells on collagen-coated Ti wire, indicating that the bactericidal and adjuvant activity of the payload nanocarrier could be leveraged to prevent MRSA colonization onto a Ti wire.

In the subsequent section, the essential findings emerging from the thesis work is summarized and the future perspective is highlighted.

SUMMARY AND FUTURE PERSPECTIVE

SUMMARY AND FUTURE PERSPECTIVE

The continuous challenge posed by MRSA in the clinics is a global healthcare concern. Owing to this crisis, there is a critical need to develop antagonistic agents that can thwart the inherent resistance mechanism and resensitize the pathogen against therapeutic antibiotics. The current investigation is an endeavor to address this challenge and illustrates the use of rationally designed low molecular weight ligands to counter the core resistance mechanism in MRSA and thereby restore susceptibility of the pathogen to low doses of a therapeutic antibiotic. The key accomplishments of the study and the future prospects of the leads are as follows:

1. A key resistance mechanism prevalent in MRSA is the presence of efflux pumps, which enable the pathogen to evade the action of an antibiotic. In order to address this problem, urea-based ligands were rationally designed as potential efflux pump inhibitor (EPI). Amongst structurally varying urea-based ligands, the ligand C8 bearing a nitro group and reasonable hydrophobicity and polarity could significantly inhibit efflux pump activity in a clinical MRSA strain. Interestingly, C8 could suppress the expression of *norA* gene encoding a major efflux pump in MRSA, reduce the MIC of ciprofloxacin (CPX) 16-fold and prevent emergence of CPX resistance in MRSA for many generations in a combinatorial therapy regimen. Based on the structural guidelines emerging from the current study, a more rigorous structure-function study with a larger repertoire of synthetic EPIs can be undertaken to strengthen the findings and discover a more potent candidate molecule for anti-MRSA therapy.
2. The potency of C8 as an efflux pump inhibitor could be leveraged in C8-loaded PLGA nanocarrier (C8-PNC), which breached the core resistance mechanism to disarm the pathogen and could subsequently eliminate MRSA in combination with only 2.0 µM ciprofloxacin. A significant highlight of the study is that the developed nanomaterial (C8-PNC) was non-toxic and could hinder adhesion of MRSA cells on collagen in combination with ciprofloxacin. In future, it would be interesting to explore the potential of C8-PNC in combination with CPX for mitigation of MRSA infection in collagen-rich tissues such as skin and bone in a suitable *in vivo* model.

3. The bacterial cell membrane is bedrock for critical physiological functions. The membrane is also a formidable permeability barrier for antibiotics. Hence, it is conceived that antibacterials that can breach the membrane or disrupt its function hold significant prospect against MRSA. The quinoxaline-based ligand C2 evaluated in the present study offers a viable approach in anti-MRSA therapy. Owing to its potent membrane-directed activity, the molecule C2 acts on a profound target and is less likely to trigger resistance development.
4. The limitations of antibiotic-mediated monotherapy combined with the prolonged process of drug discovery against MRSA has fueled a crisis in the clinics. In order to tide over this crisis, combination therapy is professed as a promising approach for mitigation of MRSA infections. The current investigation demonstrates that the membrane-targeting C2 could be effectively leveraged as an adjuvant molecule to bolster the potency of ciprofloxacin against MRSA as well as effectively counter MRSA in an *in vitro* bone cell infection model. It would be worthwhile to leverage the leads obtained from the current study and validate the potential of the combination therapy regimen in an *in vivo* bone cell infection model of MRSA.
5. Colonization of orthopaedic implant by recalcitrant MRSA biofilm can trigger serious infections leading to high rates of implant failure and associated clinical complications. In the current study, the adjuvant potential of the ligand C2 was leveraged to develop a biocompatible HSA nanocarrier, which in combination with CPX could prevent the invasion of MRSA onto Ti wire, used as a model orthopaedic implant. In future it would be interesting to explore whether the bactericidal nanocarrier can be further fortified with growth factors to support bone cell growth on the implant.
6. In order to leverage the candidate molecules C8 and C2 for anti-MRSA therapy, it will be crucial to establish their *in vivo* attributes. In this regard, an acute toxicity and histopathological study with the ligands can be conducted in future on animal models. Further, given the potent anti-MRSA activity of C2, it will be interesting to assess in an animal model whether the ligand can be used as a topical agent to prevent MRSA invasion in a wound and thereby promote wound healing.

The rational design of the adjuvants C8 and C2 is an illustration of judicious medicinal chemistry to address a pertinent global healthcare problem. The nanomaterials developed in the current study can serve as prototypes of therapeutic adjuvants to mitigate invasive MRSA infections in soft tissue and bone implants. In the domain of anti-MRSA therapeutics, C8 and C2 hold potential in combination therapy directed against a serious human pathogen. A schematic representation of the significant findings emerging from the present investigation is indicated in Scheme 1.

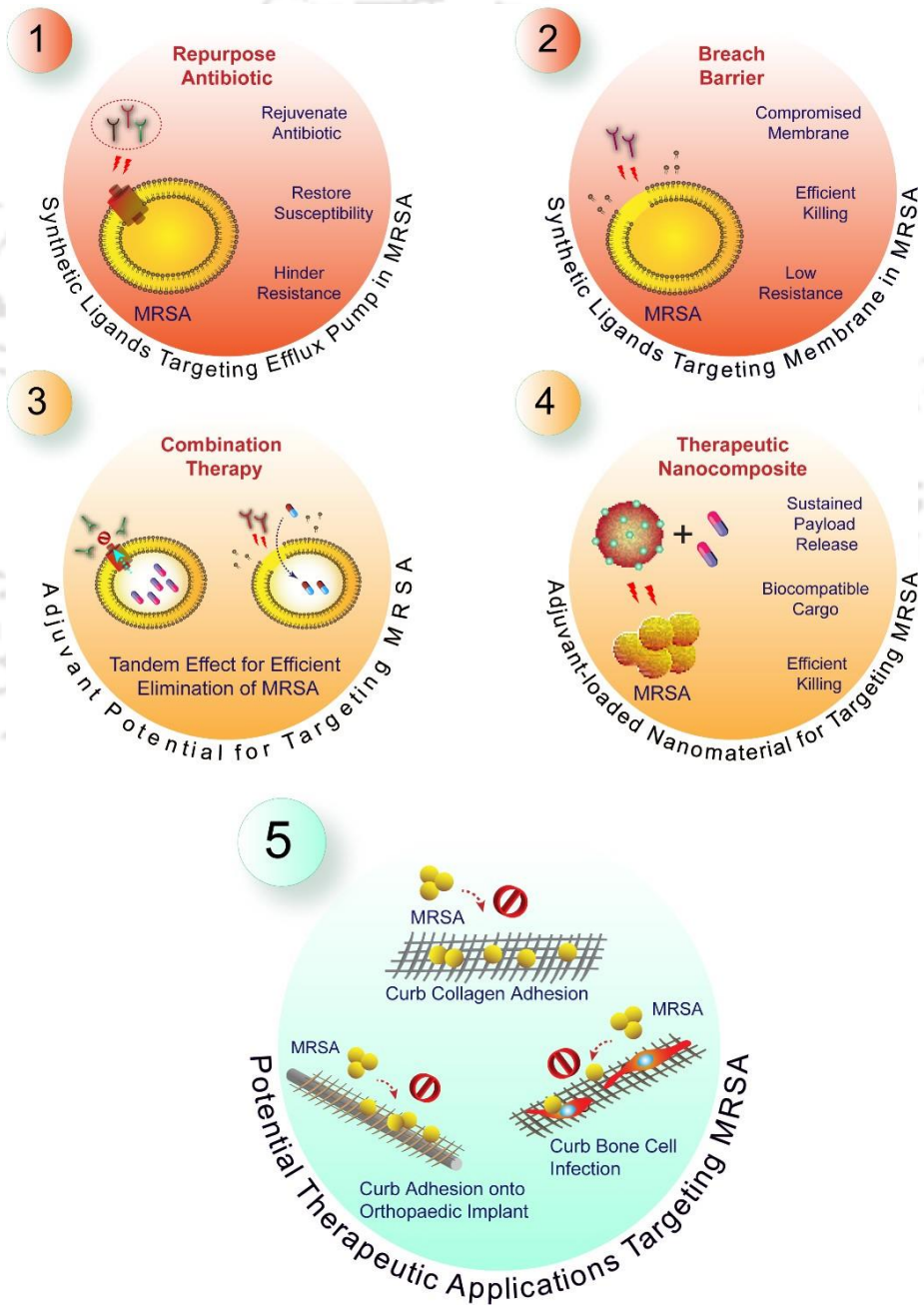

Scheme 1. Schematic representation of the significant findings of the present investigation.

BIBLIOGRAPHY

1. Adhikari, M. D.; Goswami, S.; Panda, B. R.; Chattopadhyay, A.; Ramesh, A. Membrane-directed high bactericidal activity of gold nanoparticle-polythiophene composite for niche applications against pathogenic bacteria, *Adv. Healthcare Mater*. **2013**, *2*, 599-606.
2. Al Atya A. K.; Belguesmia, Y.; Chataigne, G.; Ravallec, R,; Vachee, A.; Szunerits, S.; Boukherroub, R.; Drider, D. Anti-MRSA activities of enterocins DD28 and DD03 and their evidences on their role in the inhibition of biofilm formation. *Front. Microbiol*. **2016**, *7*, 817.
3. Arbeit, R. D.; Maki, D.; Tally, F. P.; Campanaro, E.; Eisenstein, B. I. The safety and efficacy of daptomycin for the treatment of complicated skin and skin-structure infections. *Clin. Infect. Dis*. **2004**, *38*, 1673-1681.
4. Archer, N. K.; Mazaitis, M.; Costerton, W.; Leid, G.; Powers, M. E.; Shirtliff, M. E. *Staphylococcus aureus* biofilms. *Virulence*, **2011**, *2*, 445-459.
5. Arciola, C. R.; Campoccia, D.; Speziale, P.; Montanaro, L.; Costerton, J. W. Biofilm formation in Staphylococcus implant infections. A review of molecular mechanisms and implications for biofilm-resistant materials. *Biomaterials* **2012**, *33*, 5967-5982.
6. Arciola, C.R.; Campoccia, D.; Montanaro, L. Implant infections: adhesion, biofilm formation and immune evasion, *Nat. Rev. Microbiol*. **2018,** *16*, 397-409.
7. Arpin, C.; Noury, P.; Boraud, D.; Coulange, L.; Manetti, A.; Andre, C.; M'Zali, F.; Quentin, C. NDM-1-producing *Klebsiella pneumoniae* resistant to colistin in a French community patient witYonghout history of foreign travel, *Antimicrob. Agents Chemother.* **2012,** *56*, 3432-3434.
8. Bajaj, M.; Pandey, S. K.; Nain, T.; Brar, S. K.; Singh, P.; Singh, S.; Wangoo, N.; Sharma, R. K. Stabilized cationic dipeptide capped gold/silver nanohybrids: towards enhanced antibacterial and antifungal efficacy. *Colloids Surf. B Biointerfaces* **2017**, *158*, 397-407.
9. Bakhshandeh, S.; Karaji, Z. G.; Lietaert, K.; Fluit, A. C.; Boel, C, H. E.; Vogely, H. C.; Vermonden, T.; Hennink, W. E.; Weinans, H.; Zadpoor, A. A.; Yavari, S. A. Simultaneous delivery of multiple antibacterial agents from additively manufactured porous biomaterials to fully eradicate planktonic and adherent *Staphylococcus aureus*. *ACS Appl. Mater. Interfaces* **2017**, *9*, 25691-25699.

10. Banerjee, R.; Fernandez, M. G.; Enthaler, N.; Graml, C.; Greenwood-Quaintance, K. E.; Patel, R. Combinations of cefoxitin plus other β-lactams are synergistic *in vitro* against community associated methicillin-resistant *Staphylococcus aureus*. *Eur. J. Clin. Microbiol. Infect. Dis.*, **2013**, *32*, 827-833.
11. Basak, M.; Bhattacharjee, B.; Ramesh, A.; Das, G. Self-assembled quinoxaline derivative: insight into disaggregation induced selective detection of nitro-aromatics in aqueous medium and live cell imaging. *Dyes. Pigm*. **2021**, *196*, 109779.
12. Bera, S.; Zhanel, G. G.; Schweizer, F. Antibacterial activities of aminoglycoside antibiotics-derived cationic amphiphiles. Polyol-modified neomycin B-, kanamycin A-, amikacin-, and neamine-based amphiphiles with potent broad spectrum antibacterial activity. *J. Med. Chem*. **2010**, *53*, 3626-3631.
13. Berndsen, R.; Cunningham, T.; Kaelin, L.; Callender, M.; Boldog, W. D.; Viering, B.; King, A.; Labban, N.; Pollock, J. A.; Miller, H. B.; Blackledge, M. S. Identification and evaluation of brominated carbazoles as a novel antibiotic adjuvant scaffold in MRSA. *ACS Med. Chem. Lett.* **2022**, *13*, 483-491.
14. Biek, D.; Critchley, I. A.; Diekema, D. J.; Doern, G. V. Activity of ceftaroline and epidemiologic trends in *Staphylococcus aureus* isolates collected from 43 medical centers in the United States in 2009. *Antimicrob. Agents Chemother*. **2011**, *55*, 4154-4160.
15. Bongiorno, D.; Musso, N.; Lazzaro, L. M.; Mongelli, G.; Stefani, S. Campanile, F. Detection of methicillin-resistant *Staphylococcus aureus* persistence in osteoblasts using imaging flow cytometry. *MicrobiologyOpen* **2020**, *9*, e1017.
16. Brincat, J. P.; Broccatelli, F.; Sabatini, S.; Frosini, M.; Neri, A.; Kaatz, G. W.; Cruciani, G.; Carosati, E. Ligand promiscuity between the efflux pumps human p-glycoprotein and *S. aureus* NorA. *ACS Med. Chem. Lett*., **2012**, *3*, 248-251.
17. Brink, A. J.; Coetzee, J.; Clay, C. G.; Sithole, S.; Richards, G. A.; Poirel, L.; Nordmann, P. Emergence of New Delhi Metallo-Beta-Lactamase (NDM-1) and *Klebsiella pneumoniae* Carbapenemase (KPC-2) in South Africa, *J. Clin. Microbiol.* **2012,** *50*, 525-527.
18. Brown, E.D.; Wright, G.D. Antibacterial drug discovery in the resistance era. Nature **2016**, 529, 336-343.

19. Brown, E.D.; Wright, G.D. Antibacterial drug discovery in the resistance era. *Nature* **2016**, *529*, 336-343.
20. Brown, M. H.; Skurray, R. A. Staphylococcal multidrug efflux pump protein QacA. *J. Mol. Microbiol. Biotechnol.* **2001**, *3*, 163-170.
21. Bryers, D. Medical biofilms. *Biotechnol. Bioeng*., **2008**, *100*, 1-18.
22. Cartiera, M. S.; Ferreira,E. C.; Caputo, C.; Egan, M. E.; Caplan, M. J.; Saltzman, W. M. Partial correction of cystic fibrosis defects with PLGA nanoparticles encapsulating curcumin. *Mol. Pharma*., **2009**, 7, 86-93.
23. Cascioferro, S.; Carbone, D.; Parrino, B.; Camilla, P.; Giovannetti, E.; Cirrincione, G.; Diana, P. Therapeutic strategies to counteract antibiotic resistance in MRSA biofilm-associated infections. *ChemMedChem* **2021**, *16*, 65-80.
24. Casula, A.; Fornasier, M.; Montis, R.; Bettoschi, A.; Argent, S. P.; Blake, A. J.; Lippolis, V.; Marongiu, L.; Picci, G.; Tidey, J. P.; Caltagirone, C. Halogen-substituted ureas for anion binding: solid state and solution studies. *Supramol. Chem*., **2017**, *29*, 875-886.
25. CDC. Antibiotic Resistance Threats in the United States, 2019. Atlanta, GA: U.S. Department of Health and Human Services, CDC; 2019. www.cdc.gov/DrugResistance/Biggest-Threats.html DOI: http://dx.doi.org/10.15620/cdc:82532.
26. Chambers, H. F.; Deleo, F. R.; Waves of resistance: *Staphylococcus aureus* in the Antibiotic Era. *Nat. Rev. Microbiol*, **2010,** *7*, 629–641.
27. Chen, C. J.; Huang, Y. C.; Chiu, C. H. Multiple pathways of cross-resistance to glycopeptides and daptomycin in persistent MRSA bacteraemia. *J. Antimicrob. Chemother*. **2015**, *70*, 2965-2972.
28. Chen, C.; Pan, F.; Zhang, S.; Hu, J.; Cao, M.; Wang, J.; Xu, H.; Zhao, X.; Lu, J. R. Antibacterial activities of short designer peptides: a link between propensity for nanostructuring and capacity for membrane destabilization. *Biomacromolecules*. **2010**, *11*, 402-411. Chen, L.; Gao, L.; Fang, W.; Golubovic, L. How the antimicrobial peptides kill bacteria: Computational Physics Insights 1 Introduction. *Commun. Comput.Phys.*, **2012**, *11*, 709-725.
29. Cheng, G.; Sa, W.; Cao, C.; Guo, L.; Hao, H.; Liu, Z.; Wang, X.; Yuan, Z. Quinoxaline 1,4-di-*N*-oxides: biological activities and mechanisms of actions. *Front. Pharmacol*., **2016**, *7*, 64.

30. Cheung, G. Y.; Wang, R.; Khan, B. A.; Sturdevant, D. E.; Otto, M. Role of the accessory gene regulator *agr* in community-associated methicillin-resistant *Staphylococcus aureus* pathogenesis. *Infect. Immun*. **2011**, *79*, 1927-1935.
31. Christena, L. R.; Subramaniam, S.; Vidhyalakshmi, M.; Mahadevan, V.; Sivasubramanian, A.; Nagarajan, S. Dual role of pinostrobin-a flavonoid nutraceutical as an efflux pump inhibitor and antibiofilm agent to mitigate food borne pathogens. *RSC Adv*., **2015**, *5*, 61881-61887.
32. Coelho, M. L.; Ferreira, J. H. L.; Junior, J. P.S.; Kaatz, G. W.; Barreto, H. M.; Cavalcante, A. A. C. M. Inhibition of the NorA multi-drug transporter by oxygenated monoterpenes. Microb. Path. **2016**, 99, 173-177.
33. Collin, F.; Karkare, S.; Maxwell, A. Exploiting bacterial DNA gyrase as a drug target: current state and perspectives. *Appl Microbiol Biotechnol*. **2011**, *92*, 479-497.
34. Cosgrove, S. E.; Vigliani, G. A.; Campion, M.; Fowler, V. G. Jr.; Abrutyn, E.; Corey, G. R.; Levine, D. P.; Rupp, M. E.; Chambers, H. F.; Karchmer, A. W.; Boucher, H. W. Initial low-dose gentamicin for *Staphylococcus aureus* bacteremia and endocarditis is nephrotoxic. *Clin. Infect. Dis.*, **2009**, *48*, 713-721.
35. Costa, S. S.; Viveiros, M.; Rosato, A. E.; Melo-Cristino, J.; Couto, I. Impact of efflux in the development of multidrug resistance phenotypes in *Staphylococcus aureus*. *BMC Microbiol*., **2015**, *15*, 232.
36. Craft. K. M.; Nguyen, J. M.; Berg, L. J.; Towndend, S. D. Methicillin-resistant *Staphylococcus aureus* (MRSA): antibiotic-resistance and the biofilm phenotype. *Med. Chem. Commun*. **2019**, *10*, 1231-1241.
37. Danhier, F.; Ansorena, E.; Silva, J. M.; Coco, R.; Le Breton, A.; Preat, V. PLGA-based nanoparticles: an overview of biomedical applications. *J. Control Release* **2012**, *161*, 505-522.
38. Darouiche, R.O. Treatment of infections associated with surgical implants. *N. Engl. J. Med*., **2004**, *350*, 1422-1429.
39. Das, B.; Chattopadhyay, P.; Mishra, D.; Maiti, T. K.; Maji, S.; Narayan, R.; Karak, N. Nanocomposites of bio-based hyperbranched polyurethane/funtionalized MWCNT as non-immunogenic, osteoconductive, biodegradable and biocompatible scaffolds in bone tissue engineering. *Journal of Materials Chemistry B*, **2013**, *1*, 4115-4126.

40. Davies, J.; Davies, D. Origins and evolution of antibiotic resistance. *Microbiol. Mol. Biol. Rev.*, **2010**, *74*, 417–433.
41. Davis, J. S.; Van Hal, S.; Tong. S. Y. C. Combination antibiotic treatment of serious methicillin-resistant *Staphylococcus aureus* infections. *Semin. Respir. Crit. Care Med.*, **2015**, *36*, 3-16.
42. de Kraker, M. E. A.; Stewardson, A.; Harbarth, S. Will 10 million people die a year due to antimicrobial resistance by 2050? *PLoS Med*. **2016**, *13*, e1002184.
43. Dey, P.; Das, G.; Ramesh, A. Interplay between supramolecular and coordination interactions in synthetic amphiphiles: Triggering metal starvation and anchorage onto MRSA cell surface. *Langmuir*, **2020**, *36*, 2110-2119.
44. Dey, P.; Mukherjee, S.; Das, G.; Ramesh, A. Micellar chemotherapeutic platform based on a bifunctional salicaldehyde amphiphile delivers a "combo-effect" for heightened killing of MRSA. *J. Mater. Chem. B* **2018**, *6*, 2116-2125.
45. Doran, P. M. Bioprocess Engineering Principles, (2nd Ed.). Elsevier Ltd, **2013**.
46. Duncan, B.; Li, X.; Landis, R. F.; Kim, S. T.; Gupta, A.; Wang, L. S.; Ramanathan, R.; Tang, R.; Boerth, J. A.; Rotello, V. M. Nanoparticle-stabilized capsules for the treatment of bacterial biofilms. *ACS Nano* **2015**, *9*, 7775-7782.
47. Ellington, J.K.; Harris, M.; Hudson, M. C.; Vishin, S.; Webb, L. X.; Sherertz, R. Intracellular *Staphylococcus aureus* and antibiotic resistance: implications for treatment of staphylococcal osteomyelitis. *J. Orthop. Res.* **2006**, *24*, 87-93.
48. Fair, R. J., & Tor, Y. Antibiotics and bacterial resistance in the 21st century. *Perspect. Medicin. Chem.*, **2014,** 25–64.
49. Feldman, M.; Smoum, R.; Mechoulam, R.; Steinberg, D. Potential combinations of endocannabinoid/endocannabinoid-like compounds and antibiotics against methicillin resistant *Staphylococcus aureus*. *PLoS ONE* **2020**, *15*, e0231583.
50. Finch, R. G.; Eliopoulos, G. M. Safety and efficacy of glycopeptide antibiotics. *J. Antimicrob. Chemother*., **2005**, *55*, Suppl. S2, ii5-ii13.

51. Findlay, B.; Zhanel G. G.; Schweizer, F. Cationic amphiphiles, A new generation of antimicrobials inspired by the natural antimicrobial peptide scaffold, *Antimicrob. Agents Chemother*. **2010**, *54*, 4049-4058.
52. Fischbach, M. A.; Walsh, C. T. Antibiotics for emerging pathogens, *Science* **2009**, *325*, 1089-1093.
53. Fischbach, M. Combination therapies for combating antimicrobial resistance. *Curr. Opin. Microbiol*., **2011**, *14*, 519-523.
54. Floyd, J. L.; Smith, K. P.; Kumar, S. H.; Floyd, J. T.; Varela, M. F. LmrS is a multidrug efflux pump of the major facilitator superfamily from *Staphylococcus aureus*. *Antimicrob. Agents Chemother*. **2010**, *54*, 5406-5412.
55. Fontaine, F.; Hequet, A.; Voisin-Chiret, A-S.; Bouillon, A.; Lesnard, A.; Cresteil, T.; Jolivalt, C.; Rault, S. First identification of boronic species as novel potential inhibitors of the *Staphylococcus aureus* NorA efflux pump. *J. Med. Chem.*, **2014**, *57*, 2536-2548.
56. Foster, T.J.; Geoghegan, J.A.; Vannakambadi, K.G.; Hook, M. Adhesion, invasion and evasion: the many functions of the surface proteins of *Staphylococcus aureus*. *Nat. Rev. Microbiol*., **2014**, *12*, 49-62.
57. Fuente-Nunez, C. D. L.; Reffuveille, F.; Fernandez, L.; Hancock, R. E. WW. Bacterial biofilm development as a multicellular adaptation: antibiotic resistance and new therapeutic strategies. Curr. Opin. Microbiol., **2013**, *16*, 580–589.
58. Ganesan, A.; Christena, L. R.; Subbarao, H. M. V.; Venkatasubramanian, U.; Thiagarajan, R.; Sivaramakrishnan, V.; Kasilingam, K.; Saisubramanian, N.; Ganesan, S. S. Identification of benzochromene derivatives as a highly specific NorA efflux pump inhibitor to mitigate the drug resistant strains of *S. aureus*. *RSC Adv*. **2016**, *6*, 30258-30267.
59. Gaur, R.; Gupta, V. K.; Pal, A.; Darokar, M. P.; Bhakuni, R. S.; Kumar, B. *In vitro* and *in vivo* synergistic interaction of substituted chalcone derivatives with norfloxacin against methicillin resistant *Staphylococcus aureus*. *RSC Adv*., **2015**, *5*, 5830-5845.
60. Geetha, M.; Singh, A. K.; Asokamani, R.; Gogia, A. K. Ti based biomaterials, the ultimate choice for orthopaedic implants–a review. *Prog. Mater. Sci.* **2009**, *54*, 397-425.

61. Ghimire, A.; Song, J. Anti-periprosthetic infection strategies: from implant surface topographical engineering to smart drug-releasing coatings. ACS Appl. Mater. Interfaces **2021**, *13*, 20921-20937.
62. Ghosh, D.; Basak, M.; Deka, D.; Das G. Fabrication and photophysical assessment of quinoxaline based chemosensor: selective determination of picric acid in hydrogel and aqueous medium. *J. Mol. Liq*. **2022**, 119816.
63. Giacometti, A; Oscar C.; Maria S.; Del P.; Alessandra M.; Marcello M.; D. Errico; Giorgio S. Combination studies between polycationic peptides and clinically used antibiotics against gram-positive and gram-negative bacteria., *Peptides*, **2000**, *21*, 1155-1160.
64. Gidari, A.; Sabbatini, S.; Schiaroli, E.; Perito, S.; Francisci, D.; Baldelli, F.; Monari, C. Tedizolid-rifampicin combination prevents rifampicin-resistance on *in vitro* model of *Staphylococcus aureus* mature biofilm. *Front. Microbiol*. **2020**, *11*, 2085.
65. Giraud, E.; Cloeckaert, A.; Kerboeuf, D.; Chaslus-Dancla, E. Evidence for active efflux as the primary mechanism of resistance to ciprofloxacin in *Salmonella enterica* serovar *typhimurium*. *Antimicrob. Agents Chemother*., **2000**, *44*, 1223-1228.
66. Gokel, G. W.; Negin, S. Synthetic membrane active amphiphiles. *Adv. Drug Del. Rev*., **2012**, *64*, 784-796.
67. Gootz, T. D. The global problem of antibiotic resistance. *Crit. Rev. Immun*. **2010**, *30*, 79-93.
68. Goswami, S.; Adhikari M.D.; Kar C.; Thiyagarajan D.; Das G.; Ramesh A. Synthetic amphiphiles as therapeutic antibacterials: Lessons on bactericidal efficacy and cytotoxicity and potential application as an adjuvant in antimicrobial chemotherapy. *Journal of Materials Chemistry B*, **2013**, *1*, 2612-2623.
69. Goswami, S.; Thiyagarajan, D.; Das, G.; Ramesh, A. Biocompatible nanocarrier fortified with a dipyridinium-based amphiphile for eradication of biofilm. *ACS Appl. Mater. Interfaces* **2014**, *6*, 16384-16394.
70. Gould, I. M.; David, M. Z.; Esposito, S.; Garau, J.; Lina, G.; Mazzei, T.; Peters, G. New insights into meticillin-resistant *Staphylococcus aureus* (MRSA) pathogenesis, treatment and resistance. *Int. J. Antimicrob. Agents* **2012**, *39*, 96-104.

71. Gulati, K.; Hamlet, S. M.; Ivanovski, S. Tailoring the immuno-responsiveness of anodized nano-engineered titanium implants. *J. Mater. Chem. B* **2018**, *6*, 2677-2689.
72. Guo, Y.; Hou, E.; Wen, T.; Yan, X.; Han, M.; Bai, L, P.; Fu, X.; Liu, J.; Qin, S. Development of membrane-active honokiol/magnolol amphiphiles as potent antibacterial agents against methicillin-resistant *Staphylococcus aureus* (MRSA). *J. Med. Chem.* **2021**, *64*, 12903-12916.
73. Gutsmann, T.; Seydel, U. Impact of the glycostructure of amphiphilic membrane components on the function of the outer membrane of Gram-negative bacteria as a matrix for incorporated channels and a target for antimicrobial peptides or proteins. *Eur. J. Cell Biol*. **2010**, *89*, 11-23.
74. Hall, C.W.; Mah, T.F. Molecular mechanisms of biofilm-based antibiotic resistance and tolerance in pathogenic bacteria. *FEMS Microbiol. Rev*. **2017**, *41*, 276-301.
75. Hall-Stoodley, L.; Costerton, J. W.; Stoodley, P. Bacterial biofilms: from the natural environment to infectious diseases. *Nat. Rev. Microbiol*. **2004**, *2*, 95-108.
76. Handzlik, J.; Matys, A.; Kiec-Kononowicz, K.; Recent Advances in Multi-Drug Resistance (MDR) Efflux Pump Inhibitors of Gram-Positive Bacteria *S. aureus*. *Antibiotics* **2013**, *2*, 28-45.
77. Hawas, S.; Verderosa, A.D.; Totsika, M. Combination therapies for biofilm inhibition and eradication: a comparative review of laboratory and preclinical studies. *Front. Cell. Infect. Microbiol.* **2022**, *12*, 850030.
78. Hetrick, EM; Schoenfisch, M.H. Reducing implant-related infections: active release strategies. *Chem. Soc. Rev.*, **2006,** *35*, 780–789.
79. Hoefel, D.; Grooby, W. L.; Monis, P. T.; Andrews, S.; Saint, C. P. A comparative study of carboxyfluorescein diacetate and carboxyfluorescein diacetate succinimidyl ester as indicators of bacterial activity. *J. Microbiol. Methods*. **2003**, *52*, 379-388.
80. Hoque, J.; Akkapeddi, P.; Yarlagadda, V.; Uppu, D. S.; Kumar, P.; Haldar, J. Cleavable cationic antibacterial amphiphiles: synthesis, mechanism of action, and cytotoxicities, *Langmuir* **2012,** *28*, 12225-12234.
81. Horn, J.; Stelzner, K.; Rudel, T.; Fraunholz, M. Inside job: *Staphylococcus aureus* host-pathogen interactions. *Int. J. Med. Microbiol.* **2018**, *308*, 607-624.

82. Houlihan, H.H.; Mercier, R. C.; Rybak, M. J. Pharmacodynamics of vancomycin alone and in combination with gentamicin at various dosing intervals against methicillin-resistant *Staphylococcus aureus*-infected fibrin-platelet clots in an *in vitro* infection model. *Antimicrob. Agents Chemother*., **1997**, *41*, 2497-2501.
83. Hu, H.; Zhang, W.; Qiao, Y.; Jiang, X.; Liu, X.; Ding, C. Antibacterial activity and increased bone marrow stem cell functions of Zn-incorporated TiO_2 coatings on titanium. *Acta Biomater*. **2012**, *8*, 904-915.
84. Huh, A.J.; Kwon, Y. J. "Nanoantibiotics": A new paradigm for treating infectious diseases using nanomaterials in the antibiotics resistant era. *J. Control. Release* **2011**, *156*, 128-145.
85. Hurdle, J. G.; O'Neill, A. J.; Chopra, I.; Lee, R. E. Targeting bacterial membrane function: an underexploited mechanism for treating persistent infections. *Nat. Rev. Microbiol*. **2011**, *9*, 62-75.
86. Jang, S. Multidrug efflux pumps in *Staphylococcus aureus* and their clinical implications. *J. Microbiol*., **2016**, *54*, 1-8.
87. Jarraud, S.; Lyon, G. J.; Figueiredo, A. M.; Lina, G.; Vandenesch, F.; Etienne, J.; Muir, T, W.; Novick, R. P. Exfoliatin-producing strains define a fourth agr specificity group in *Staphylococcus aureus*. J. Bacteriol. 2000, 182, 6517-6522.
88. Jevon, M.; Guo, C.; Ma, B.; Mordan, N.; Nair, S.P.; Harris, M.; Henderson, B.; Bentley, G.; Meghji, S. Mechanisms of internalization of *Staphylococcus aureus* by cultured human osteoblasts. *Infect. Immun*. **1999**, *67*, 2677-2681.
89. Jin, Y.; Shao, C.; Li, J.; Fan, H.; Bai, Y.; Wang, Y. Outbreak of multidrug resistant NDM-1-producing *Klebsiella pneumoniae* from a neonatal unit in Shandong Province, China, *PLoS One*, **2015,** *10*, e0119571.
90. Jose, D. A.; Kumar, D. K.; Kar, P.; Verma, S.; Ghosh, A.; Ganguly, B.; Ghosh, H. N.; Das, A. Role of positional isomers on receptor–anion binding and evidence for resonance energy transfer. *Tetrahedron*, **2007**, *63*, 12007-12014.
91. Kaatz, G.W.; Seo, S.M.; Ruble, C.A. Efflux-mediated fluoroquinolone resistance in *Staphylococcus aureus*. *Antimicrob. Agents Chemother.* **1993**, *37*, 1086-1094.
92. Kaatz, G.W.; Thyagarajan, R.V.; Seo, S.M. Effect of promoter region mutations and MgrA overexpression on transcription of norA, which encodes a *Staphylococcus aureus* multidrug efflux transporter. *Antimicrob. Agents Chemother*. **2005**, *49*, 161-169.

93. Kang, H. K.; Park, J.; Seo, C. H.; Park, Y. PEP27-2, a potent antimicrobial cell-penetrating peptide, reduces skin abscess formation during *Staphylococcus aureus* infections in mouse when used in combination with antibiotics. *ACS Infect. Dis.* **2021**, *7*, 2620-2636.
94. Kaye, K. S.; Kaye, D. Multidrug-resistant pathogens: mechanisms of resistance and epidemiology. *Curr. Infect. Dis. Rep*. **2000**, *2*, 391-398.
95. Kim, W.; Zou, G.; Hari, T. P. A.; Wilt, I. K.; Zhu, W.; Galle, N.; Faizi, H. A.; Hendricks, G. L.; Tori, K.; Pan, W.; Huang, X.; Steele, A. D.; Csatary, E. E.; Dekarske, M. M.; Rosen, J. L.; Ribeiro, N. Q.; Lee, K.; Port, J.; Fuchs, B. B.; Vlahovska, P. M.; Wuest, W. M.; Gao, H.; Ausubel, F. M.; Mylonakis, E. A selective membrane-targeting repurposed antibiotic with activity against persistent methicillin-resistant *Staphylococcus aureus*. *Proc. Natl. Acad. Sci*, **2019**, *116*, 16529-16534.
96. Kohanski, M. A.; Dwyer, D. J.; Collins, J. J. How antibiotics kill bacteria: from targets to networks. *Nat. Rev. Microbiol*. **2010**, *8*, 423-435.
97. Kokubo, T.; Kushitani, H.; Sakka, S.; Kitsugi, T.; Yamamuro, T. Solutions able to reproduce *in vivo* surface-structure changes in bioactive glass–ceramic A-W. *J. Biomed. Mater. Res*. **1990**, *24*, 721-734.
98. Kouidhi, B.; Zmantar, T.; Hentati, H.; Bakhrouf, A. Cell surface hydrophobicity, biofilm formation, adhesives properties and molecular detection of adhesins genes in *Staphylococcus aureus* associated to dental caries. *Microb. Pathog.*, **2010**, *49*, 14–22.
99. Kuroda, K.; DeGrado, W. F. Amphiphilic polymethacrylate derivatives as antimicrobial agents. *J. Am. Chem. Soc*. **2005**, *127*, 4128-4129
100. Lam, A. K.; Moen, E. L.; Pusavat, J.; Wouters, C. L.; Panlilio, H.; Ferrell, M. J.; Houck, M. B.; Glatzhofer, D. T.; Rice, C. V. PEGylation of polyethylenimine lowers acute toxicity while retaining anti-biofilm and β lactam potentiation properties against antibiotic-resistant pathogens. *ACS Omega* **2020**, *5*, 26262-26270.
101. Lange, R. P.; Locher, H. H.; Wyss, P. C.; Then, R. L. The targets of currently used antibacterial agents: lessons for drug discovery. *Curr Pharm Des*. **2007**, *13*, 3140-3154.

102. Langer, K.; Balthasar, S.; Vogel, V.; Dinauer, N.; von Briesen, H.; Schubert, D. Optimization of the preparation process for human serum albumin (HSA) nanoparticles. *Int. J. Pharmaceutics* **2003**, *257*, 169-180.

103. Lee, A. S.; Lencastre, H. D.; Garau, Javier.; Kluytmans, J.; Malhotra-kumar, S.; Peschel, A.; Harbarth, S. Methicillin-resistant *Staphylococcus aureus*. *Nat. Rev. Dis. Primer*, **2018**, *4*, 18033.

104. Lee, H. J.; Kim, B.; Kim, S.; Cho, D. H.; Jung, H.; Kim, W.; Kim, Y. G.; Kim, J. S.; Joo, H. S.; Lee, S.H.; Yang, Y. H. Leucyl-tRNA synthetase inhibitor, d-norvaline, in combination with oxacillin, is effective against methicillin-resistant *Staphylococcus aureus*. *Antibiotics* **2022**, *11*, 683.

105. Lepri, S.; Buonerba, F.; Goracci, L.; Velilla, I.; Ruzziconi, R.; Schindler, B. D.; Seo, S. M.; Kaatz, G. W.; Cruciani, G. Indole based weapons to fight antibiotic resistance: a structure-activity relationship study. *J. Med. Chem.*, **2016**, *59*, 867-891.

106. Lewies, A.; Wentzel, J. F.; Jordaan, A.; Bezuidenhout, C.; Du Plessis, L. H. Interactions of the antimicrobial peptide nisin Z with conventional antibiotics and the use of nanostructured lipid carriers to enhance antimicrobial activity. *Int. J. Pharm*. **2017**, *526*, 244-253.

107. Li, X. Z.; Nikaido, H. Efflux-mediated drug resistance in bacteria: an update. *Drugs*, **2009**, *69*, 1555-1623.

108. Liu, C.; Bayer, A,; Cosgrove. S. E.; Daum, R. S.; Fridkin, S. K.; Gorwitz, R. J.; Kaplan. S. L.; karchmer, A. W.; Levine, D. P.; Murray, B. E.; Rybak, M. J.; Talan, D. A.; Chambers, H. F. Clinical practice guidelines by the Infectious Diseases Society of America for the treatment of methicillin-resistant *Staphylococcus aureus* infections in adults and children. *Clin. Infect. Dis*. **2011**, *52*, e18-55.

109. Livak, K. J.; Schmittgen, T. D. Analysis of relative gene expression data using real-time quantitative PCR and the $2^{-\Delta\Delta CT}$ method. *Methods*, **2001**, *25*, 402-408.

110. Lowy, F.D. *Staphylococcus aureus* infections. *N. Engl. J. Med*., **1998**, *339*, 520-532.

111. M. Basak.; Das, G. Supramolecular self-assembly of nitro-incorporated quinoxaline framework: insights into the origin of fluorescence turn-on response towards benzene group of VOCs. *Analyst* **2021**, *146*, 6239-6244.

112. Manna, U.; Chutia, R.; Das, G. Entrapment of cyclic fluoride-water and sulfate-water-sulfate cluster within the self-assembled structure of linear meta-

phenylenediamine based bis-urea receptors: positional isomeric effect. *Cryst. Growth Des*., **2016**, *16*, 2893-2903.

113. Manna, U.; Nayak, B.; Das, G. Dual guest [(Chloride)$_3$-DMSO] encapsulated cation-sealed neutral trimeric capsular assembly: meta-substituent directed halide and oxyanion binding discrepancy of isomeric neutral disubstituted bis-urea receptors. *Cryst. Growth Des*., **2016**, *16*, 7163-7174.
114. Marr, A. K.; Gooderham, W. J.;Hancock, R. E. W. Antibacterial peptides for therapeutic use : obstacles and realistic outlook. *Curr. Opin. Pharmacol.*, **2006**, 468-472.
115. Mather, A. E.; Reid, S. W.; Maskell, D. J.; Parkhill, J.; Fookes, M. C.; Harris, S. R.; Brown, D. J.; Coia, J. E.; Mulvey, M. R.; Gilmour, M. W.; Petrovska, L.; de Pinna, E.; Kuroda, M.; Akiba, M.; Izumiya, H.; Connor, T. R.; Suchard, M. A.; Lemey, P.; Mellor, D. J.; Haydon, D. T.; Thomson, N. R. Distinguishable epidemics of multidrug-resistant *Salmonella Typhimurium* DT104 in different hosts. *Science* **2013**, *341*, 1514-1517.
116. McCoy, L. S.; Xie, Y.; Tor, Y. Antibiotics that target protein synthesis. *Wiley Interdiscip. Rev. RNA.* **2011**, *2*, 209-232.
117. Melander, R. J.; Melander, C. The challenge of overcoming antibiotic resistance: an adjuvant approach? *ACS Infect. Dis.* **2017**, *3*, 559-563.
118. Moretti, A.; Weeks, R. M.; Chikindas, M.; Uhrich, K. E. Cationic amphiphiles with specificity against gram-positive and gram-negative bacteria: chemical composition and architecture combat bacterial membranes. *Langmuir* **2019**, *35*, 5557-5567.
119. Mukherjee, S.; Ramesh, A. Dual label flow cytometry-based host cell adhesion assay to ascertain the prospect of probiotic *Lactobacillus plantarum* in niche-specific antibacterial therapy. *Microbiology* **2017**, *163*, 1822-1834.
120. Mukherjee, S; Ramesh, A. Bacteriocin-producing strains of *Lactobacillus plantarum* inhibit adhesion of *Staphylococcus aureus* to extracellular matrix: Quantitative insight and implications in antibacterial therapy. *J. Med. Microbiol*., **2015**, *64*, 1514-1526.
121. Mullick, P.; Das, G.; Ramesh, A. 2-Dodecylmalonic acid-mediated synthesis of mineralized hydroxyapatite amicable for bone cell growth on orthopaedic implant. *J. Colloid Inter. Sci*. **2022**, *608*, 2298-2309.

122. Mullick, P.; Das, G.; Ramesh, A. Probiotic bacteria cell surface-associated protein mineralized hydroxyapatite incorporated in porous scaffold: in vitro evaluation for bone cell growth and differentiation. *Mater. Sci. Eng.*: *C* **2021**, *126*, 112101.

123. Musso, N.; Caruso, G.; Bongiorno, D.; Grasso, M.; Bivona, D.A.; Campanile, F.; Caraci, F.; Stefani, S. Different modulatory effects of four methicillin-resistant *Staphylococcus aureus* clones on MG-63 osteoblast-like cells. *Biomolecules* **2021**, *11*, 72.

124. Mwangi, M. M.; Wu, S. W.; Zhou, Y.; Sieradski, K.; de Lencastre, H.; Richardson, P.; Bruce, D.; Rubin, E.; Myers, E.; Siggia, E. D.; Tomasz, A. Tracking the *in vivo* evolution of multidrug resistance in *Staphylococcus aureus* by whole-genome sequencing. *Proc. Natl. Acad. Sci*. **2007**, *104*, 9451-9456.

125. Namivandi-Zangeneh, R.; Wong, E. H. H.; Boyer, C. Synthetic antimicrobial polymers in combination therapy: tackling antibiotic resistance. *ACS Infect. Dis*. **2021**, *7*, 215-253.

126. Neyfakh, A.A.; Borsch, C.M.; Kaatz, G.W. Fluoroquinolone resistance protein NorA of *Staphylococcus aureus* is a multidrug efflux transporter. *Antimicrob. Agents Chemother*. **1993**, *37*, 128-129.

127. Ng E. Y. W.; Trucksis, M.; Hooper, D. C. Quinolone resistance mediated by norA: physiologic characterization and relationship to flqB, a quinolone resistance locus on the *Staphylococcus aureus* chromosome. *Antimicrob. Agents Chemother*. **1994**, *38*, 1345-1355.

128. Nikaido, H. Multidrug resistance in bacteria. *Annu. Rev. Biochem.*, **2010**, *78*, 119–146.

129. Nordmann, P.; Poirel, L.; Walsh, T. R.; Livermore, D. M. The emerging NDM carbapenemases. *Trends Microbiol*. **2011**, *19*, 588-595.

130. Novick, R.P. Autoinduction and signal transduction in the regulation of staphylococcal virulence. *Mol. Microbiol*. **2003**, *48*, 1429-1449.

131. Oliveira, W.F.; Silva, P.M.S.; Silva, R.C.S.; Silva, G.M.M.; Machado, G.; Coelho, L.; Correia, M.T.S. *Staphylococcus aureus* and *Staphylococcus epidermidis* infections on implants. *J. Hosp. Infect.* **2018**, *98*, 111-117.

132. Otto, M. Staphylococcal biofilms. *Curr. Top. Microbiol. Immunol.*, **2008**, *322*, 207–228.

133. Owens, R. C. Jr.; Ambrose, P. G. Antimicrobial safety: focus on fluoroquinolones. *Clin. Infect. Dis*., **2005**, *41*, S144-S157.
134. Palmer, A. C.; Kishony, R. Opposing effects of target overexpression reveal drug mechanisms. *Nat. Commun*. **2014**, *5*, 4296.
135. Papkou. A.; Hedge, J.; Kapel, N.; Young, B.; Craig MacLean, R. Efflux pump activity potentiates the evolution of antibiotic resistance across *S. aureus* isolates. *Nat. Commun*., **2020**, *11*, 3970.
136. Petchiappan, A.; Chatterji, D. Antibiotic resistance: current perspectives. *ACS Omega* **2017**, *2*, 7400-7409.
137. Peterson, E.; Kaur, P. Antibiotic resistance mechanisms in bacteria: relationships between resistance determinants of antibiotic producers, environmental bacteria, and clinical pathogens. *Front. Microbiol*., **2018**, *9*, 2928.
138. Pieroni, M.; Dimovska, M.; Brincat, J. P,; Sabatini, S.; Carosati, E.; Massari, S.; Kaatz, G. W.; Fravolini, A. From 6-aminoquinolone antibacterials to 6-amino-7-thiopyranopyridinylquinolone ethyl esters as inhibitors of *Staphylococcus aureus* multidrug efflux pumps. *J. Med. Chem.* **2010**, *53*, 4466-4480.
139. Radix, S.; Jordheim. A. D.; Rocheblave, L.; N' Digo, S.; Prignon, A-L.; Commun, C.; Michalet, S.; Dijoux-Franca, M-G.; Mularoni, A.; Walchshofer, N. N, N'-disubstituted cinnamamide derivatives potentiate ciprofloxacin activity against overexpressing NorA efflux pump *Staphylococcus aureus* 1199B strains. *Eur. J. Med. Chem*., **2018**, *150*, 900-907.
140. Radovic-Moreno, A. F.; Lu, T. K.; Puscasu, V. A.; Yoon, C. J.; Langer, R.; Farokhzad, O. C. Surface charge-switching polymeric nanoparticles for bacterial cell wall-targeted delivery of antibiotics. *ACS Nano* **2012**, *6*, 4279-4287.
141. Rasigade J.P.; Trouillet-Assant, S.; Ferry, T.; Diep, B. A.; Sapin, A.; Lhoste, Y.; Ranfaing, J.; Badiou, C.; Benito, Y.; Bes, M.; Couzon, F.; Tigaud, S.; Lina, G.; Etienne, J.; Vandenesch, F.; Laurent, F. PSMs of hypervirulent *Staphylococcus aureus* act as intracellular toxins that kill infected osteoblasts. *PLoS ONE* **2013**, *8*, e63176.
142. Ribeiro, M.; Monteiro, F.J.; Ferraz, M.P. Infection of orthopedic implants with emphasis on bacterial adhesion process and techniques used in studying bacterial-material interactions. *Biomaterials* **2012**, *2*, 176-194.

143. Rossi, F.; Diaz, L.; Wollam, A.; Panesso, D.; Zhou, Y.; Rincon, S.; Narechania, A.; Xing, G.; Di Gioia, T. S. R.; Doi, A.; Tran, T.; Reyes, J.; Munita, J. M.; Carvajal, L. P.; Hernandez-Roldan, A; Brandao, D.; van der Heijden, I. M.; Murray, B. E.; Planet, P. J.; Weinstock, G. M.; Arias, C. A. Transferable vancomycin resistance in a community-associated MRSA lineage. *N. Engl. J. Med*., **2014**, *370*, 1524-1531.

144. Rouch, D. A.; Cram, D. S.; DiBerardino, D.; Littlejohn, T. G.; Skurray, R. A. Efflux-mediated antiseptic resistance gene qacA from *Staphylococcus aureus*: common ancestry with tetracycline- and sugar-transport proteins. *Mol. Microbiol.* **1990**, *4*, 2051-2062.

145. Sabatini, S.; Gosetto, F.; Iraci, N.; Barreca, M. L.; Massari, S.; Sancineto, L.; Manfroni, G.; Tabarrini, O.; Dimovska, M.; Kaatz, G. W.; Cecchetti, W. Re-evolution of the 2-phenylquinolines: ligand-based design, synthesis, and biological evaluation of a potent new class of *Staphylococcus aureus* NorA efflux pump inhibitors to combat antimicrobial resistance. *J. Med. Chem*., **2013**, *56*, 4975-4989.

146. Sabatini, S.; Gosetto, F.; Manfroni, G.; Tabarrini, O.; Kaatz, G. W.; Patel, D.; Cecchetti, V. Evolution from a natural flavones nucleus to obtain 2-(4 propoxyphenyl) quinoline derivatives as potent inhibitors of the *S. aureus* NorA efflux pump. *J. Med. Chem*., **2011**, *54*, 5722-5736.

147. Sabatini, S.; Gosetto, F.; Serritella, S.; Manfroni, G.; Tabarrini, O.; Iraci, N.; Brincat, J. P.; Carosati, E.; Villarini, M.; Kaatz, G. W.; Cecchetti, V. Pyrazolo[4,3-c][1,2]benzothiazines 5,5-dioxide: a promising new class of *Staphylococcus aureus* NorA efflux pump inhibitors. *J. Med. Chem*., **2012**, *55*, 3568-3572.

148. Sabatini, S.; Kaatz, G. W.; Rossolini, G. M.; Brandini, D.; Fravolini, A. From phenothiazine to 3-phenyl-1,4-benzothiazine derivatives as inhibitors of the *Staphylococcus aureus* NorA multidrug efflux pump. *J. Med. Chem*., **2008**, *51*, 4321-4330.

149. Saha, B.; Das, S.; Saikia, J.; Das, G. Preferential and enhanced adsorption of different dyes on iron oxide nanoparticles: a comparative study. *J. Phy. Chem. C*, **2011**, *115*, 8024-8033.

150. She, P.; Zhou, L.; Li, S.; Liu, Y.; Xu, L.; Chen, L.; Luo, Z.; Wu, Y. Synergistic microbicidal effect of auranofin and antibiotics against planktonic and biofilm- encased *S. aureus* and *E. faecalis*. *Front. Microbiol*. **2019**, *10*, 2453.

151. Shintre, S. A.; Ramjugernath, D.; Shahidul Islam, Md.; Mopuri, R.; Mocktar, C.; Koorbanally, N. A. Synthesis, *in vitro* antimicrobial, antioxidant, and antidiabetic activities of thiazolidine-quinoxaline derivatives with amino acid side chains. *Med. Chem. Res*., **2017**, *26*, 2141-2151.

152. Silva, N. C.; Silva, S.; Sarmento, B.; Pintado, M. Chitosan nanoparticles for daptomycin delivery in ocular treatment of bacterial endophthalmitis. *Drug Deliv*. **2015**, *22*, 885-893.

153. Silver, L. L. Challenges of antibacterial discovery. *Clin Microbiol Rev*. **2011**, *24*, 71-109.

154. Singh, A. K.; Mukherjee, S.; Adhikari, M. D.; Ramesh, A. Fluorescence-based comparative evaluation of bactericidal potency and food application potential of antilisterial bacteriocin produced by lactic acid bacteria isolated from indigenous samples. *Probiotics Antimicrob. Proteins* **2012**, *4*, 122-132.

155. Singh, R.; Kumar, C. S.; Banerjee, M.; Gupta, S. A dual drug delivery platform for cancer-bacteria cotargeting. *ACS Appl. Bio Mater*. **2019**, *2*, 5032-5041.

156. Sinha, B.; Fraunholz, M. *Staphylococcus aureus* host-cell invasion and post-invasion events. *Int. J. Med. Microbiol.* **2010**, *300*, 170-175.

157. Smith, K..; Perez, A.; Ramage, G.; Gemmell, C. G.; Lang, S. Comparison of biofilm-associated cell survival following in vitro exposure of meticillin-resistant *Staphylococcus aureus* biofilms to the antibiotics clindamycin, daptomycin, linezolid, tigecycline and vancomycin. *Int. J. Antimicrob. Agents* **2009**, *33*, 374-378.

158. Song, A.; Walker, S. G.; Parker, K. A.; Sampson, N. S. Antibacterial studies of cationic polymers with alternating, random, and uniform backbones, *ACS Chem Biol.* **2011,** *6*, 590-599.

159. Song, H. S.; Choi, T. R.; Bhatia. S. K.; Lee, S. M.; Park. S. L.; Lee, H. S.; Kim, Y. G.; Kim. J. S.; Kim, W.; Yan, Y. H. Combination therapy using low-concentration oxacillin with palmitic acid and span85 to control clinical methicillin-resistant *Staphylococcus aureus*. *Antibiotics*, **2020**, *9*, 682.

160. Spriano, S.; Yamaguchi, S.; Baino, F.; Ferraris, S. A critical review of multifunctional titanium surfaces: new frontiers for improving osseointegration and host response, avoiding bacteria contamination. *Acta Biomater*. **2018**, *79*, 1-22.

161. Steinbuch, K. B.; Fridman, M. Mechanisms of resistance to membrane-disrupting antibiotics in gram-positive and gram-negative bacteria. *Med. Chem. Commun.*, **2016,** *7*, 86-102.

162. Stoodley, P; Ehrlich, G.D.; Sedghizadehc, P.P.; Hall-Stoodley, L; Baratze, M. E.; Altmane, D.T.; Sotereanose, N.G.; Costertone, J.W.; DeMeoe, P. Orthopaedic biofilm infections, *Curr. Orthop. Pract*., **2011**, *22*, 558–563.

163. Stryjewski, M. E.; Graham, D. R.; Wilson, S. E.; O'Riordan, W.; Young, D.; Lentek, A.; Ross, D. P.; Fowler, V. G.; Hopkins, A.; Friedland, H. D.; Barriere, S. L.; Kitt, M. M.; Corey, G. R. Telavancin versus vancomycin for the treatment of complicated skin and skin structure infections caused by gram-positive organisms. *Clin. Infect. Dis*. **2008**, *46*, 1683-1693.

164. Sun, Z, L.; He, J. M.; Wang, S. Y.; Ma, R.; Khondkar, P.; Kaatz, G. W.; Gibbons, S.; Mu, Q. Benzocyclohexane oxide derivatives and neolignans from Piper betle inhibit efflux-related resistance in *Staphylococcus aureus*. *RSC Adv*., **2016**, *6*, 43518-43525.

165. Sundaramoorthy, N. S.; Mitra, K.; Ganesh, J. S.; Makala, H.; Lotha, R.; Bhanuvalli, S. R.; Ulaganathan, V.; Tiru, V.; Sivasubramanian, A.; Nagarajan, S. Ferulic acid derivative inhibits NorA efflux and in combination with ciprofloxacin curtails growth of MRSA *in vitro* and *in vivo*. *Microb. Path*., **2018**, *124*, 54-62.

166. Swider, E.; Koshkina, O.; Tel, J.; Cruz, L. J.; de Vries, I. J. M.; Srinivas, M. Customizing poly(lactic-co-glycolic acid) particles for biomedical applications. *Acta Biomater*. **2018**, *73*, 38-51.

167. Tacconelli, E.; Carrara, E.; Savoldi, A.; Harbarth, S.; Mendelson, M.; Monnet, D. L.; Pulcini, C.; Kahlmeter, G.; Kluytmans, J.; Carmeli, Y.; Ouellette, M.; Outterson, K.; Patel, J.; Cavaleri, M.; Cox, E. M.; Houchens, C. R.; Grayson, M. L.; Hansen, P.; Singh, N.; Theuretzbacher, U.; Magrini, N.; the WHO Pathogens Priority List Working Group; Discovery, research, and development of new antibiotics: the WHO priority list of antibiotic-resistant bacteria and tuberculosis *Lancet Infect. Dis*., **2017**, *18*, 318-324.

168. Tambat, R.; Jangra, M.; Mahey, N.; Chandal, N.; Kaur, M.; Chaudhary, S.; Verma, D.K.; Thakur, K. G.; Raje, M.; Jachak, S.; Khatri, N. and Nandanwar, H. Microbe-derived indole metabolite demonstrates potent multidrug efflux pump inhibition in *Staphylococcus aureus*. *Front. Microbiol*. **2019**, *10*, 2153

169. Tang, H. J.; Chen, C. C.; Cheng, K. C.; Wu, K. Y.; Lin, Y. C.; Zhang, C. C.; Weng, T. C. *In vitro* efficacies and resistance profiles of rifampin-based combination regimens for biofilm-embedded methicillin-resistant *Staphylococcus aureus Antimicrob. Agents Chemother*. **2013**, *57*, 5717-5720.

170. Tenland, E.; Pochert, A.; Krishnan, N.; Umashankar Rao, K.; Kalsum, S.; Braun, K.; Glegola-Madejska, I.; Lerm, M.; Robertson, B. D.; Linden, M.; Godaly, G. Effective delivery of the anti-mycobacterial peptide NZX in mesoporous silica nanoparticles. *PLoS ONE* **2019**, *14*, e0212858.

171. Thangamani, S.; Mohammad, H.; Abushahba, M. F. N.; Sobreira, T. J. P.; Hedrick, V. E.; Paul, L. N.; Seleem, M. N. Antibacterial activity and mechanism of action of auranofin against multi-drug resistant bacterial pathogens. *Sci. Rep*., **2016**, *6*, 22571.

172. Thappeta, K. R. V.; Vikhe, Y. S.; Yong, A. M. H.; Chan-Park, M. B.; Kline, K. A. Combined efficacy of an antimicrobial cationic peptide polymer with conventional antibiotics to combat multidrug-resistant pathogens. *ACS Infect. Dis*. **2020**, *6*, 1228-1237.

173. Thiyagarajan D.; Das G.; Ramesh A. Amphiphilic cargo-loaded nanocarrier enhances antibiotic uptake and perturbs efflux: effective synergy for mitigation of methicillin-resistant *Staphylococcus aureus*. *ChemMedChem*, **2017**, *12*, 1125-1132.

174. Thiyagarajan, D.; Goswami, S.; Kar, C.; Das, G.;Ramesh, A. A prospective antibacterial for drug-resistant pathogens: a dual warhead amphiphile designed to track interactions and kill pathogenic bacteria by membrane damage and cellular DNA cleavage. *Chem. Commun.*, **2014**, *50*, 7434-7436.

175. Tong, S.Y.C.; Davis, J.S.; Eichenberger, E.; Holland, T.L.; Fowler, V.G., Jr. *Staphylococcus aureus* infections: epidemiology, pathophysiology, clinical manifestations, and management. *Clin. Microbiol. Rev*., **2015**, *28*, 603-661.

176. Toprak, E.; Veres, A.; Michel, J. B.; Chait, R.; Hartl, D. L.; Kishony, R. Evolutionary paths to antibiotic resistance under dynamically sustained drug selection. *Nat. Genet*. **2012**, *44*, 101-105.

177. Truong-Bolduc, Q. C.; Zhang, X.; and Hooper, D.C. Characterization of NorR protein, a multifunctional regulator of NorA expression in *Staphylococcus aureus*. *J. Bacteriol*. **2003**, *185*, 3127-3138.

178. Truong-Bolduc, Q.C.; Hooper, D. C. Phosphorylation of MgrA and its effect on expression of the NorA and NorB efflux pumps of *Staphylococcus aureus*. *J. Bacteriol*. **2010**, *192*, 2525-2534.

179. Truong-Bolduc, Q.C.; Hooper, D. C. The transcriptional regulators NorG and MgrA modulate resistance to both quinolones and beta-lactams in *Staphylococcus aureus*. *J. Bacteriol*. **2007**, *189*, 2996-3005.

180. Tsuji, B.T.; Rybak, M. J. Short-course gentamicin in combination with daptomycin or vancomycin against *Staphylococcus aureus* in an *in vitro* pharmacodynamic model with simulated endocardial vegetations. *Antimicrob. Agents Chemother*., **2005**, *49*, 2735-2745.

181. Tuchscherr, L.; Medina, E.; Hussain, M.; Volker, W.; Heitmann, V.; Niemann, S.; Holzinger, D.; Roth, J.; Proctor, R. A.; Becker, K.; Peters, G.; Loffler, B. *Staphylococcus aureus* phenotype switching: an effective bacterial strategy to escape host immune response and establish a chronic infection. *EMBO Mol. Med.* **2011**, *3*, 129-141.

182. Turner, N, A., Sharma-Kuinkel, B. K.; Maskarinec, S. A.; Eichenberger, E. M.; Shah, P. P.; Carugati, M.; Holland, T. L.; Fowler Jr., V, G. Methicillin-resistant *Staphylococcus aureus*: an overview of basic and clinical research. *Nat. Rev. Microbiol*., **2019**, *17*, 203-218.

183. Tyuleva, S. N.; Allen, N.; White, L. J.; Pepes, A.; Shepherd, H. J.; Saines, P. J.; Ellaby, R. J.; Mulvihill, D. P.; Hiscock, J. R. A Symbiotic supramolecular approach to the design of novel amphiphiles with antibacterial properties against MSRA. *Chem. Commun*., **2019**, *55*, 95-98.

184. Van Bambeke, F.; Mingeot-Leclercq, M. P.; Struelens, M. J.; Tulkens, P. M. The bacterial envelope as a target for novel anti-MRSA antibiotics. *Trends Pharmacol. Sci*. **2008**, *29*, 124-134.

185. Vermote, A.; Brackman, G.; Risseeuw, M. D. P.; Cappoen, D.; Cos, P.; Coenye, T.; Van Calenbergh, S. Novel potentiators for vancomycin in the treatment of

biofilm related MRSA infections via a mix and match approach. *ACS Med. Chem. Lett*. **2017**, *8*, 38-42.

186. Visperas, A.; Santana, D.; Klika, A. K.; Higuera- Rueda, C. A.; Piuzzi, N. S. Current treatments for biofilm- associated periprosthetic joint infection and new potential strategies. *J. Orthop. Res*. **2022**, *40*, 1477- 1491.
187. Viveiros, M.; Martins, A.; Paixao, L.; Rodrigues, L.; Martins, M.; Couto, I.; Fahnrich, E.; Kern, W. V.; Amaral, L. Demonstration of intrinsic efflux activity of *Escherichia coli* K-12 AG100 by an automated ethidium bromide method. *Int. J. Antimicrob. Agents*, **2008**, *31*, 458-462.
188. Wan, F.; Bohr, S. S. R.; Klodzinska, S. N.; Jumaa, H.; Huang, Z.; Nylander, T.; Thygesen, M. B.; Sorensen, K. K.; Jensen, K. J.; Sternberg, C.; Hatzakis, N.; Nielsen, H. M.; Ultrasmall TPGS−PLGA hybrid nanoparticles for site-specific delivery of antibiotics into *Pseudomonas aeruginosa* biofilms in lungs. *ACS Appl. Mater. Interfaces* **2020**, *12*, 380-389.
189. Wang, C.; Ye, C.; Liao, L.; Wang, Z.; Hu, Y.; Deng, C.; Liu, L. Adjuvant β-lactam therapy combined with vancomycin or daptomycin for methicillin-resistant *Staphylococcus aureus* bacteremia: a systematic review and metaanalysis. *Antimicrob. Agents Chemother*. **2020**, *64*, e01377-20.
190. Wang, S.; Liu, X. Q.; Kang, O. H.; Kwon, D. Y. Combination of sanguisorbigenin and conventional antibiotic therapy for methicillin-resistant *Staphylococcus aureus*: inhibition of biofilm formation and alteration of cell membrane permeability. *Int. J. Mol. Sci.* **2022**, *23*, 4232.
191. Weidenmaier, C.; Peschel, A. Teichoic acids and related cell-wall glycopolymersin gram-positive physiology and host interactions. *Nat. Rev. Microbiol*. **2008**, *6*, 276-287.
192. Weigel, L. M.; Clewell, D. B.; Gill, S. R.; Clark, N. C.; McDougal, L. K.; Flannagan, S. E.; Kolonay, J. F.; Shetty, J.; Killgore, G. E.; Tenover, F. C. Genetic analysis of a high-level vancomycin-resistant isolate of *Staphylococcus aureus*. *Science* **2003**, *302*, 1569-1571.
193. Wilson, D. N. Ribosome-targeting antibiotics and mechanisms of bacterial resistance. *Nat. Rev. Microbiol*. **2014**, *12*, 35-48.
194. Wimley, W. C.; Hristova, K. Antimicrobial peptides: successes, challenges and unanswered questions. *J. Membrane Biol*. **2011**, *239*, 27-34.
195. World Health Organization (WHO). Antimicrobial resistance: Global report on

surveillance (2014). Available from: http://www.who.int/drugresistance/documents/surveillancereport/en/.

196. Worthington, R.; Melander, C. Combination approaches to combat multidrug-resistant bacteria. *Trends Biotechnol*., **2013**, *31*, 177-184.

197. Wright, G. D. Molecular mechanisms of antibiotic resistance. *Chemical Communications*, **2011,** *47*, 4055-4061.

198. Wunderink, R. G.; Niederman, M. S.; Kollef, M. H.; Shorr, A. F.; Kunkel, M. J.; Baruch, A.; McGee, W. T.; Reisman, A.; Chastre, J. Linezolid in methicillin-resistant *Staphylococcus aureus* nosocomial pneumonia: a randomized, controlled study. *Clin. Infect. Dis.* **2012**, *54*, 621-629.

199. Wuthrich, D.; Cuenod, A.; Hinic, V.; Morgenstern, M.; Khanna, N.; Egli, A.; Kuehl, R. Genomic characterization of inpatient evolution of MRSA resistant to daptomycin, vancomycin and ceftaroline. *J. Antimicrob. Chemother*. **2011**, *74*, 1452-1454.

200. Xiong. Y.; Kong, J.; Yi, S.; Tan, Q.; Bai, E.; Ren, N.; Huang, Y.; Duan, Y.; Zhu, X. Lipopeptide surfactin ameliorates the cell uptake of platensimycin and enhances its therapeutic effect on treatment of MRSA skin infection. *J Antimicrob. Chemother*. **2022**.

201. Yamada, Y.; Hideka, K.; Shiota, S.; Kuroda, T.; Tsuchiya, T. Gene cloning and characterization of SdrM, a chromosomally-encoded multidrug efflux pump, from *Staphylococcus aureus*. *Biol. Pharm. Bull*. **2006**, *29*, 554-556.

202. Yamakami, K.; Tsumori, H.; Sakurai, Y.; Shimizu, Y.; Nagatoshi, K.; Sonomoto, K. Sustainable inhibition efficacy of liposome-encapsulated nisin on insoluble glucan-biofilm synthesis by *Streptococcus mutans*. *Pharm. Biol*. **2013**, *51*, 267-270.

203. Yan, Q.; Karau, M. J.; Raval, Y. S.; Patel, R. Evaluation of oritavancin combinations with rifampin, gentamicin, or linezolid against prosthetic joint infection-associated methicillin-resistant *Staphylococcus aureus* biofilms by time-kill assays. *Antimicrob. Agents Chemother*. **2018**, *62*, e00943-18.

204. Yeh, Y.C.; Huang, T. H.; Yang, S.C.; Chen, C.C.; Fang, J. Y. Nano-based drug delivery or targeting to eradicate bacteria for infection mitigation: a review of recent advances. *Front. Chem*. **2020**, *8*, 286.

205. Yong, D.; Toleman, M. A.; Giske, C. G.; Cho, H. S.; Sundman, K.; Lee, K.; Walsh. T. R. Characterization of a new metallo-beta-lactamase gene, bla (NDM-

1), and a novel erythromycin esterase gene carried on a unique genetic structure in *Klebsiella pneumoniae* sequence type 14 from India. *Antimicrob. Agents Chemother*. **2009**, *53*, 5046-5054.

206. Yoshida, H.; Bogaki, M.; Nakamura, S.; Ubukata, K.; Konno, M. Nucleotide sequence and characterization of the *Staphylococcus aureus* norA gene, which confers resistance to quinolones. *J. Bacteriol*., **1990**, 172, 6942-6949.
207. Yu Y.; Huang H. L.; Ye, X. Q., Cai D. T.; Fang J.T.; Sun, J.; Liao, X. P.; Liu, Y. H. Synergistic potential of antimicrobial combinations against methicillin-resistant *Staphylococcus aureus*. *Front. Microbiol*. **2020**, *11*, 1919.
208. Zhang, M.; Liao, Y.; Tong, X.; Yan, F. Novel urea derivative-loaded PLGA nanoparticles to inhibit caries-associated *Streptococcus mutans*. *RSC Adv*. **2022**, *12*, 4072-4080.
209. Zhao, Q.; Yi, L.; Jiang, L.; Ma, Y.; Lin, H.; Dong, J. Surface functionalization of titanium with zinc/strontium-doped titanium dioxide microporous coating via microarc oxidation. *Nanomed.: Nanotech. Biol. Med.* **2019**, *16*, 149-161.
210. Zwietering, M. H.; Jongenburger, I.; Rombouts, F. M.; Riet, K. Van't. Modeling of the bacterial growth curve. *Appl. Env. Microbiol*. **1990**, *56*, 1875-1881.

APPENDIX

APPENDIX

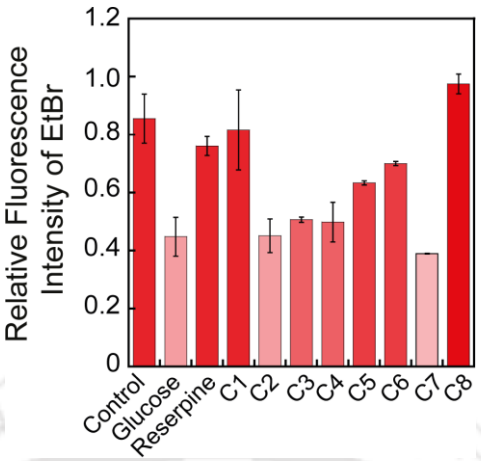

Figure A2.1. Effect of urea-based ligands on EtBr efflux in *S. aureus* 4s cells. The data point represents end-point analysis of samples following 10 minutes of treatment of *S. aureus* 4s cells with urea-based ligands (10 µM each). Reserpine (40 µM) was used as positive control for the assay.

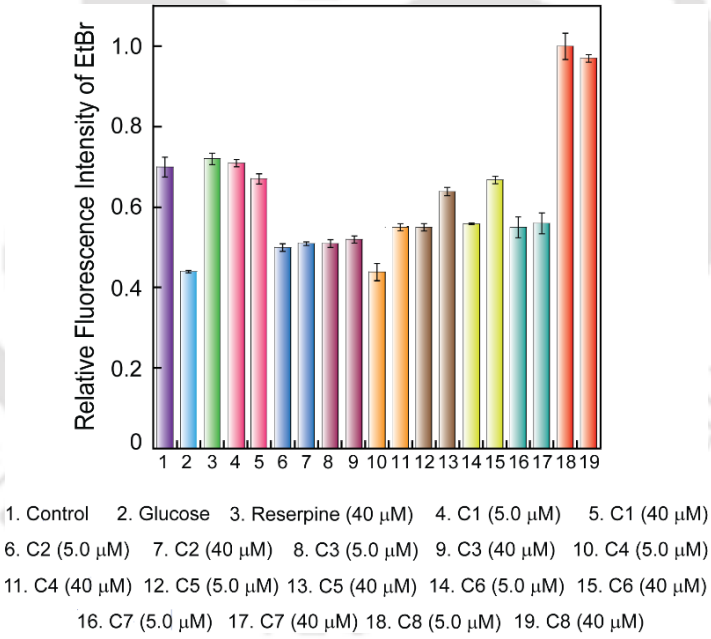

Figure A2.2. Effect of urea-based ligands on EtBr efflux in *S. aureus* 4s cells. The data point represents end-point analysis of samples following 10 minutes of treatment of *S. aureus* 4s cells with urea-based ligands (5.0 µM and 40 µM each). Reserpine (40 µM) was used as positive control for the assay.

Table A2.1. Statistical analysis for cellular fluorescence obtained in EtBr accumulation assay in *S. aureus* 4s cells treated with C1 and C8.

Sl. No.	Comparison Group	Significant Difference in Cellular Fluorescence Intensity Measured in EtBr Accumulation Assay *	Concentration of Compounds in EtBr Accumulation Assay
1.	C8 versus untreated cells	Yes	Reserpine: 40 µM C1: 40 µM C8: 10 µM
2.	C8 versus positive control (+ glucose)	Yes	
3.	C8 versus Reserpine	Yes	
4.	C1 versus untreated cells	Yes	
5.	C1 versus positive control (+ glucose)	Yes	
6.	C1 versus Reserpine	Yes	
7.	Positive control (+ glucose) versus untreated cells	Yes	

* Significant difference implies *p* value < 0.001 based on analysis of variance (ANOVA) followed by all pair wise multiple comparisons (Holm-Sidak method) of relative end-point fluorescence measured in EtBr efflux assay.

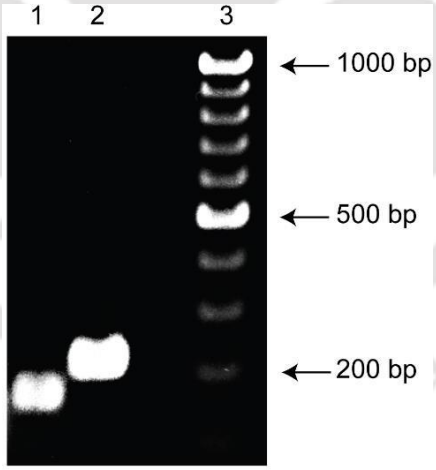

Figure A2.3. Agarose gel electrophoresis of amplicons obtained from the MRSA strain *S. aureus* 4s using gene specific primers for *norA* and *16S rRNA* gene. Lane 1: Amplicon for *norA* gene; Lane 2: Amplicon for *16S rRNA* gene; Lane 3: 100 bp DNA size marker.

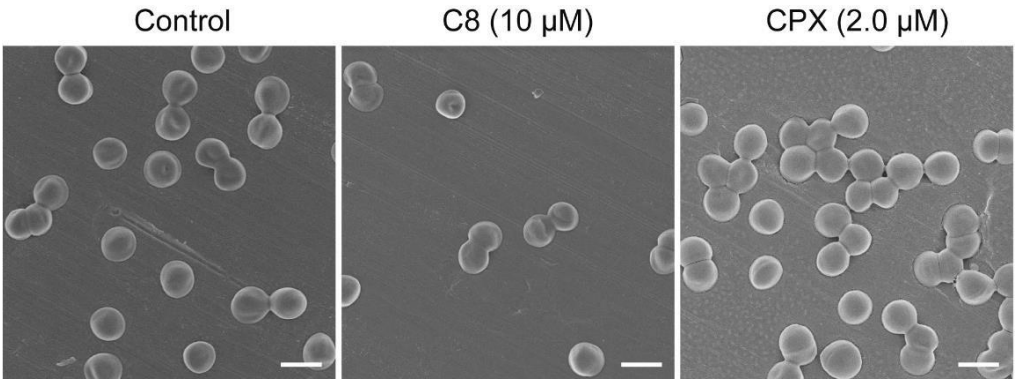

Figure A2.4. FESEM analysis of (i) untreated, (ii) C8-treated and (iii) CPX-treated *S. aureus* 4s cells. Scale bar for the images is 1.0 μm.

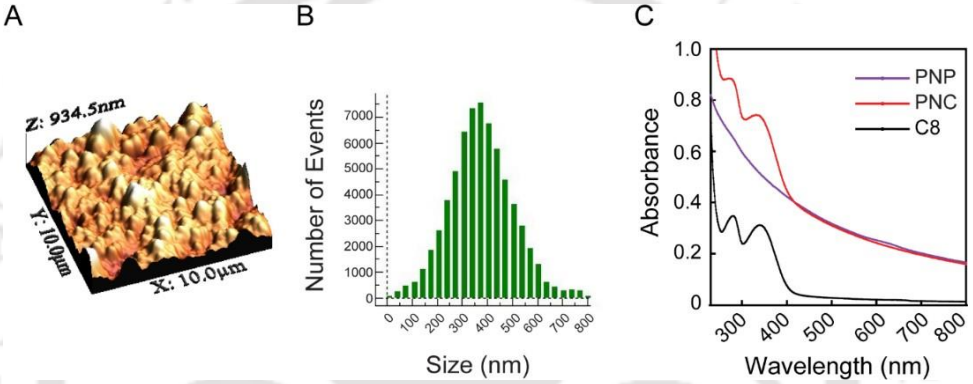

Figure A3.1. (A) 3D topography AFM image of C8-PNC. (B) Height profile of C8-PNC assessed by analysis of the image shown in (A). (C) Characterization of C8-PNC by UV-visible absorption spectroscopy.

Table A3.1. Statistical analysis for relative end-point fluorescence obtained in EtBr efflux assay using *S. aureus* 4s cells treated with C8-PNC or C8.

Sl. No.	Comparison Group	Significant Difference in Relative End-point Fluorescence Measured in EtBr Efflux Assay *	Concentration of C8 in EtBr Efflux Assay
1.	C8-PNC versus Control (+ glucose)	Yes	C8-PNC: loaded with 50 µM C8 C8 alone: 10 µM
2.	C8-PNC versus Reserpine	Yes	
3.	C8-PNC versus C8	Yes	
4.	C8 versus Control (+ glucose)	Yes	
5.	C8 versus Reserpine	Yes	

* Significant difference implies *p* value < 0.001 based on analysis of variance (ANOVA) followed by all pair wise multiple comparisons (Holm-Sidak method) of relative end-point fluorescence measured in EtBr efflux assay.

Table A3.2. MTT assay to ascertain the cytotoxic effect of varying concentrations of C8 on cultured HEK 293 cells.

Sl. No.	Concentration of C8 in MTT Assay (µM)	Growth of HEK 293 Cells* (% ± Standard Deviation)
1.	5.0	63.22 ± 0.065
2.	10	41.92 ± 0.174
3.	20	23.73 ± 0.047
4.	40	10.41 ± 0.010

* Each data point represents mean ± standard deviation from six samples.

A4.1. Synthesis and Characterization of Ligands

Synthesis and spectroscopic characterization of C1, C2 and C3 have been reported previously (Basak *et al*., 2021; Basak and Das, 2021; Ghosh *et al*., 2022). The same protocol was essentially followed for synthesis of C4. To a suspension of 3,4- diaminobenzoic acid (152.15 mg, 1.0 mmol) in 20 ml glacial acetic acid, isatin (176.56 mg, 1.0 mmol) was added portion-wise at room temperature. The reaction

mixture was allowed to reflux overnight. After stirring for 24 hours, it was cooled to room temperature, and crushed ice was added slowly to obtain a precipitate. The precipitate was filtered and washed several times with methanol/acetic acid followed by ether to obtain the pure product C4.

C4: brown solid (95% yield); MALDI-MS (*m/z*): calculated for $C_{15}H_{10}N_3O_2$ $[M+H]^+$: 264.077; found: 264.650; ^{1}H NMR (500 MHz, DMSO-d_6): 12.118 (s, 1H), 12.044 (s, 1H), 8.953 (s, 1H), 8.427-8.413 (d, 1H), 8.336-8.323 (d, 1H) , 8.066-8.040(d, 1H), 7.910-7.895 (d, 1H), 7.705-7.674 (t, 1H), 7.419-7.378 (dd, 1H) ; ^{13}C NMR (150 MHz, DMSO-d_6):167.68, 150.51, 149.53, 147.08, 146.54, 143.61, 137.83, 134.01, 130.77, 127.85, 125.06, 123.79, 1194.04, 116.28, 111.90; FT-IR (KBr pellets, cm^{-1}): 3418(O-H stretching), 3097(N-H stretching), 2983(C-H stretching), 1708(C=O stretching), 1596(C=N), 1391(C-N stretch), 747(N-H wagging).

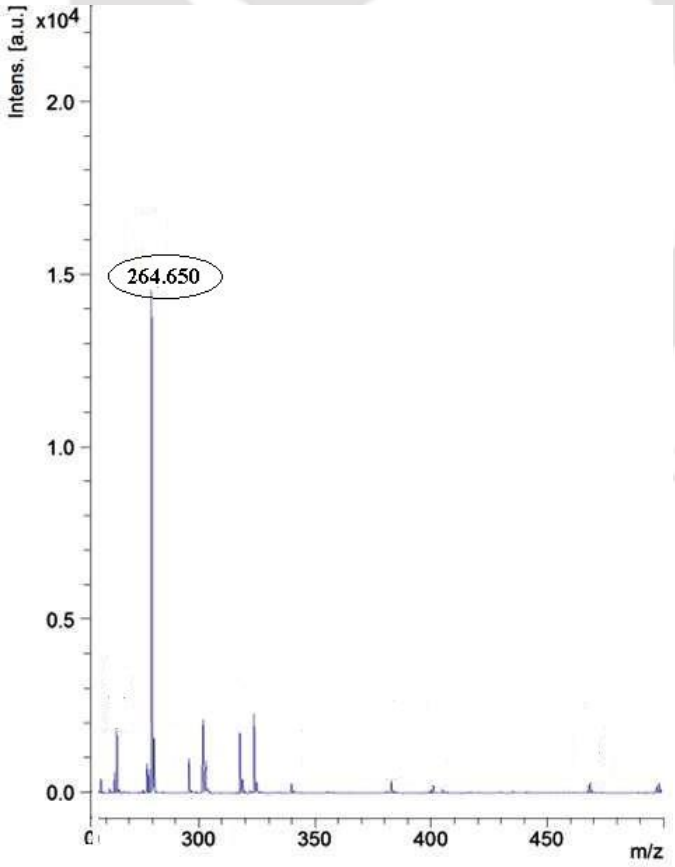

Figure A4.1. MALDI-MS spectra of C4 in dichloromethane in positive ionization mode. Calculated Mass $[M + H^+]$ = 264.077; Obtained Mass $[M + H^+]$ = 264.650.

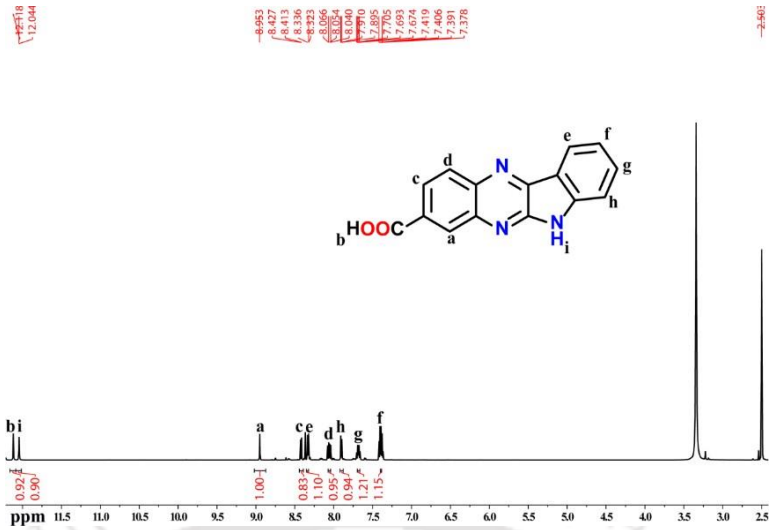

Figure A4.2. ^{1}H NMR of C4 in DMSO-d_6 at room temperature.

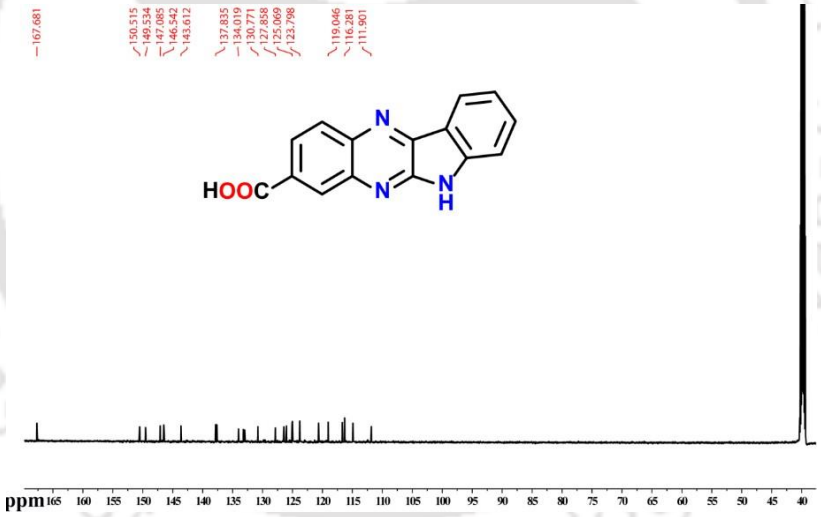

Figure A4.3. ^{13}C NMR of C4 in DMSO-d_6 at room temperature.

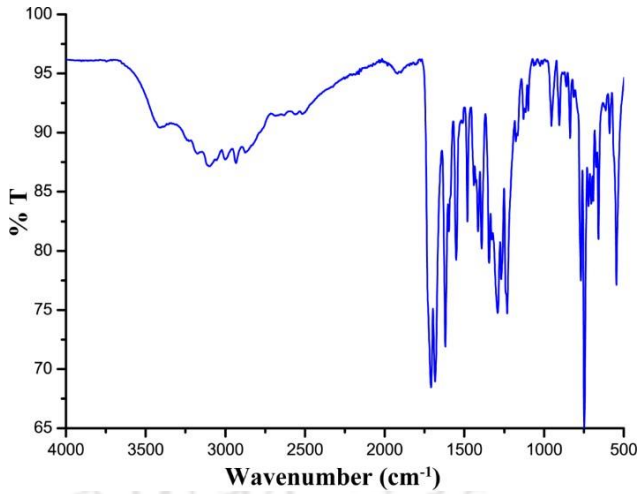

Figure A4.4. FTIR spectrum of C4 recorded at room temperature.

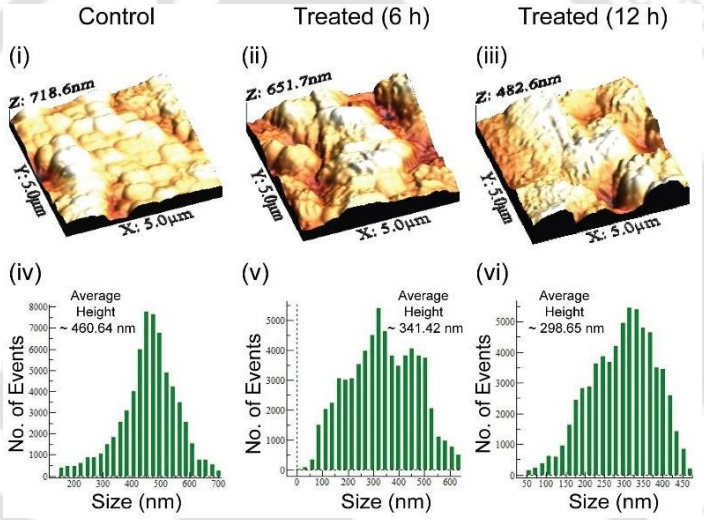

Figure A4.5. Bactericidal activity of C2 (32 µM) against *S. aureus* 4s cells ascertained by AFM analysis. Panels (i-iii) indicate 3D topography images and panels (iv-vi) represent the corresponding height profile.

Table A5.1. MTT assay to ascertain the cytotoxic effect of varying concentrations of C2 on cultured MG-63 cells.

Treatment	Growth of MG-63 Cells* (% ± Standard Deviation)
10 µM C2	89.15 ± 1.50
12 µM CPX	99.95 ± 0.66
10 µM C2 + 12 µM CPX	90.96 ± 0.52

* Each data point represents mean ± standard deviation from six samples.

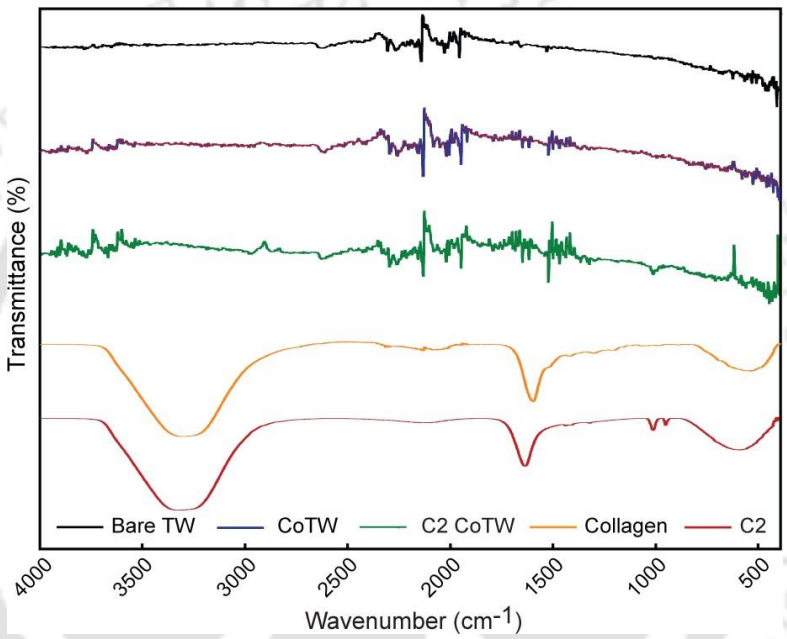

Figure A6.1. Characterization of bare titanium wire, collagen coated titanium wire (Co-TW) and C2-incorporated collagen-coated titanium wire (C2-Co-TW) by FTIR analysis.

LIST OF PUBLICATIONS

Publications from Ph.D. Thesis Work:

(A) Journal Publications:

1. **Bhattacharjee, B.;** Das, A.; Das, G.; Ramesh, A. Urea-based ligand as an efflux pump inhibitor: warhead to counter ciprofloxacin resistance and inhibit collagen adhesion by MRSA. *ACS Applied Bio Materials* **2022**, *5*, 1710-1720.
2. **Bhattacharjee, B.;** Basak, M.; Das, G.; Ramesh, A. Quinoxaline-based membrane-targeting therapeutic material: implications in rejuvenating antibiotic and curb MRSA invasion in an *in vitro* bone cell infection model. *Biomaterials Advances* **2022**, Manuscript Number BIOADV-D-22-02041 **(Under Review).**
3. **Bhattacharjee, B.;** Basak, M.; Das, G.; Ramesh, A. Biocompatible nanocarrier fortified with a membrane-targeting adjuvant enables effective combination therapy to prevent MRSA invasion in orthopaedic implant **(Manuscript under preparation)**.

(B) Conference Presentations:

1. **Bhattacharjee, B.,** Mukherjee, S., Manna, U., Das, A., Das, G. and Ramesh, A. (2018). Nanocomposite loaded with a synthetic adjuvant to potentiate the activity of ciprofloxacin against methicillin-resistant Staphylococcus aureus. Presented in 59th Annual Conference of Association of Microbiologists of India (AMI), University of Hyderabad, 9-12 December 2018.

(C) Publications from Other Research Projects:

1. Halder, S.; Nayak, B.; **Bhattacharjee, B.**, Ramesh, A.; Das, G. Insight into the aggregation prospective of Schiff base AIEgens enabling an efficient hydrazine sensor in their aggregated state. *Journal of Materials Chemistry C* **2021**, *9*, 8596-8605.
2. Basak, M.; **Bhattacharjee, B.**; Ramesh, A.; Das, G. Self-assembled quinoxaline derivative: Insight into disaggregation induced selective detection of nitro-aromatics in aqueous medium and live cell imaging. *Dyes and Pigments* **2021**, *196*, 109779.